UNCLASSIFIED

SECURITY CLASSIFICATION OF THIS PAGE *(When Data Entered)*

REPORT DOCUMENTATION PAGE		READ INSTRUCTIONS BEFORE COMPLETING FORM
1. REPORT NUMBER AFFDL-TR-74-29	2. GOVT ACCESSION NO.	3. RECIPIENT'S CATALOG NUMBER
4. TITLE *(and Subtitle)* The Dynamic Response of Aircraft Encountering Aircraft Wake Turbulence		5. TYPE OF REPORT & PERIOD COVERED Final 6. PERFORMING ORG. REPORT NUMBER
7. AUTHOR*(s)* Robert C. Nelson		8. CONTRACT OR GRANT NUMBER*(s)*
9. PERFORMING ORGANIZATION NAME AND ADDRESS AF Flight Dynamics Laboratory Wright-Patterson AFB, Ohio		10. PROGRAM ELEMENT, PROJECT, TASK AREA & WORK UNIT NUMBERS Proj/Task: 192903
11. CONTROLLING OFFICE NAME AND ADDRESS Control Criteria Branch (FGC) AF Flight Dynamics Laboratory		12. REPORT DATE June 1974 13. NUMBER OF PAGES 141
14. MONITORING AGENCY NAME & ADDRESS*(if different from Controlling Office)*		15. SECURITY CLASS. *(of this report)* Unclassified 15a. DECLASSIFICATION/DOWNGRADING SCHEDULE

16. DISTRIBUTION STATEMENT *(of this Report)*

Approved for public release; distribution unlimited

17. DISTRIBUTION STATEMENT *(of the abstract entered in Block 20, if different from Report)*

18. SUPPLEMENTARY NOTES

19. KEY WORDS *(Continue on reverse side if necessary and identify by block number)*

Trailing Vortices
Aircraft Wake Turbulence

20. ABSTRACT *(Continue on reverse side if necessary and identify by block number)*

This investigation deals with the dynamic behavior of an airplane encountering aircraft wake turbulence. A digital computer simulation was developed to study the response of an aircraft flying into a trailing vortex wake. The simulation includes the complete six degree of freedom equations of motion, a description of the vortex velocity field, unsteady aerodynamics, and pilot control input. The parameters, varied in this simulation, include the penetration angle, separation distance, aircraft size (for both the penetrating and generating aircraft), and pilot control input (single- or multi-axes).

DD FORM 1 JAN 73 1473 EDITION OF 1 NOV 65 IS OBSOLETE

UNCLASSIFIED

SECURITY CLASSIFICATION OF THIS PAGE *(When Data Entered)*

Predicted vortex induced motions are presented for a variety of probe aircraft. The probe aircraft selected are representative of general aviation, business, and light jet transport type aircraft. Whereas, the aircraft used to generate the vortex wakes are representative of the commercial transport fleet. The computer predictions indicate that relatively large aircraft (light jet transport) can experience unacceptable vortex-induced roll excursions. Also the results from the simulation were found to compare favorably with flight test data. In addition to evaluating the vortex induced responses, the effect of pilot control input was assessed. It was found that pilot control input was momentarily out of phase with the vortex induced disturbance. Thus the pilot's control tended to aggravate the vortex induced upset.

FOREWORD

This report describes the results of an inhouse investigation dealing with an analysis of the response of aircraft encountering aircraft wake turbulence. The work was partially sponsored by The Pennsylvania State University and later by the Air Force Flight Dynamics Laboratory. Both organizations supplied the author with computer time.

Special recognition should be given to Drs. B. W. McCormick and J. J. Eisenhuth of The Pennsylvania State University and Dr. G. Kurylowich of the Air Force Flight Dynamics Laboratory for their technical guidance.

This investigation was performed during the period from September 1972 to April of 1974. The manuscript was submitted by the author on 10 June 1974.

TABLE OF CONTENTS

LIST OF ILLUSTRATIONS

LIST OF TABLES

Nomenclature

a	core radius constant of proportionality and slope of lift curve
A_{ij}	aerodynamic influence coefficients
b	wing span
B_{ij}	aerodynamic influence coefficients
c	wing chord
$\bar{c}$	mean chord
c_o	root chord
C_ℓ	sectional lift coefficient
C_{ℓ_o}	mid-span sectional lift coefficient
C_L	lift coefficient
$C_\int$	roll moment coefficient
g	acceleration due to gravity
h	added mass term
$h_{z_{g_w}}$	indicial function (gust velocity)
$h_{z_{m_w}}$	indicial function (vehicle motion)
I_{xx}, I_{yy}, I_{zz}	moments of inertia referred to body axes
k_2, k_3	empirical constants used in vortex model
k_p	pilot gain
k_{p_ϕ}	pilot gain in roll
k_{p_ψ}	pilot gain in heading
k_{p_θ}	pilot gain in pitch
ℓ	lift, width of panel section
ℓ_g	lift due to gust penetration
ℓ_m	lift due to vehicle motion
ℓ_t	tail moment arm

L	roll moment
L_p	$C_{\ell_p}(\frac{b}{2u})\ QSb/I_{xx}$
L_{δ_a}	$C_{\ell_{\delta_a}} QSb/I_{xx}$
M	pitching moment
M_δ	$C_{m_\delta}\ QSc/I_{yy}$
M_q	$C_{m_q}(c/2u)\ QSc/I_{yy}$
M_u	$C_{m_u}\ \rho\ SWc/I_{yy}$
M_w	$C_{m_\alpha}\ \rho\ Sc^2/I_{yy}$
m	mass
m_a	aspect ratio correction
N	yaw moment
N_β	$C_{n_\beta}\ QSb/I_{zz}$
N_δ	$C_{n_\delta}\ QSb/I_{zz}$
N_r	$C_{n_r}\ (\frac{b}{2u})\ QSb/I_{zz}$
N_v	N_β/U
P	roll rate
Q	pitching rate, dynamic pressure
q	velocity
R	yaw rate
R_a	region over the wing
R_w	region over the wake
R_{1j}	distance of port vortex from the jth control point
R_{2j}	distance of starboard vortex from the jth control point
r	radius
S	wing area

S_t	tail area
s	Laplace transform variable
t	time
u_g	component of gust velocity in x direction (body axis)
$\bar{u}_g$	component of gust velocity in x direction (inertial axis)
U	component of velocity along x direction (body axes)
V	component of velocity along y direction (body axes)
V_θ	tangential velocity
V_{θ_o}	maximum tangential velocity immediately behind the wing
$V_{\theta_{1j}}$	tangential velocity of port vortex at jth control point
$V_{\theta_{2j}}$	tangential velocity of starboard vortex at jth control point
W	component of velocity along z direction (body axes)
w_g	gust velocity
$w_{3/4c}$	vehicle velocity at control point
$\bar{w}_g$	component of gust velocity in z direction (inertial)
x	force in x direction (body axes)
x,y,z	body axes coordinates
$\bar{x},\bar{y},\bar{z}$	inertial coordinates
x_u	$\rho\ SU(-C_D - C_{D_u})/m$
x_w	$\rho\ SU(C_L - C_{D_\alpha})/2m$
$[x_{c_{p_j}}, y_{c_{p_j}}, z_{c_{p_j}}]$	control point coordinates in body frame
$[\bar{x}_{c_{p_j}}, \bar{y}_{c_{p_j}}, \bar{z}_{c_{p_j}}]$	control point coordinates in inertial frame
y	side force
Y_a	aircraft transfer function

$Y_{O.L.}$	Open loop transfer function. The product of all series transfer functions.
Y_δ	C_{y_δ} QS/m
Y_r	$C_{y_r}(\frac{b}{2u})$ QS/m
Y_v	C_{y_β} QS/(um), lateral distance to port vortex
Y_{v_d}	lateral distance to starboard vortex
z	force in z direction, also axial distance downstream
z_δ	C_{z_δ} QS/m
z_q	$C_{z_q}(\frac{c}{2u})$ QS/m
z_u	ρ SU$(-C_L - C_{L_u})$/m
z_v	vertical distance to vortex
z_w	ρ SU$(-C_{L_\alpha} - C_D)$/2m
$\dot{z}_w$	ρ Sc$(-C_{L_\alpha})$/4m

Greek Symbols

α	angle of attack
β	angle of side slip
γ	circulation per unit chord
Γ	circulation
ϵ	eddy viscosity
ζ	damping ratio
δ	circulation per unit span
δ_a	aileron deflection, also circulation per unit span
δ_e	elevator deflection
δ_r	rudder deflection
$[\eta,\xi]$	wing coordinates
θ	pitch angle
θ_c	commanded pitch attitude
θ_e	error in pitch attitude
λ	sweep angle
ν	kinematic viscosity
ρ	density of air
τ	time constant
τ_e	effective time constant
τ_L	lead constant
τ_I	lag constant
τ_{L_ϕ}	pilot lead in roll
τ_{L_θ}	pilot lead in pitch
τ_{L_ψ}	pilot lead in yaw

Φ	Wagner function
ϕ	roll angle
ϕ_e	error in roll orientation
ψ	yaw angle or Kussner function
ψ_e	error in yaw orientation
ω	undamped natural frequency

Notation

C_ϕ	cos ϕ
C_θ	cos θ
C_ψ	cos ψ
S_ϕ	sin ϕ
S_θ	sin θ
S_ψ	sin ψ

SECTION I

INTRODUCTION

The wing of an airplane generates from its trailing edge a vortex sheet which rapidly rolls up into two trailing tip vortices. These vortices have been observed to persist for distances of up to 10 miles or more behind large aircraft. It can be easily shown that the strength of the trailing vortices increases with the size of the aircraft that generates them, whereas the maximum tangential velocity increases inversely with the velocity of the aircraft. Hence the most severe vortex system to be expected is that generated by a large aircraft during either take-off or landing. Therefore the vortex hazard is greatest in the terminal area. The probability of a vortex related accident is becoming more severe with the growing disparity in aircraft size and with increasing air traffic. During the past several years, there has been a renewed interest in the hazard due to aircraft trailing vortices. Much of the analytical and experimental research conducted during this period deals with methods of predicting the vortex velocity field as well as its rate of decay. There are, however, two areas which have not received much attention. These are the effect of atmospheric conditions on the transport and decay of the vortices and the dynamic behavior of an aircraft penetrating the vortex system. It is the latter topic which is the subject of this report.

The need to know the dynamic behavior of an aircraft encountering a vortex wake becomes clear when one reviews the present goals of the Federal Aviation Administration (FAA). The FAA plans to increase

airport and airway capacity by a factor of two by 1980 and by a factor of five by 1995. In order to accomplish a two fold increase by 1980 the FAA proposes to improve landing aids, reduce separation distances between aircraft to two miles, and to utilize dual runways which are less than 2500 feet apart.[1] This of course is in direct opposition to the suggestion that aircraft be separated by greater distances to insure adequate safety from aircraft wake turbulence. The FAA recognizes that the vortex hazard poses a serious threat to aircraft safety and airport utilization and is attempting to find a solution by supporting research in the areas of vortex dissipation and vortex detection.

Efforts to eliminate the vortex hazard by causing the vortices to decay earlier have not as yet been successful. The various concepts which have been considered include wing design, mass injection, spoilers, oscillating control surfaces, engine location, and trailing bodies. The subject of vortex dissipators is treated in reference 2. All of these devices change the velocity field in the vicinity of the wing. However, these devices do not appear to change the vortex system at distances far downstream of the aircraft. For example, it was suggested by Corsiglia, Jacobsen, and Chigier[2] that placing a small vertical panel near the wing tip would cause a modification of the vortex. Wind tunnel results seemed to verify their idea. However, when the device was placed on a Convair 990 the results were inconclusive. The pilots of the aircraft probing the 990's wake reported that they were unable to detect any difference between the Convair 990 with or without the vortex dissipator.

The leading candidate for a vortex detection system is an acoustic sensor. There are several devices presently under consideration. They all have limited range and can only determine the vortices located in a very narrow field of view. Figure 1 taken from reference 1 shows an artist's conception of the planned vortex detection system.

Even if an operational vortex detection system is developed within the next few years one still needs to know how hazardous a detected vortex is to the next aircraft to pass through the same airspace. The information included in this dissertation will aid in determining safe operating procedures in the terminal area.

This report attempts to evaluate the relationship between the motion of the penetrating aircraft and the size and operating conditions of the generating aircraft. It also considers the age of the vortex and the manner in which the vortex is encountered.

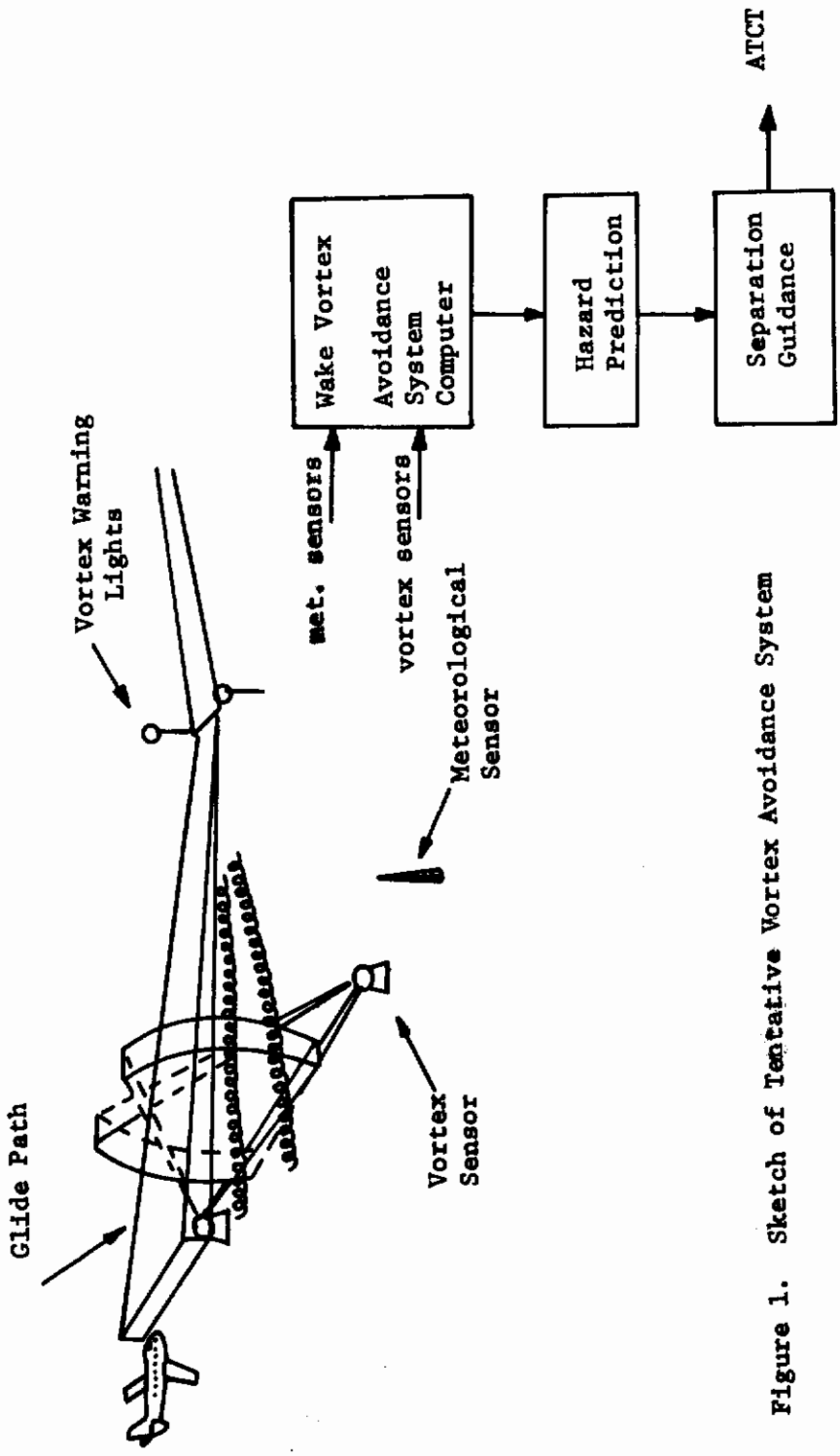

Figure 1. Sketch of Tentative Vortex Avoidance System

SECTION II

PREVIOUS INVESTIGATIONS

The problem associated with an aircraft penetrating the trailing vortex system of another aircraft was first analyzed by Bleviss[3]. In his analysis he determined the maximum roll rate to be expected if the aircraft were suddenly immersed along the axis of one of the vortices as shown in Figure 2. The induced roll rate was compared with the roll rate available using aileron control. The analysis pointed out the hazard to light aircraft encountering the wake of a civilian transport aircraft.

Introduction of jet transports into commercial aviation in the late fifties prompted a renewed interest in the vortex hazard. Several papers by McGowan[4, 5, 6] and Wetmore and Reeder[7] were published in the sixties. McGowan analyzed the behavior of an aircraft traversing the vortex system (see Figure 2). He was the first to include unsteady aerodynamics into the modeling of the problem. Some typical results from his analysis are shown in Figure 3. His calculations indicated that light normal- category and light transport - category aircraft could experience loading conditions that exceed the design limit and in some cases the design ultimate load factors. He also concluded that the pilot would aggravate the loading condition by his phasing of the elevator deflection.

Wetmore and Reeder used McGowan's and Bleviss' results to develop procedures in the airport terminal area. Their main conclusion was that the vortex hazard could be substantially reduced by developing air-traffic control procedures which emphasized appropriate

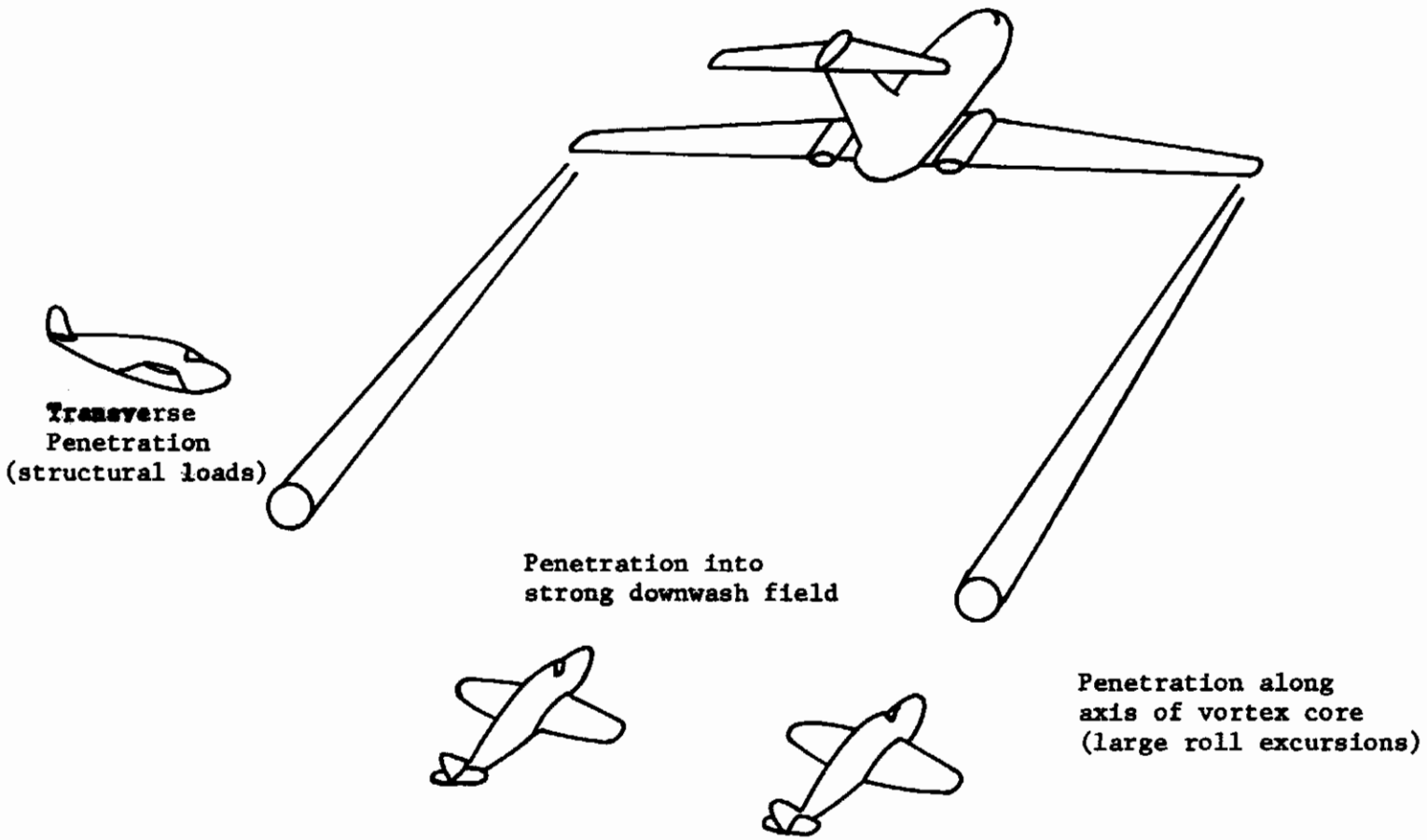

Figure 2. Hazards Associated with Trailing Vortex Wake Encounters

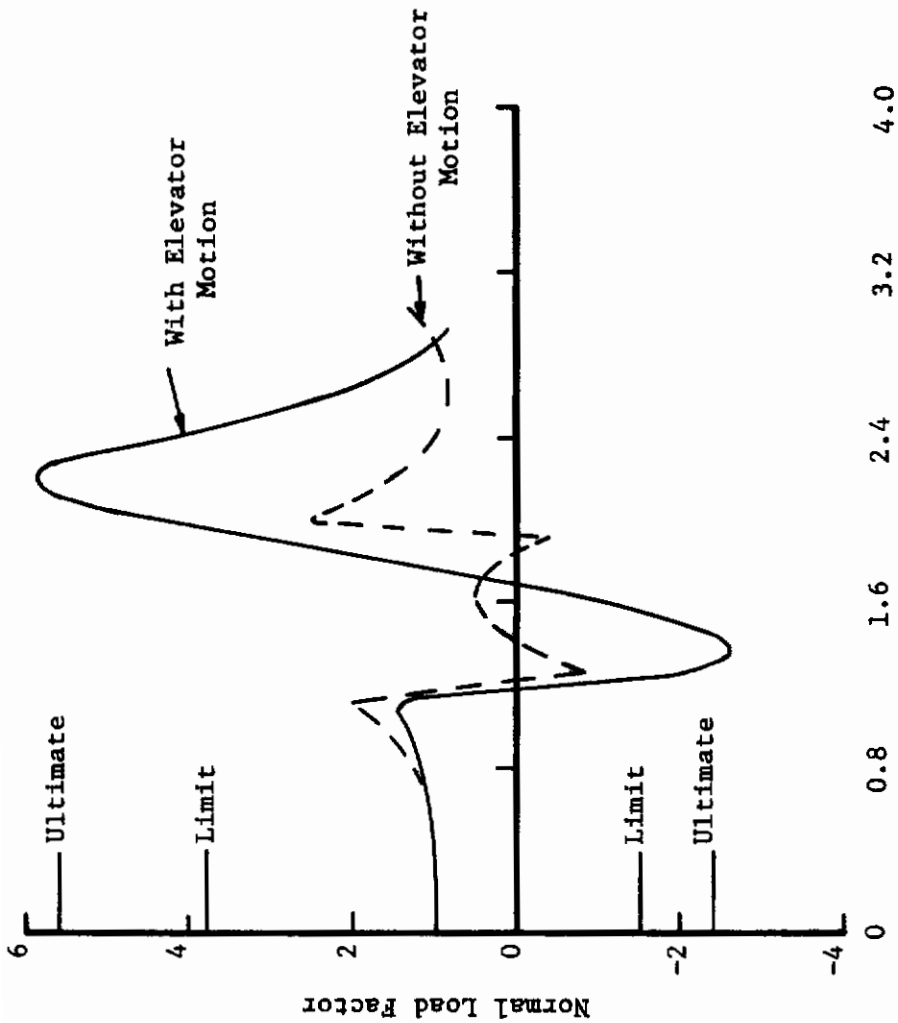

Figure 3. Calculated Load Factor on a Light Aircraft Traversing the Wake of a Jet Transport

spacing and control of flight paths.

In the late sixties and early seventies the interest in vortex wakes was renewed with the advent of the so called "Jumbo Jet". Several symposiums were held to express ideas on how to solve the vortex problem. Most of the papers presented at these symposia dealt with the theories of vortex decay, atmospheric effects on the vortices and means of alleviating the vortex hazard by hastening the vortex breakup. Several papers on the dynamics of a vortex encounter were presented by Hackett and Theisen[8], Andrews[9,10] and Condit and Tracy[11].

Hackett and Theisen presented results from a computer simulation of a vortex encounter. Their results indicated the significant effect that the vertical tail has on the vortex upset. Figure 4 taken from their paper shows the response of a jet transport to an encounter with the wake of a Jumbo Jet. Their results also indicate that the pilot's reaction could aggravate the vortex upset. This can be explained by examining Figure 4. As the aircraft enters the vortex from the top side the aircraft starts to roll in a counter clockwise direction. The vertical tail is subjected to a lateral velocity to the left causing the aircraft to yaw to the right. As the aircraft moves to the right the left wing experiences the high velocity upwash of the right vortex. This causes the aircraft to roll in a clockwise direction which is opposite of the initial roll disturbance. Thus the pilot's attempt to control the aircraft would be momentarily out of phase with the motion of the aircraft.

Andrews presented the results of tests conducted at the NASA Flight Research Center in which probe aircraft were flown into the

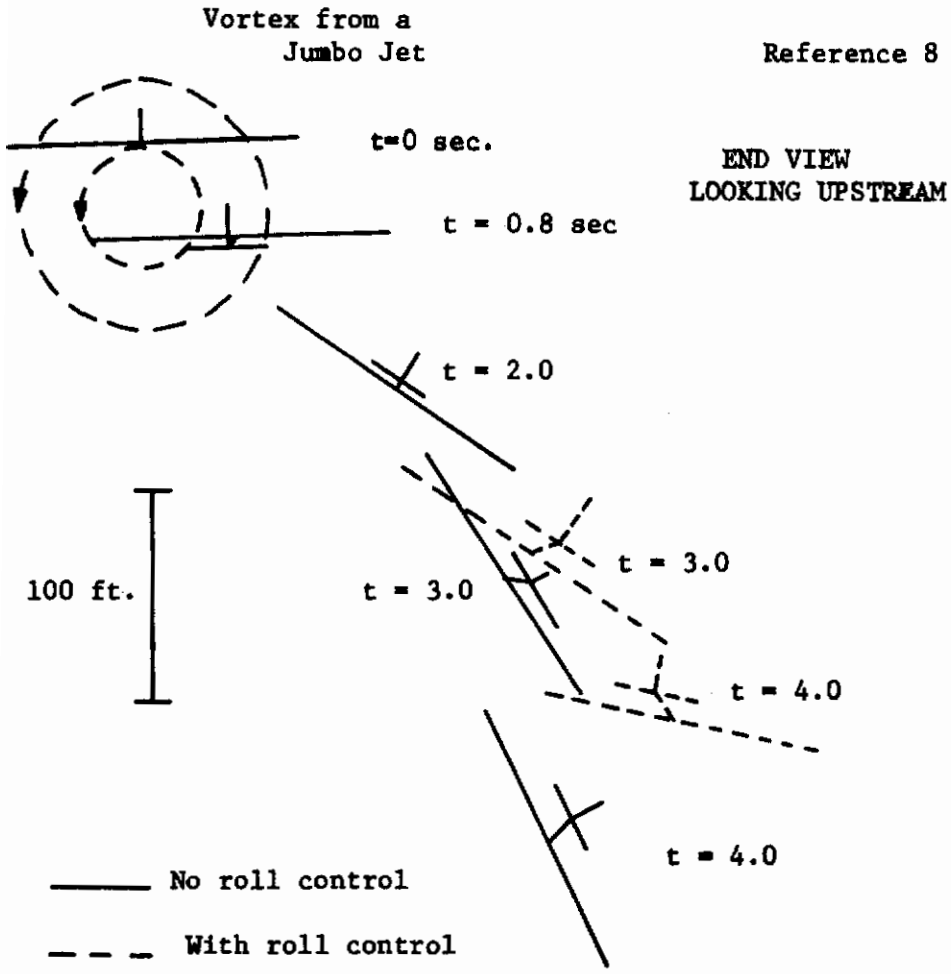

Figure 4. Wake Upset Simulation

wakes of heavy Jumbo Jet-type aircraft. Test results indicated that aircraft with short wing spans could experience uncontrolled upsets for up to 8 nautical miles behind a Jumbo Jet. They also concluded that the maximum induced rolling moments exceeded the lateral control power of most of the probe aircraft* when they were within the minimum separation distances normally maintained during take-off and landing operations.

Condit and Tracy presented the results of Boeing's wake turbulence investigations. Based on their tests and analysis they recommended that the FAA use a 5 mile separation for light airplanes following heavy transports. They also concluded that the 747 and 707 produced similar dynamic responses to aircraft encountering their respective wakes.

The most recent works on aircraft vortex interaction are by Bernstein and Iversen[12] and by Nelson and McCormick[13]. Bernstein and Iversen developed a 3 degree of freedom analog simulation of the vortex problem. They were primarily concerned with penetrations along the axis of the vortex cores. Their results showed that the response of a C-130 encountering the wake of a C-5A at a distance of 2 nautical miles was more severe than the response of a C-130 260 feet behind another C-130. Thus their results indicate the importance of the relative size of the penetrating aircraft to that

---

* The probe aircraft were a Convair 990, DC-9, Learjet and a Cessna 210.

of the generating aircraft.

Nelson and McCormick showed that relatively large aircraft can be susceptible to vortices generated by large jet transports. Their conclusions were based upon a review of accident records as well as a computer simulation of the aircraft vortex penetration. The computer simulation consisted of the equations of motion with 6 degrees of freedom and also included control input by the pilot. Figure 5 taken from reference 13 shows the response of a light jet transport (DC-9) to an encounter with the wake of a Jumbo Jet (DC-10). It should be noted that the maximum roll angle exceeded 50 degrees even with pilot feedback.

This brief survey of the papers dealing with aircraft vortex interaction is by no means complete. There are other papers published on this topic and the reader is referred to a paper by McCormick [14] for an extensive bibliography on trailing vortex systems and aircraft responses. The papers presented in this section are in the author's opinion the most significant ones dealing with the dynamics of a vortex penetration.

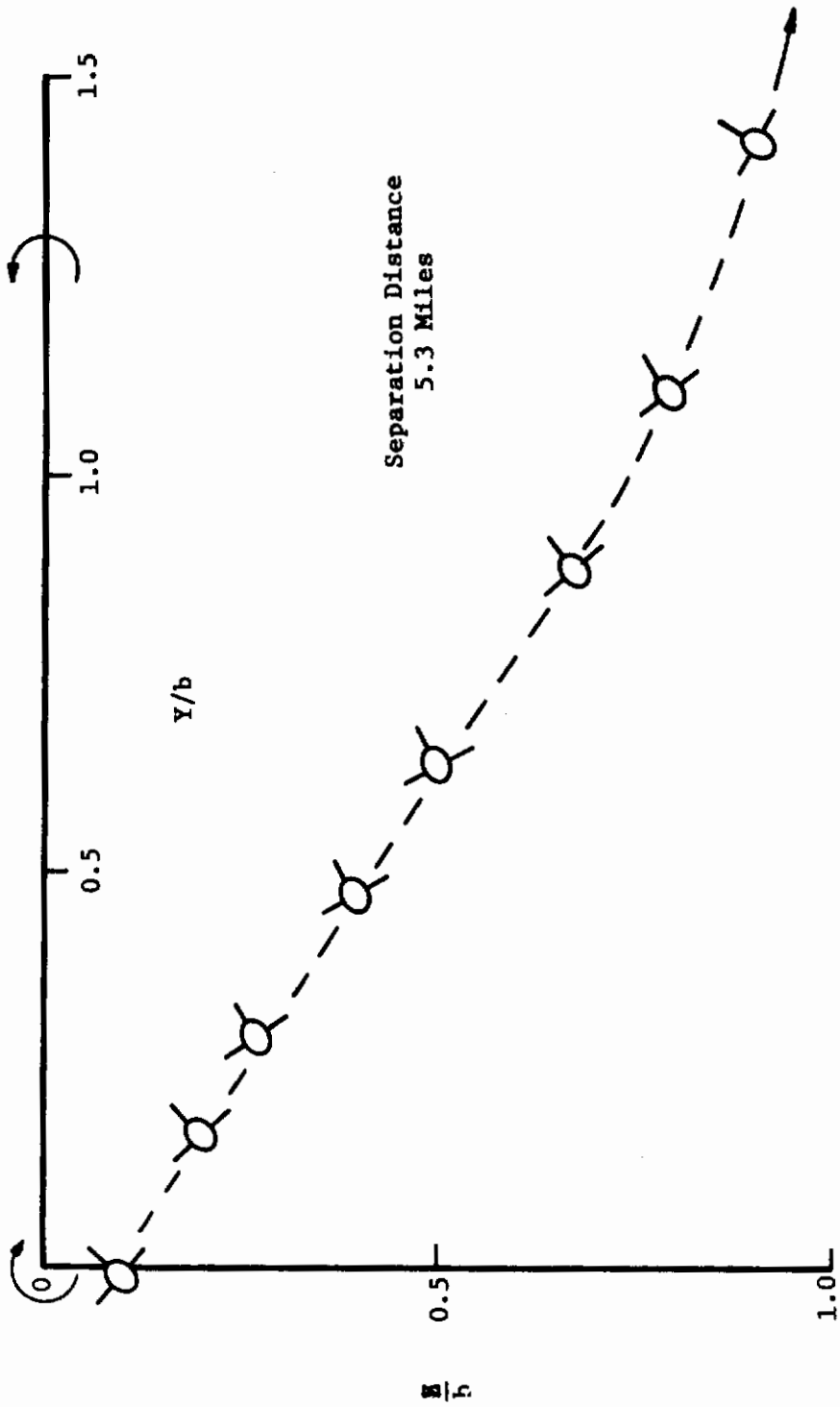

Figure 5. Response of a Light Jet Transport in the Wake of a Jumbo Jet

SECTION III

ANALYTICAL STUDY

To investigate the dynamic behavior of an aircraft penetrating a vortex wake a computer simulation was developed. The program was written in the FORTRAN IV language and consists of nine subroutines and seven function subprograms. In order to accurately model the penetration problem the computer program had to include the following:

i a realistic description of the vortex velocity field

ii a means of determining the induced velocity distribution affecting the penetrating aircraft

iii a means of computing the unsteady aerodynamics associated with the vortex velocity field

iv the complete set of rigid body equations of motion

v and finally a means of introducing pilot control.

Each of the above topics is discussed in detail in the following sections. Included in the discussion are the reasons for the selection of one theory over another as well as the assumptions made in the equations used in the program.

Vortex Decay

The rate of decay of the velocities within the vortex wake at a given distance behind the generating aircraft are difficult to calculate and to a certain extent largely unknown. There are numerous theories which can be used to calculate the velocity

distribution. However, most of these theories prove to be inadequate when compared with experimental data. Several theories for vortex decay will be discussed and some of the theories will be compared with experimental data obtained by the Federal Aviation Administration at their National Aviation Facilities Experimental Center (NAFEC).

The most familiar solution for the diffusion of a line vortex is that obtained by Lamb[15].

$$V_\theta(r,t) = \frac{\Gamma}{2\pi r}\left[1-e^{-\frac{r^2}{4\nu t}}\right]$$

where Γ is the circulation and ν is the kinematic viscosity. Various experimenters such as Rose and Dee[16], Bisgood, Maltby and Dee[17], and Squire[18] have tried to use a modified form of Lamb's solution,

$$V_\theta(r,t) = \frac{\Gamma}{2\pi r}\left[1-e^{-\frac{r^2}{4(\nu+\epsilon)t}}\right]$$

where ϵ is the eddy viscosity. The value of the eddy viscosity is assumed to be proportional to the circulation, i.e.,

$$\epsilon = a\Gamma$$

The constant of proportionality, however, has proved to be very difficult to measure and in fact has been found to lie between 10^{-3} and 10^{-4}. On the other hand Newman[19] and Dosanjh[20] replaced the kinematic viscosity by an eddy viscosity ν_T. Newman found that the ratio of eddy viscosity to the kinematic viscosity ν_T/ν had to be varied from one axial station to another in order to match the data. Dosanjh found good correlation with his data by using an eddy viscosity of $\nu_T = 10\nu$. Recently, Kurylowich[21] applied the same type of analysis to flight test data and arrived at a value for ν_T of $260\nu/\cos^2\lambda_{c/4}$ where $\lambda_{c/4}$

is the sweep angle of the wing quarter chord line. Kurylowich's equations for the eddy viscosity, core radius, and tangential velocity are as follows:

$$\nu_T = \frac{260\nu}{\cos^2\lambda_{c/4}} \left(1+k_2 w_b+k_3 w_b^{\,2}\right)$$

$$a = \sqrt{\frac{1310\,\nu c\left(1+k_2 w_b+k_3 w_b^{\,2}\right)}{V_\infty \cos^2\lambda_{c/4}}}$$

and

$$V_\theta(r,t) = \frac{\Gamma}{2\pi r}\left[1-e^{-\frac{V_\infty r^2}{4\nu_T z}}\right] \qquad r \leq 2a$$

$$V_\theta = \frac{\Gamma}{2\pi r} \qquad r > 2a$$

The additional terms in the preceding expressions are included to take into account the effect of mass flow injection into the vortex core. Inclusion of these terms was based upon results obtained by Poppleton[22]. Poppleton found that the core radius and turbulence levels increased as the mass flow injected into the vortex core was increased. Therefore the constants, k_2 and k_3, which must be determined experimentally are included to take into account the increased eddy viscosity due to mass injection.

McCormick, Tangler, and Sherrieb[23] showed that the trailing vortices could be described by geometric similarity considerations. Their work was based upon analysis of wind tunnel and flight test data. The expressions developed in their analysis are

$$V_{\theta_o}(a) = .53\, C_L\, V$$

$$\Gamma(a) = .16\Gamma_\infty$$

$$\frac{V_\theta(a)}{V_{\theta_o}(a)} = (1 + .0065\ z/\bar{c})^{-1/2}$$

$$\frac{\Gamma}{\Gamma(a)} = 1 + \ln(r/a)$$

$$\frac{V_\theta(r)}{V_\theta(a)} = \frac{1 + \ln\ r/a}{r/a}$$

where

$V_{\theta_o}(a)$ = the maximum tangential velocity immediately behind the wing.

$V_\theta(a)$ = the maximum tangential velocity at a distance z downstream of the aircraft.

$V_\theta(r)$ = the tangential velocity at any radius.

$\Gamma(a)$ = the circulation at the core radius.

Γ_∞ = the total circulation.

Γ = the circulation at any radius.

The expressions for $V_\theta(a)/V_{\theta_o}(a)$ and $\Gamma(a)$ were determined from wind tunnel and flight test data. However, the expression used for the circulation is based upon the analysis of Hoffman and Joubert[24]. Their analysis predicts a logarithmic variation of the circulation with the radius.

In a later paper dealing with an analysis of experimental measurements of the vortex wake behind large jet transports Eisenhuth, McCormick, Nelson and Garodz[25] suggested that $\Gamma(a)/\Gamma_\infty$ depends upon the lift coefficient instead of being a constant. Figure 6 shows a plot of $\Gamma(a)/\Gamma_\infty$ versus C_L which does indeed appear to vary in a linear manner. Eisenhuth, et al, suggest that the following equations should

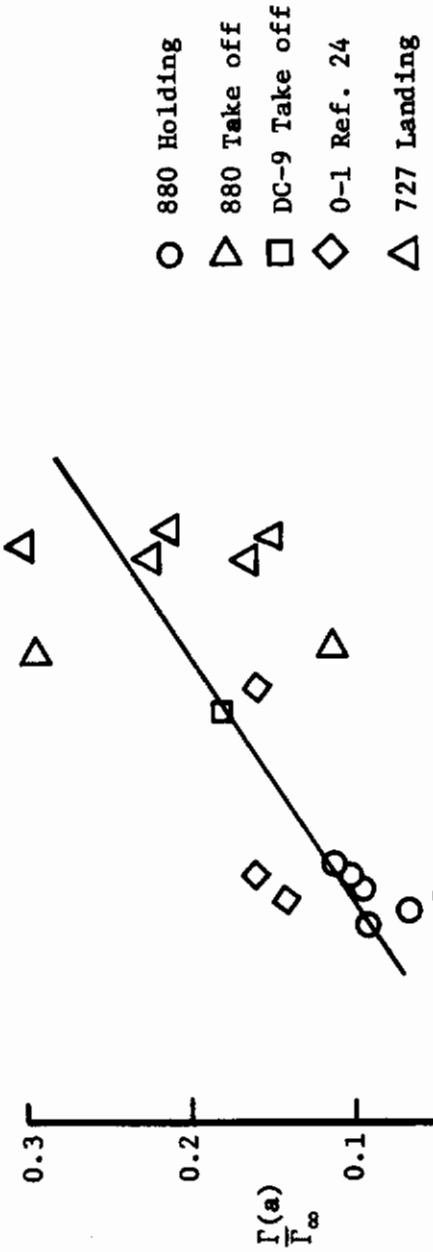

Figure 6. Dimensionless Core Circulation vs. C_L

be used to predict the velocity distribution through the vortex.

$$\frac{\Gamma}{\Gamma(a)} = .17\ C_L$$

$$\frac{a}{c_o C_{\ell_o}} = .02(1 + .00063\ z/\bar{c}\ C_L)^{1/2}$$

$$\Gamma(a) = .085\ C_L{}^2\ c_o\left(\frac{C_{\ell_o}}{C_L}\right) V$$

$$V_\theta(a) = .68\ C_L\ V\ (1 + .00063\ \frac{z}{\bar{c}\ C_L})^{-1/2}$$

$$\frac{V_\theta(r)}{V_\theta(a)} = \frac{1 + \ln r/a}{r/a}$$

In several recent papers Donaldson[26, 27] has proposed using Betz's[28] analysis to describe the roll up process as well as the velocity distribution through the vortex system. Betz used the following facts in his analysis.

1. All the vorticity shed by each half of the wing is found rolled up into the trailing vortex behind the appropriate half of the wing.
2. The "center of gravity" of the vorticity distribution remains at a constant distance from the plane of lateral symmetry.
3. The "moment of inertia" of the vorticity shed by each half of the wing about its "center of gravity" is a constant.

Rewriting these statements in mathematical form yields.

$$\int_o^{b/2} \frac{d\Gamma}{dy}\, dy = \Gamma_o = \int_o^{b/2} \frac{d\Gamma}{dr}\, dr$$

$$\int_o^{b/2} y\, \frac{d\Gamma}{dy}\, dy = \bar{y}\, \Gamma_o = \frac{\pi b}{8}\, \Gamma_o \qquad \text{(for elliptic distribution)}$$

$$\int_o^{b/2} (\bar{y}-y)^2\, \frac{d\Gamma}{dy}\, dy = \int_o^{b/2} r^2\, \frac{d\Gamma}{dr}\, dr = \text{const.}$$

Betz used these expressions to determine a circulation distribution as shown in Figure 7. Donaldson developed an approximation to this distribution which is

$$\frac{\Gamma}{\Gamma_o} = [6(r/b) - 9(r/b)^2]^{1/2} \qquad 0 < r/b \leq 1/3$$

$$\frac{\Gamma}{\Gamma_o} = 1 \qquad r/b > 1/3$$

Stated in terms of the tangential velocity the expressions are

$$V_\theta = \frac{\Gamma}{2\pi r} [6(r/b) - 9(r/b)^2]^{1/2} \qquad 0 \leq r/b \leq 1/3$$

$$V = \frac{\Gamma_o}{2\pi r} \qquad r/b > 1/3$$

In a later paper Donaldson extended the preceding analysis to include aircraft having flaps deflected. Figure 8 taken from reference 27 shows a comparison of his technique with experimental data.

The methods discussed in this section were compared with experimental data obtained by the FAA's Wake Turbulence Program.[29, 30, 31, 32] Data was obtained by flying aircraft of various sizes past an instrumented tower. The tower was equipped with hot wire and hot film

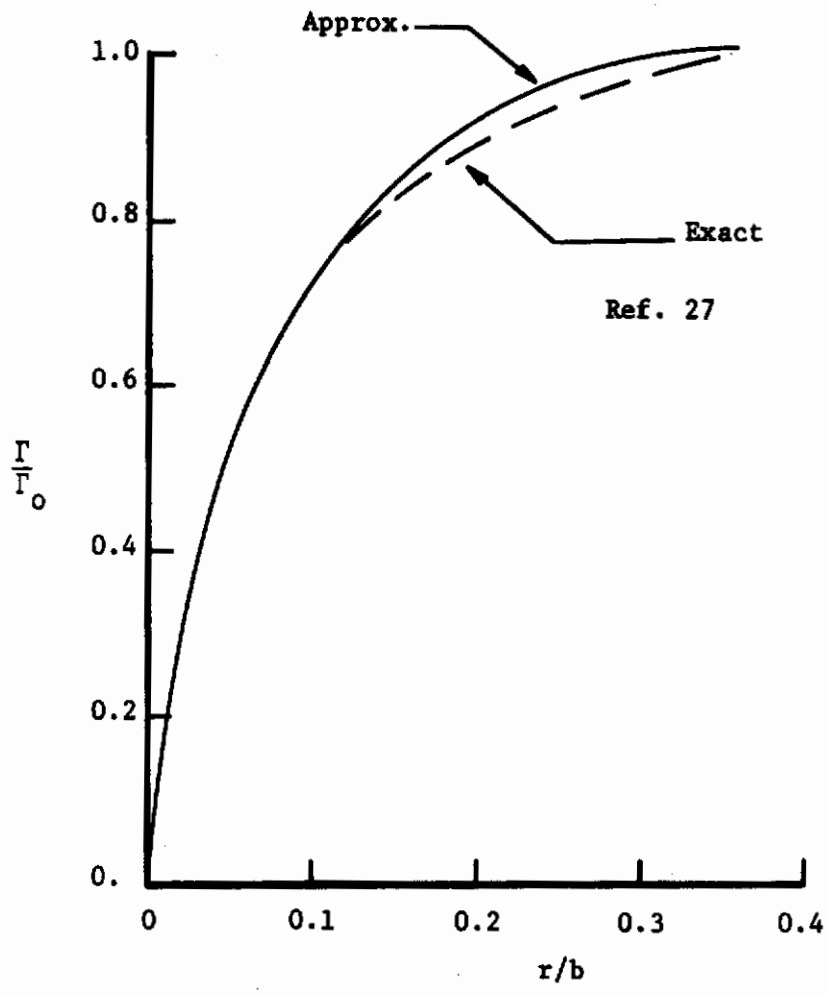

Figure 7. Donaldson's Approximation to Betz's Circulation Distributions

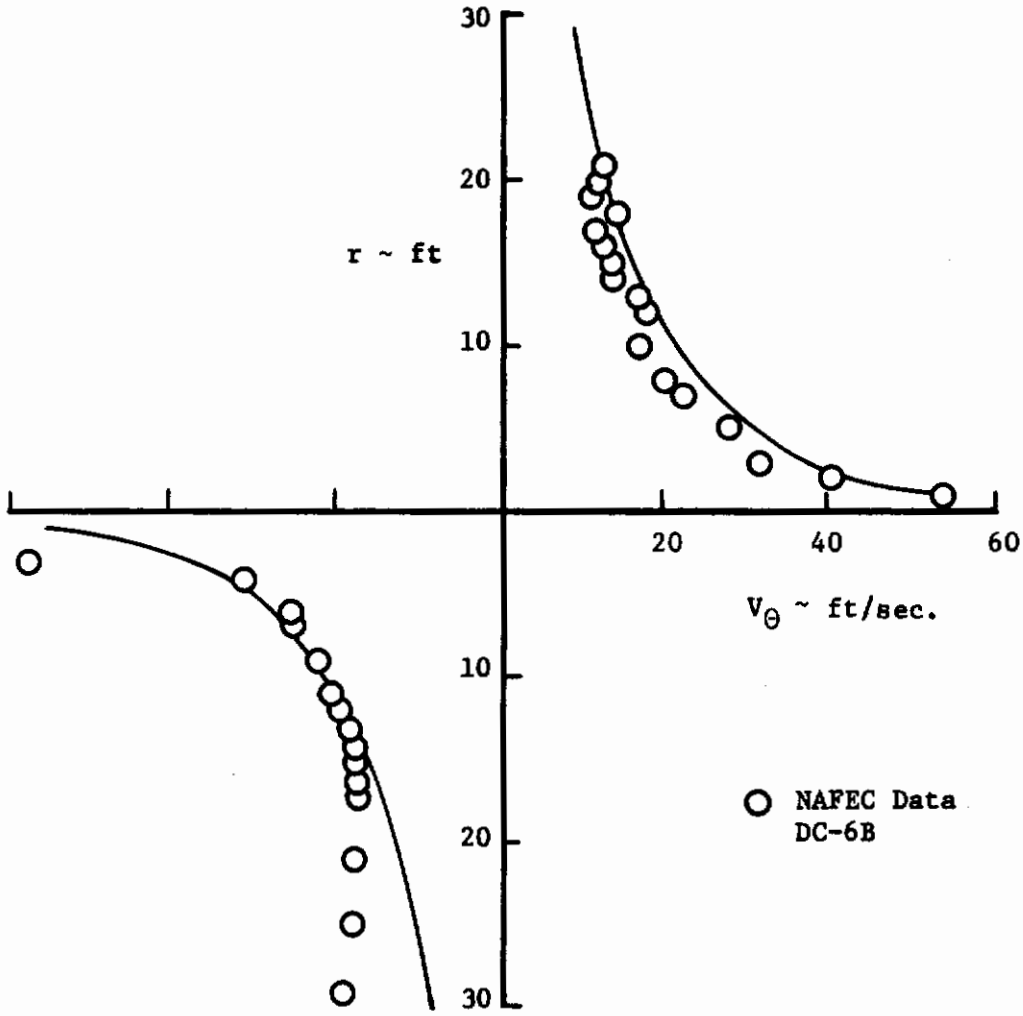

Figure 8. Comparison of Donaldson's Method with Flight Test Data

velocity sensors. Vortices of different ages were obtained by appropriately spacing the aircraft vertically and laterally so that it would take a longer time for the vortices to reach the tower. Figure 10 shows a sketch of the tower fly-by technique. It should be mentioned that the data was accumulated in ground effect. This was due to the relatively low height of the test tower. For more information on the test facilities the reader is referred to a paper presented by Garodz[33] which describes the test procedures in detail.

Figures 10 a-h show the comparison between the vortex theories and the experimental data. The airplanes used to generate these data range from a DC-6B up to a wide body jet transport. The vortex ages range from 7.7 to 31 seconds which correspond to distances of 1770 to 7150 feet behind the generating aircraft. Only the theories which compared favorably with the data were plotted on the figures. Examination of the figures show that Eisenhuth's[25] expressions consistently match the data with the exception of the 747 runs. It should be recalled that the expressions proposed by Eisenhuth, et al[25] were based on McCormick's[23] analysis. The disagreement between the predicted and measured data for the 747 is not easily explained. It has been suggested in the literature that the exhaust from the 747's outboard engines is entrained in the vortex and alters its structure. This seems plausible when one examines the data obtained by Marchman and Mason[34] or Poppleton[22]. These investigators studied the effect of air injection into the vortex core. Figures 11 and 12 taken from reference 34 show the effect of axial blowing (injection) on the velocity distribution, vortex core, and circulation. The data show that blowing

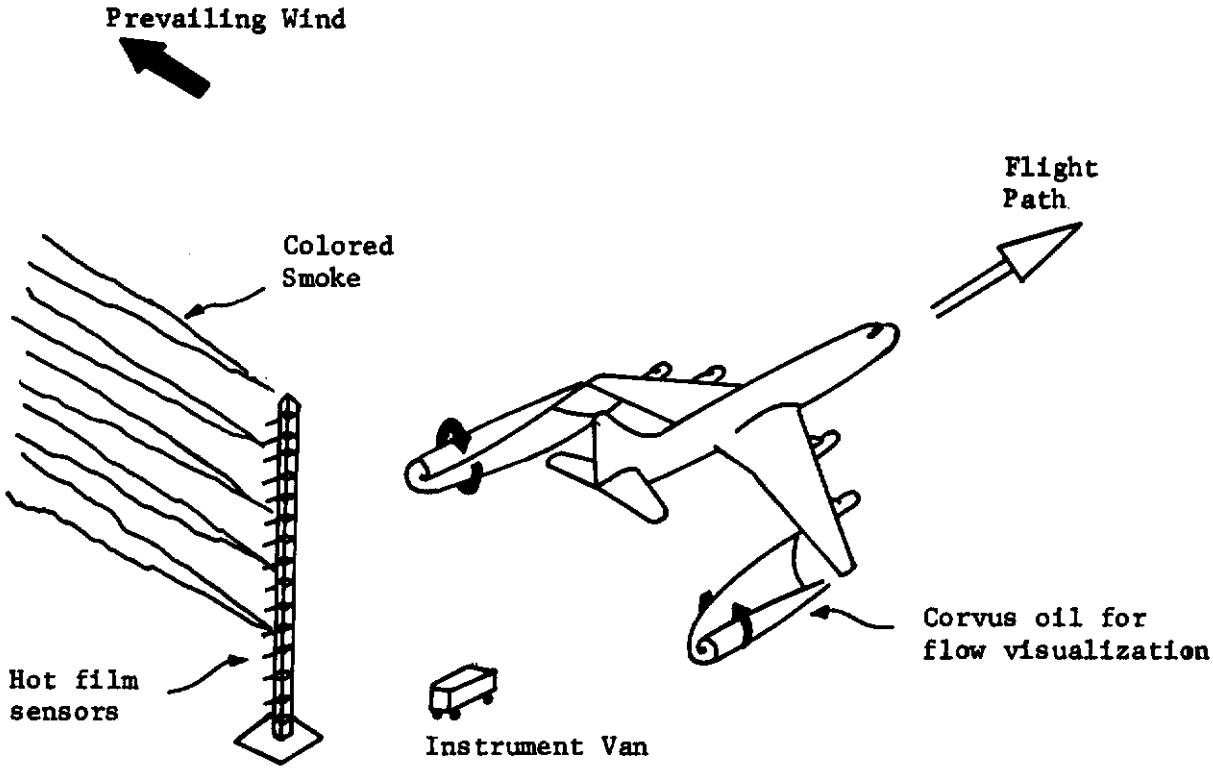

Figure 9. Schematic of Tower Fly-by Technique

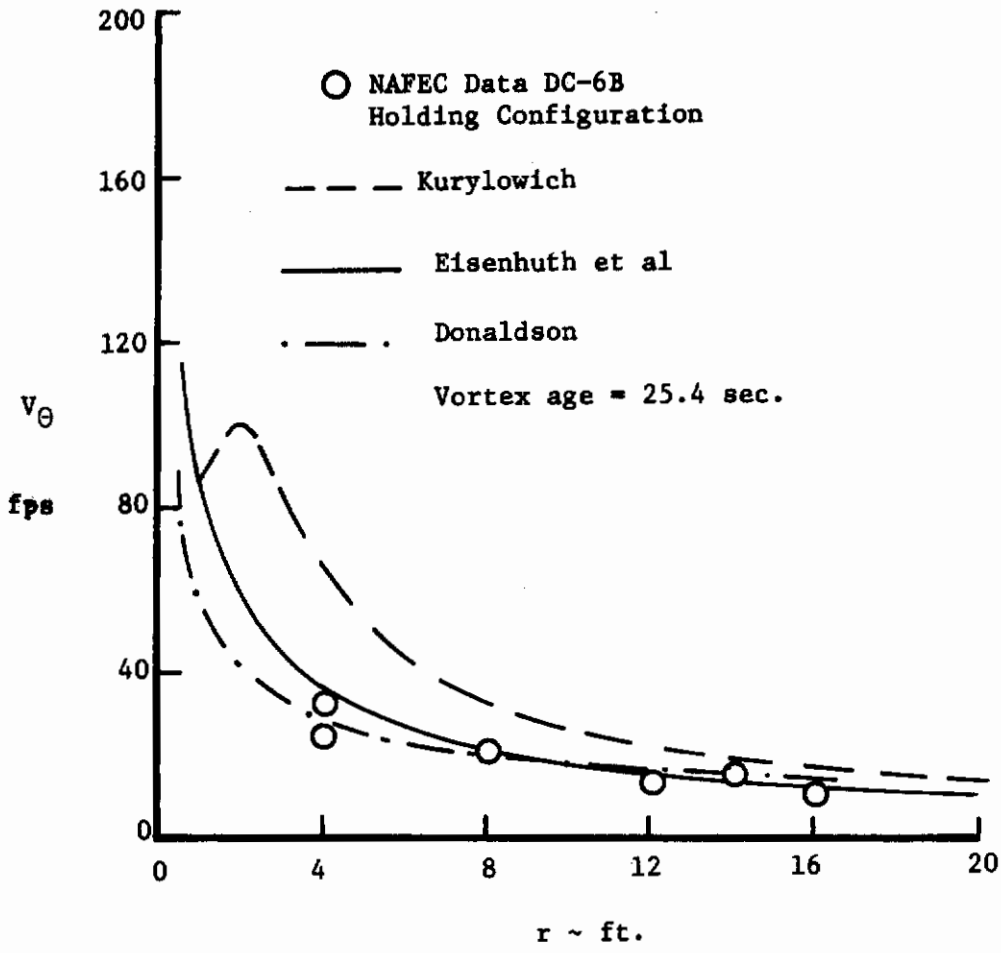

Figure 10a. Continued

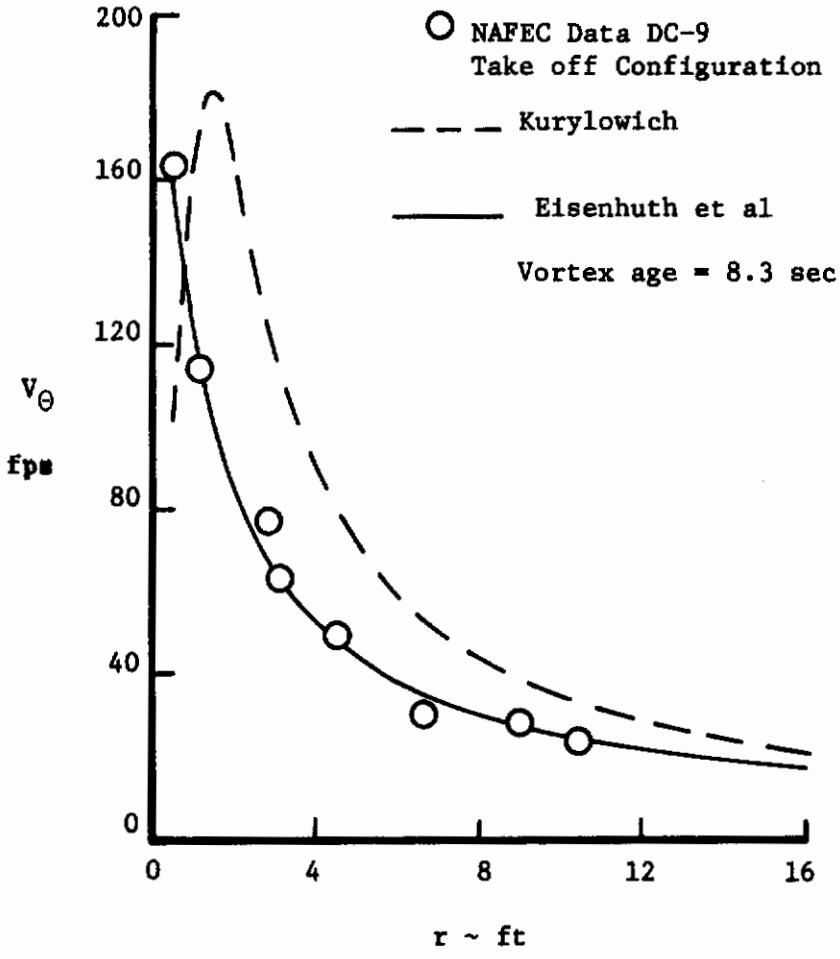

Figure 10b. Continued

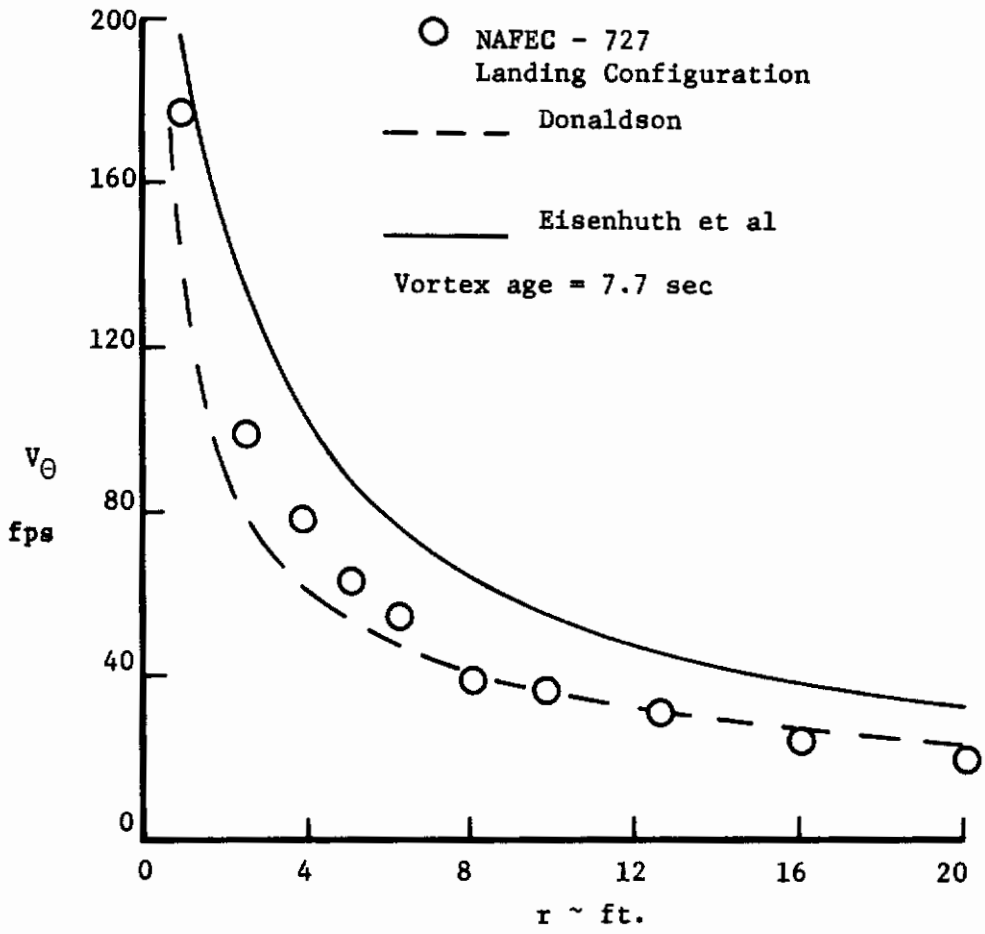

Figure 10c. Continued

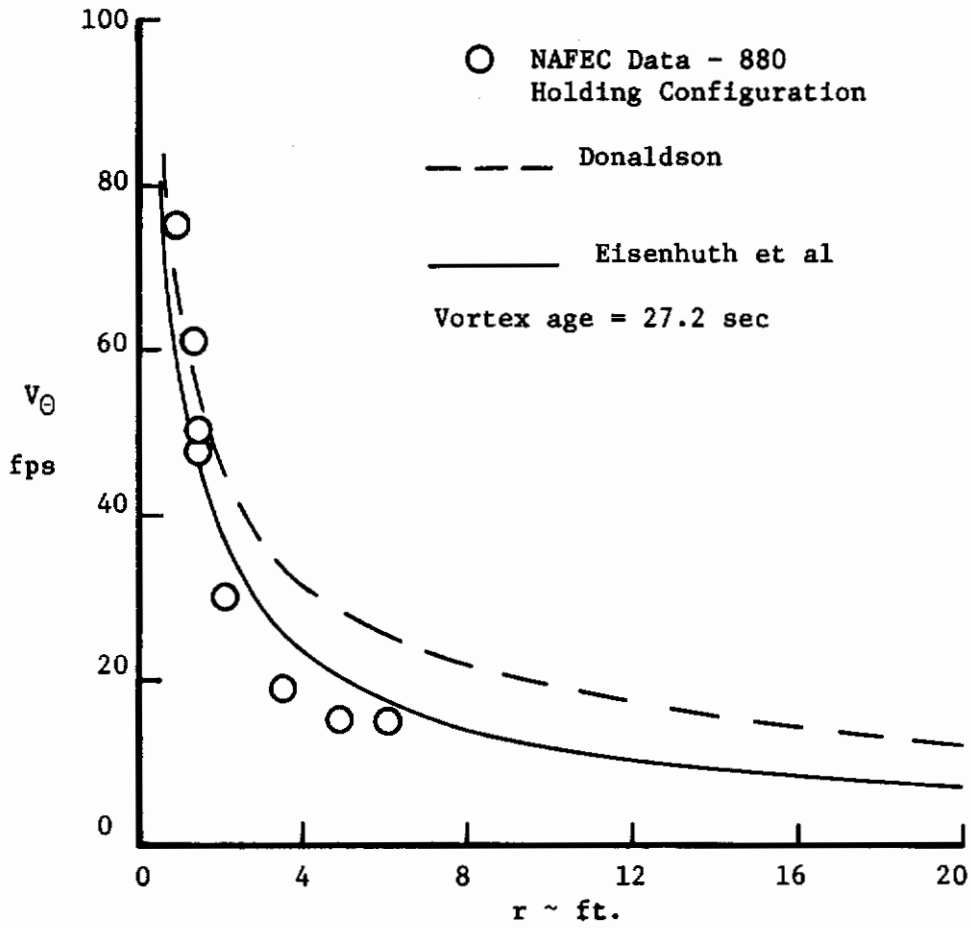

Figure 10d. Continued

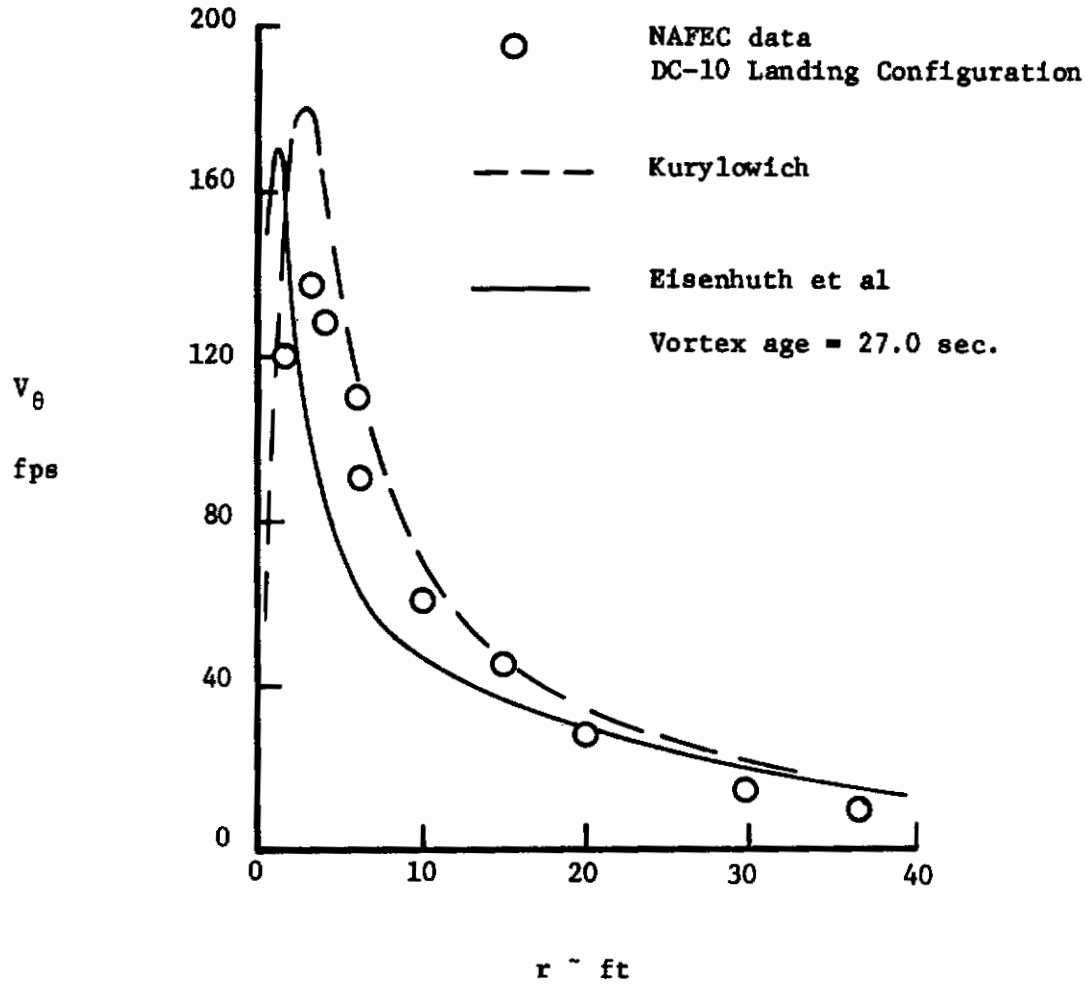

Figure 10e. Continued

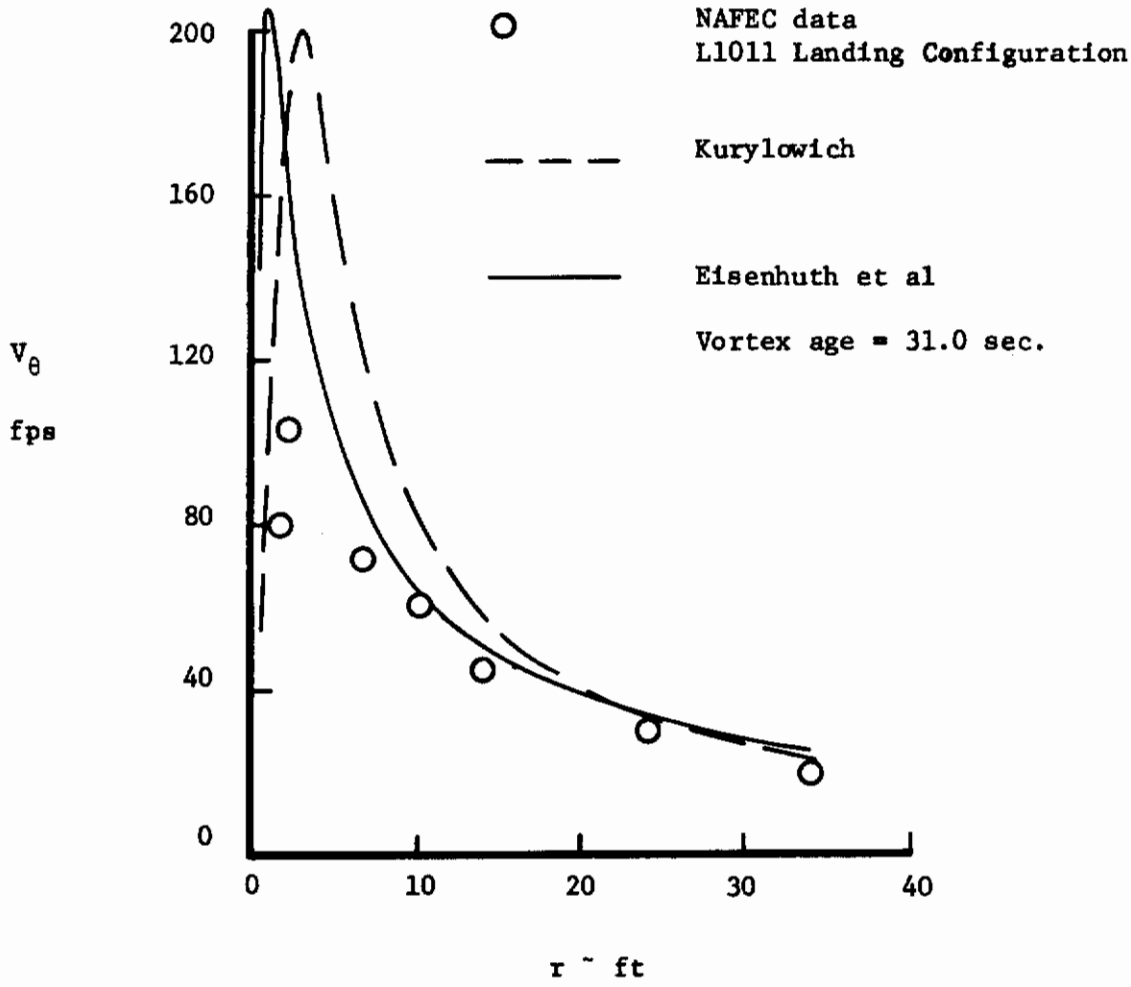

Figure 10f. Continued.

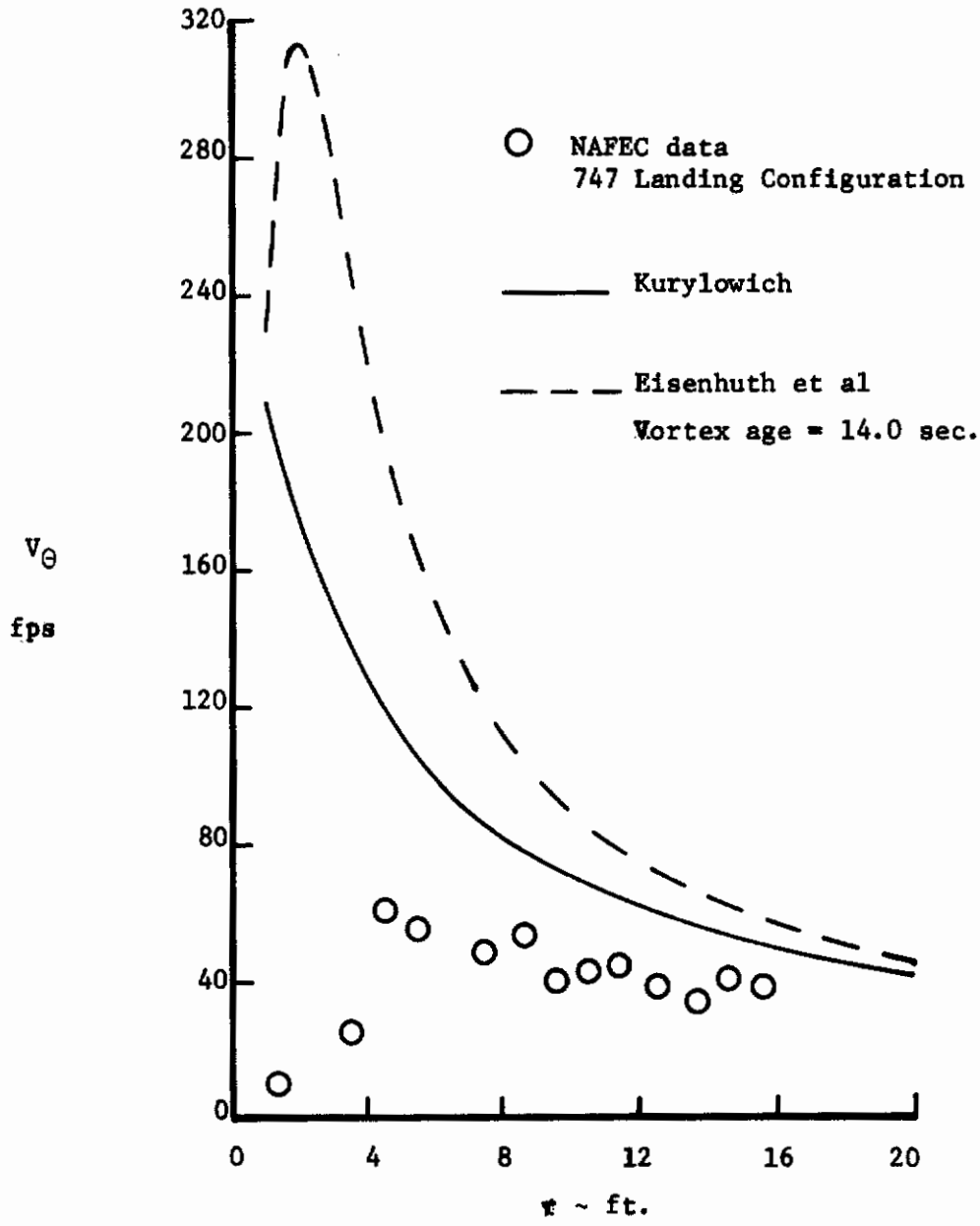

Figure 10g. Continued

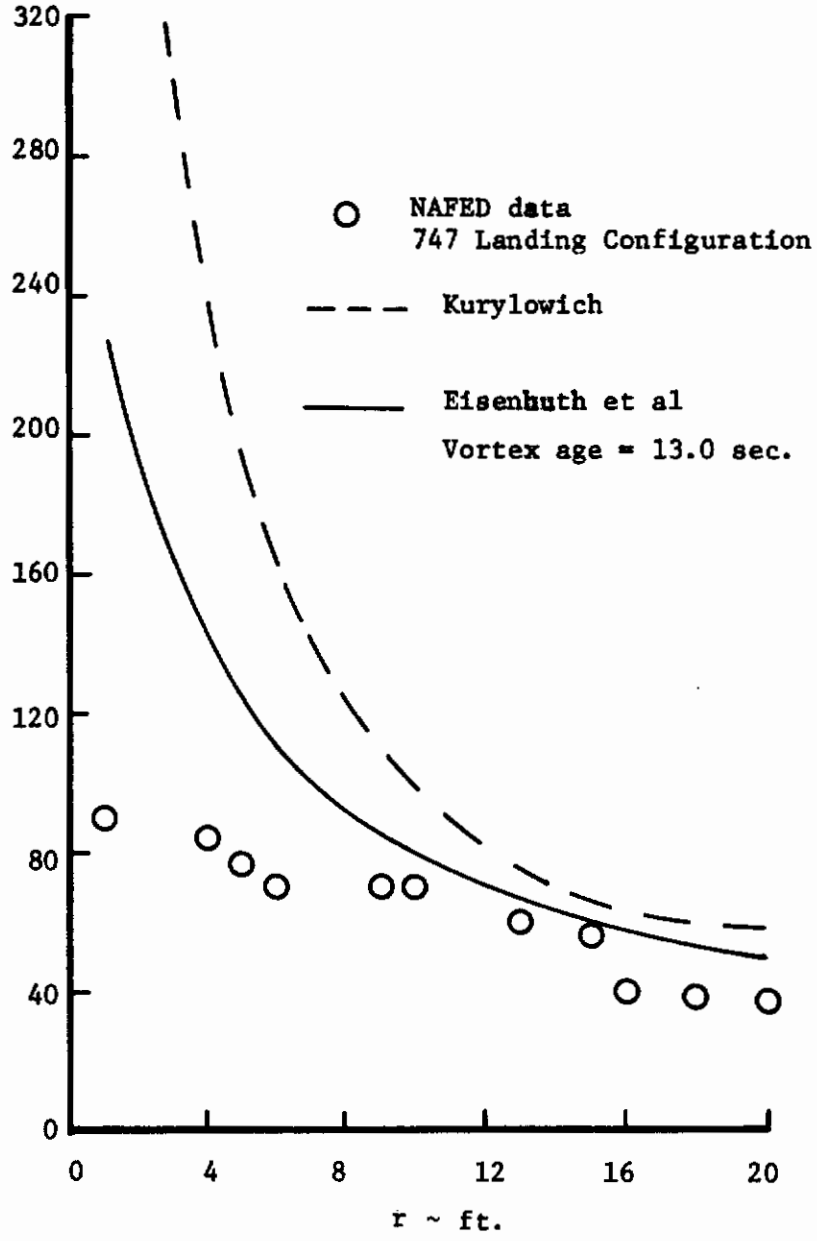

Figure 10h. Continued

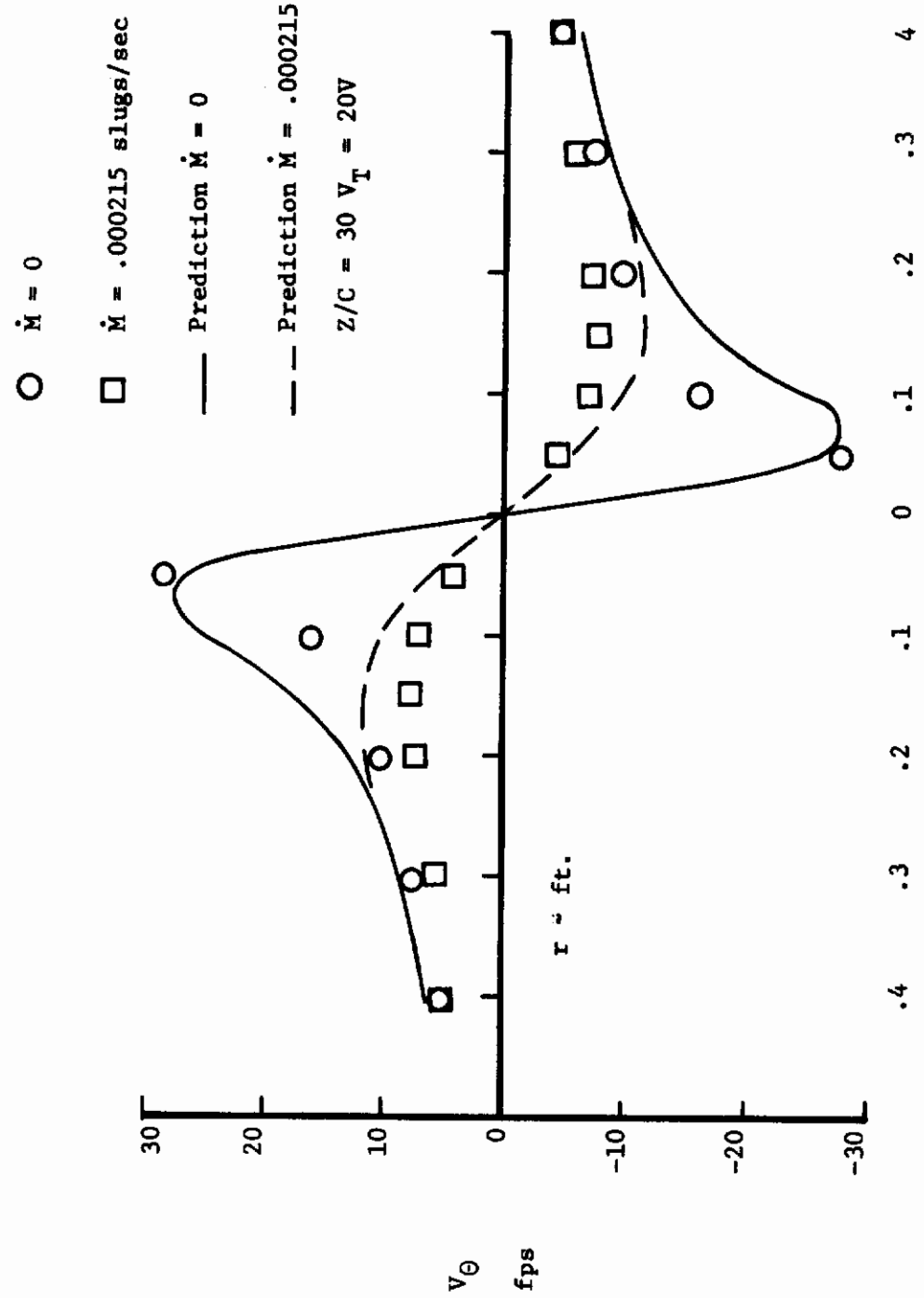

Figure 11. Effect of Blowing on the Velocity Distribution Through the Vortex

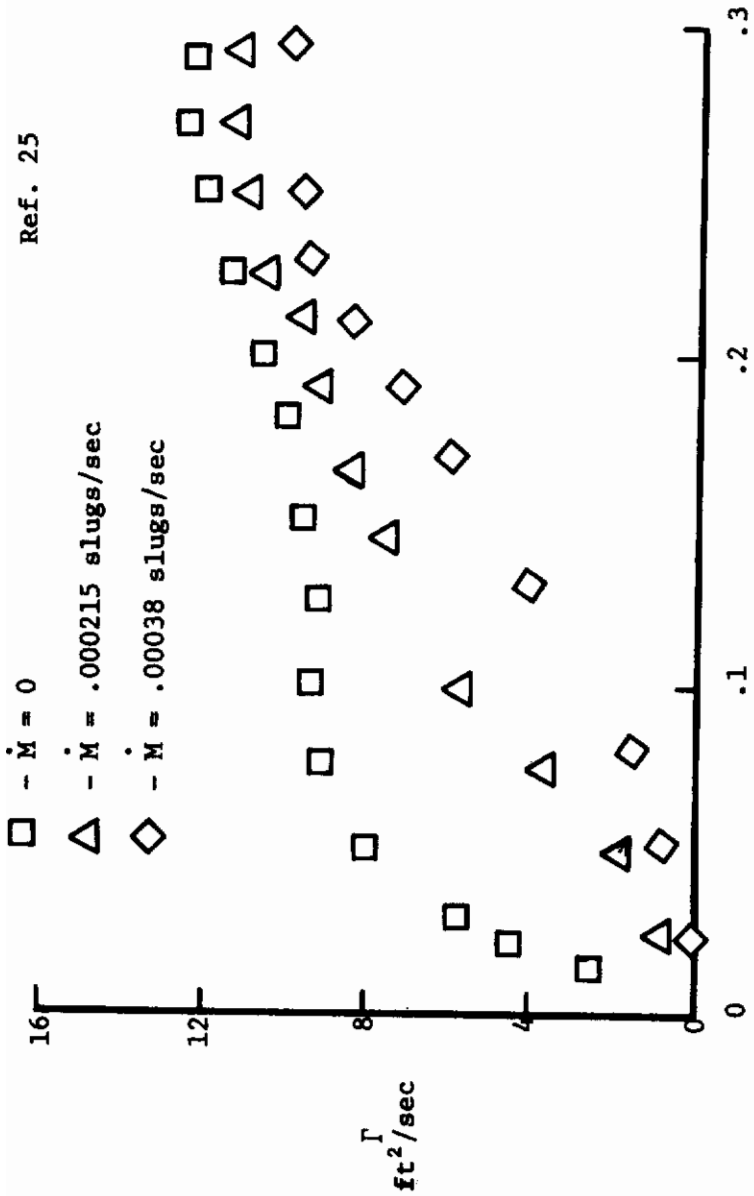

Figure 12. Effect of Blowing on the Circulation Distribution

into the vortex core reduces the maximum tangential velocity and increases the core radius. The circulation distribution is altered in the vicinity of the vortex core, however; at radial distances greater than the vortex radius, the circulations approach the theoretical bound vortex strength. Also included in Figure 11 is a prediction based on Kurylowich's method. It should be noted that the eddy viscosity had to be adjusted to a value of 20ν. These figures were included to help explain the difference between the data of the 747 and the other aircraft. In a later section the effect of modifying the vortex velocity field on the dynamic response of a following aircraft will be discussed.

Based on the comparisons presented and others not included in this report it was concluded that Eisenhuth's expressions could be used to accurately model the velocity distribution through the vortex system.

Vortex Induced Velocities

The wing is divided into N strips as shown in Figure 13. The velocity induced by the trailing vortex system is resolved into components $[U_g(t), V_g(t), W_g(t)]$ at control points located at the 3/4 chord point of each strip on the wing and tail surfaces.

The procedure for resolving the induced velocity into its components $[U_g(t), V_g(t), W_g(t)]$ is as follows:

1. The inertial axes system is aligned so that the X axis is parallel to the axis of the vortex filaments. (See Figure 14)

2. Using the transformation shown below the control points can be resolved into the inertial frame.

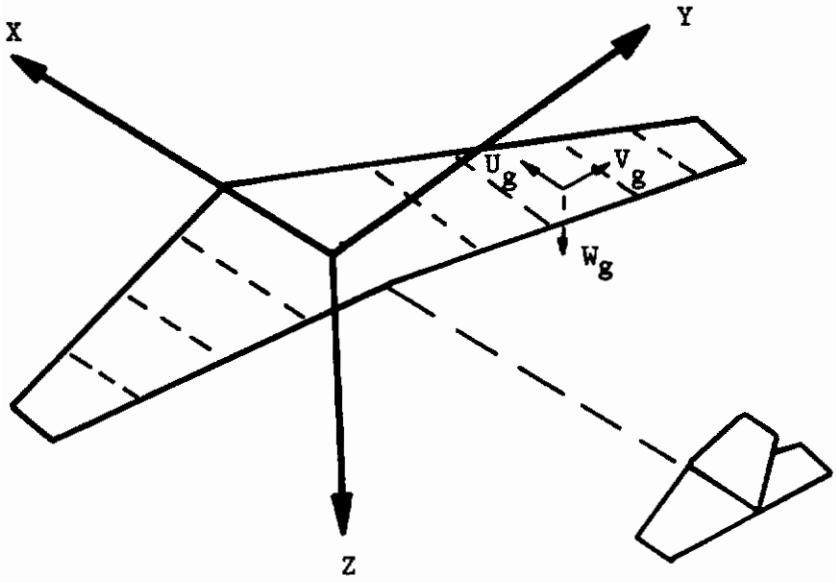

Figure 13. Wing Divided into N Panels

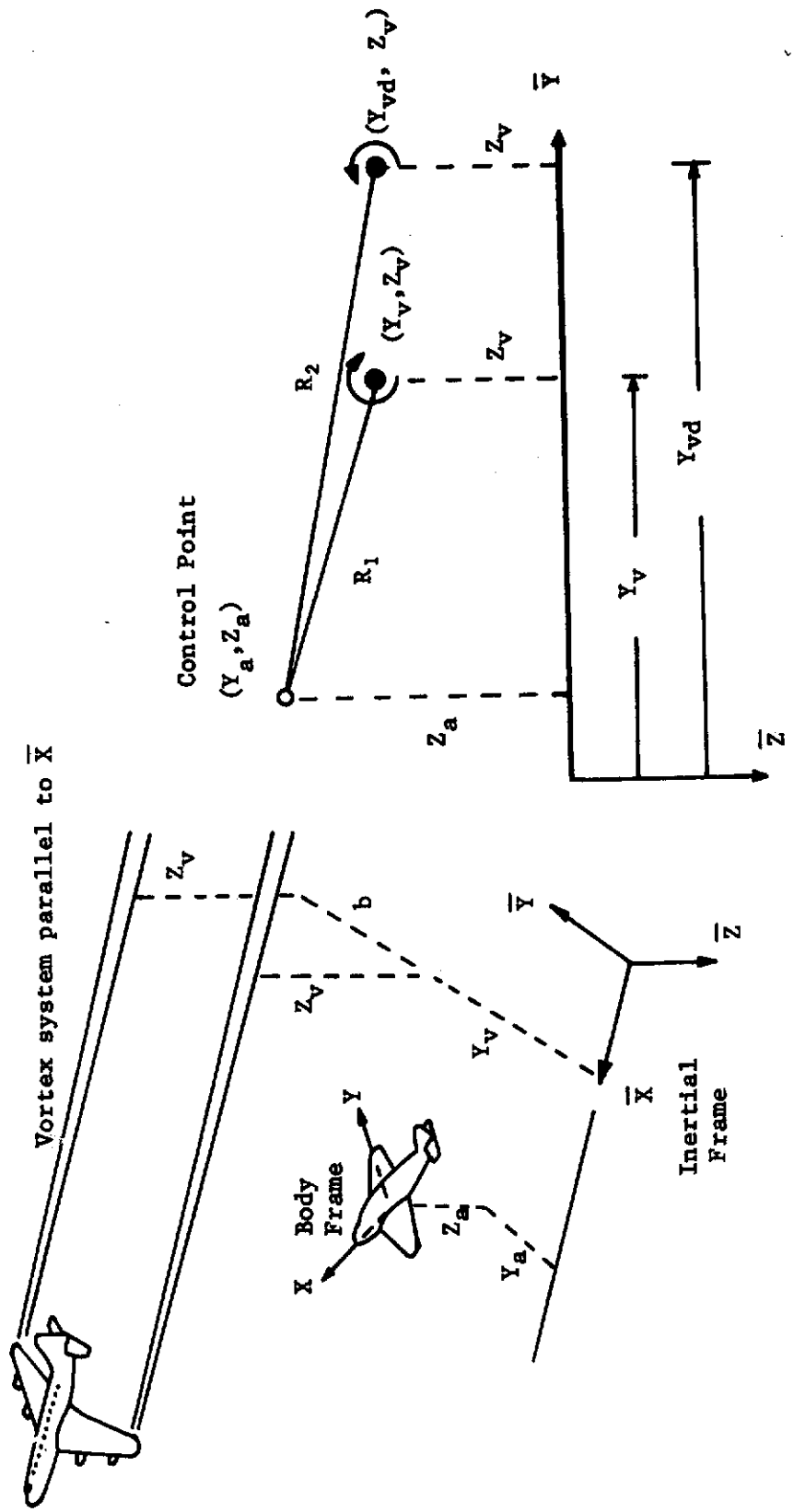

Figure 14. Distance from Control Points to Vortex System.

$$\begin{bmatrix} \bar{X}_{cp_j} \\ \bar{Y}_{cp_j} \\ \bar{Z}_{cp_j} \end{bmatrix} = \begin{bmatrix} C_\theta C_\psi & S_\phi S_\theta C_\psi - S_\psi C_\phi & C_\psi C_\phi S_\theta + S_\psi S_\phi \\ C_\theta S_\psi & S_\psi S_\theta S_\phi + C_\psi C_\phi & S_\psi C_\phi S_\theta - C_\psi S_\phi \\ -S_\theta & S_\phi C_\theta & C_\phi C_\theta \end{bmatrix} \begin{bmatrix} X_{cp_j} \\ X_{cp_j} \\ Z_{cp_j} \end{bmatrix}$$

3. The perpendicular distance of each control point from the vortex filaments is equal to the following expressions.

$$Y_j = Y_{cg} + \bar{Y}_{cp_j}$$

$$Z_j = Z_{cg} + \bar{Z}_{cp_j}$$

$$R_{1_j} = \{(Y_i - Y_v)^2 + (Z_i - Z_v)^2\}^{1/2}$$

$$R_{2_j} = \{(Y_i - Y_{v_d})^2 + (Z_i - Z_v)^2\}^{1/2}$$

4. The velocity components in the inertial frame are

$$\bar{W}_{g_j} = V_{\theta 1_j} \left(\frac{Y_j - Y_v}{R_{1_j}}\right) - V_{\theta 2_j} \left(\frac{Y_j - Y_{v_d}}{R_{2_j}}\right)$$

$$\bar{V}_{g_j} = -V_{\theta 1_j} \left(\frac{Z_j - Z_v}{R_{1_j}}\right) + V_{\theta 2_j} \left(\frac{Z_j - Z_v}{R_{2_j}}\right)$$

if the control point lies outside the core, and

$$\bar{W}_{g_j} = V_{\theta 1_j} \left(\frac{Y_j - Y_v}{a}\right)$$

port vortex core

$$\bar{V}_{g_j} = -V_{\theta 1_j} \left(\frac{Z_j - Z_v}{a}\right)$$

or

$$\bar{W}_{g_j} = -V_{\theta 2_j} \left(\frac{Y_j - Y_{v_d}}{a}\right)$$

starboard vortex core

$$\bar{V}_{g_j} = V_{\theta 2_j} \left(\frac{Z_j - Z_v}{a}\right)$$

if the control point lies within the vortex core.

5. The velocity components referred to the body axes system are obtained by using the following transformation.

$$\begin{bmatrix} U_{g_j} \\ V_{g_j} \\ W_{g_j} \end{bmatrix} = \begin{bmatrix} C_\theta C_\psi & C_\theta S_\psi & -S_\theta \\ S_\phi S_\theta C_\psi - S_\psi C_\phi & S_\psi S_\theta S_\phi + C_\psi C_\phi & S_\phi C_\theta \\ C_\psi C_\phi S_\theta + S_\psi S_\phi & S_\psi C_\phi S_\theta - C_\psi S_\phi & C_\phi C_\theta \end{bmatrix} \begin{bmatrix} \bar{U}_{g_j} \\ \bar{V}_{g_j} \\ \bar{W}_{g_j} \end{bmatrix}$$

However, $\bar{U}_{g_j}$ is assumed to be zero, i.e., zero axial velocity in the vortex field. This allows the expressions to be reduced to the following form.

$$\begin{bmatrix} U_{g_j} \\ V_{g_j} \\ W_{g_j} \end{bmatrix} = \begin{bmatrix} C_\theta S_\psi & -S_\theta \\ S_\psi S_\theta S_\phi + C_\psi C_\phi & S_\phi C_\theta \\ S_\psi C_\phi S_\theta - C_\psi S_\phi & C_\phi C_\theta \end{bmatrix} \begin{bmatrix} \bar{V}_{g_j} \\ \bar{W}_{g_j} \end{bmatrix}$$

Aerodynamics

The problem of determining the aerodynamic forces acting on an aircraft in a time-varying velocity field is indeed quite formidable. However, in order to accurately predict the response of an aircraft penetrating a vortex system, some means of incorporating the unsteady aerodynamics into the equations of motion of the aircraft is necessary.

There have of course been numerous lifting surface theories developed over the years. In the early sixties two techniques dominate the literature; they are the vortex and doublet lattice methods. The use of discrete vortices for the solution of the steady lifting surface problem was first used by Falkner[35]. Falkner, however, had to make assumptions on the load distributions in order to keep the number of unknowns to a minimum. In the sixties, Hedman[36], Giesing[37], Rubbert[38], Woodward[39], Albano and Rodden[40] and others developed lifting surface theories which did not make any prior assumptions on the load distribution. This was possible due to the feasibility of using modern digital computers to invert the matrices associated with the finite element methods.

The method discussed in this section is an unsteady vortex lattice technique. This technique is an extension of Rudhman's[41] work to the finite wing.

Now consider the integral equation of the linearized lifting surface theory as formulated by Reissner[42] and others,

$$W(x,y,z,t) = \frac{1}{4\pi}\iint_{R_a} \frac{\gamma_a(\xi,\eta,t)[x-\xi]+\delta_a(\xi,\eta,t)[y-\eta]}{[(x-\xi)^2+(y-\eta)^2+z^2]^{3/2}}\, d\xi d\eta$$

$$- \frac{1}{4\pi}\iint_{R_W} \frac{\gamma_w(\xi,\eta,t)[x-\xi]+\delta_w(\xi,\eta,t)[y-\eta]}{[(x-\xi)^2+(y-\eta)^2+z^2]^{3/2}}\, d\xi d\eta$$

where R_a = wing region

R_W = wake region

γ & δ = the circulation per unit chord and per unit span, respectively.

See Figure 15 for clarification of the above symbols. The integral equation relates the downwash distribution to the unknown running circulations. The boundary condition which must be satisfied is as follows:

$$W(x,y,o,t) = \frac{\partial Z_a}{\partial t}(x,y,o,t) + U\frac{\partial Z_a(x,y,o,t)}{\partial x}$$

This is a mathematical statement of the flow tangency condition.

If a discrete vortex method is used the above integral equation is replaced by a system of simultaneous algebraic equations.

$$W_i = A_{ij}\,\Gamma_j$$

or in matrix notation

$$\{W\} = [A]\{\Gamma\}$$

where

$\{W\} = \{W_B\} + \{W_w\}$

$\{W_B\}$ = normalwash which is known from the boundary condition.

$\{W_w\}$ = upwash (downwash) due to vortices shed into the wake.

$[A]$ = matrix of aerodynamic influence coefficients relating the upwash (downwash) at a point i due to a singularity at point j.

$\{\Gamma\}$ = horseshoe vortex strength.

In the above formulation both $\{W_B\}$ and $\{W_w\}$ are known. $\{W_B\}$ is determined from the boundary condition. $\{W_w\}$ is determined from the following equation

$$\{W_w\} = \sum_{k=1}^{n} [B]_k \{\Gamma\}_k$$

where

$[B]_k$ = matrix of influence coefficients relating the upwash (downwash) at a point i (on the wing) due to a

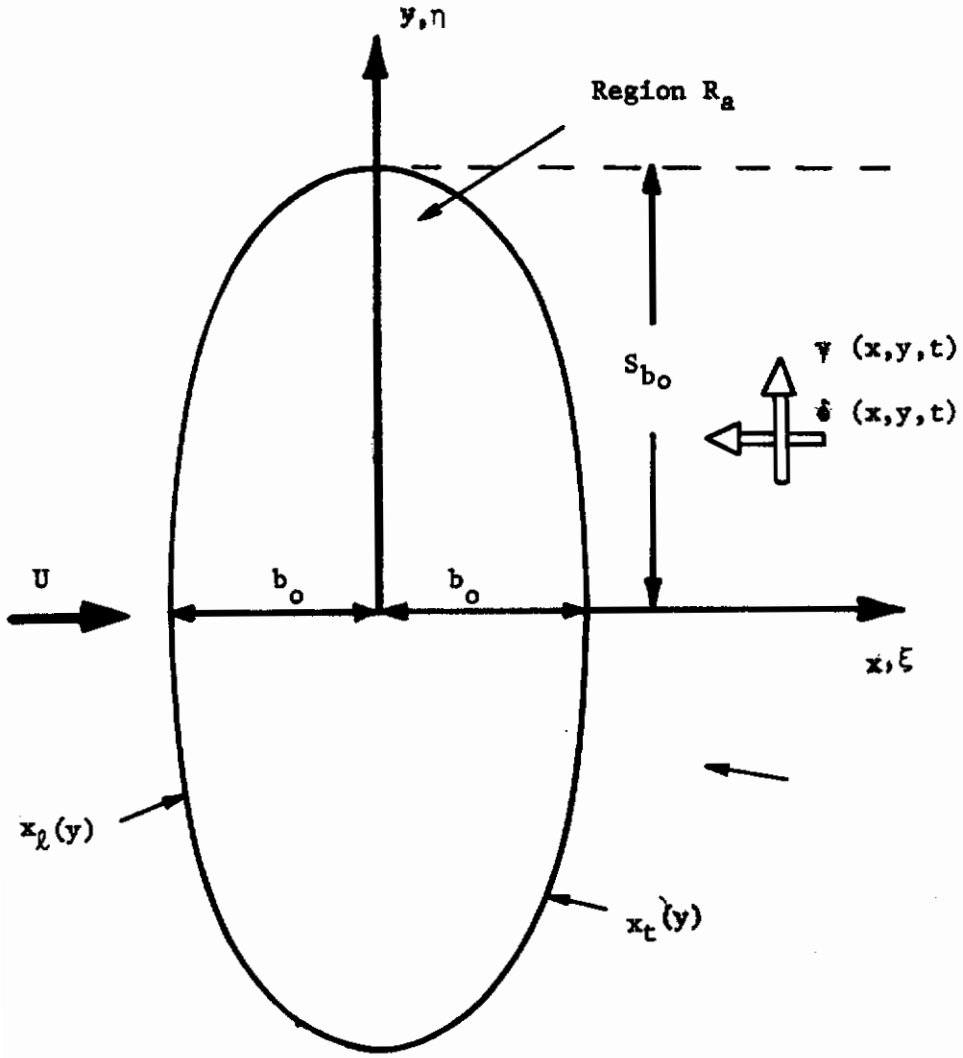

$\gamma(x,y,t)$ and $\delta(x,y,t)$ are the circulations per unit length in the x and y directions

Figure 15. Vortex Model of the Finite Wing

singularity at point j (in the wake).

$\{\Gamma\}_k$ = strength of vortices shed into the wake.

n = number of time steps or $\{\Gamma\}$'s shed into the wake.

It should be noted that $\{\Gamma\}_k$ is known. This is so because the circulation shed into the wake is related to the change in wing circulation. That is the wake circulation shed during a time interval Δt is equal and opposite to the change in wing circulation during the same time interval.

The approach used in solving the unsteady lifting surface problem is to represent the wing by a network of closed horseshoe vortices which are distributed in both the chordwise and spanwise directions. The wake is constructed as shown by the simple sketch in Figure 16. The strength of the individual vortices are determined by applying the wing boundary condition at as many control points on the wing as there are vortices. The resulting system of simultaneous equations is then solved to determine the strength of the vortex filaments.

The spacing and location of vortex filaments is shown in Figure 17. Notice that the bound vortices are located at the 1/4 chord of each chordwise panel. The control point is located at the 3/4 chord point of the panels. This choice of control point location has been shown by James[43] and De Young[44] to be the optimum for the two dimensional cases. Although nothing has been said about imposing the Kutta condition in this method, it has been found by numerical experimentation that the Kutta condition will be satisfied when the control point is located at the 3/4 chord location. The location of the trailing filament was obtained by using the following transformation.

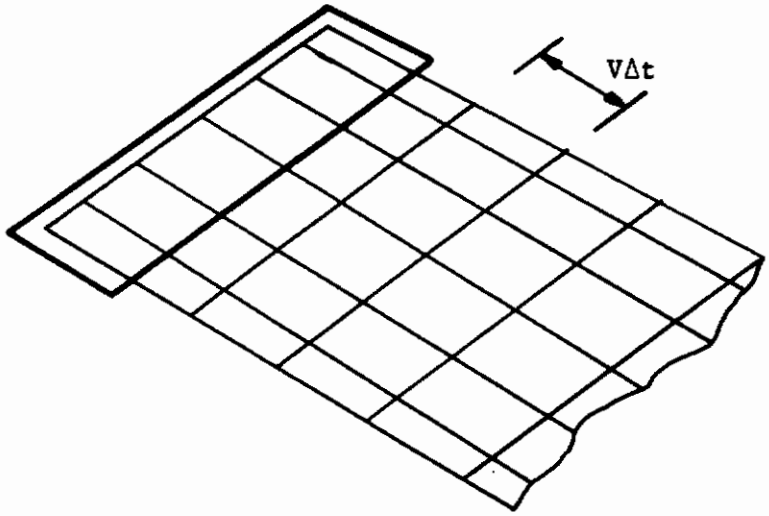

Figure 16. Vortex Wake

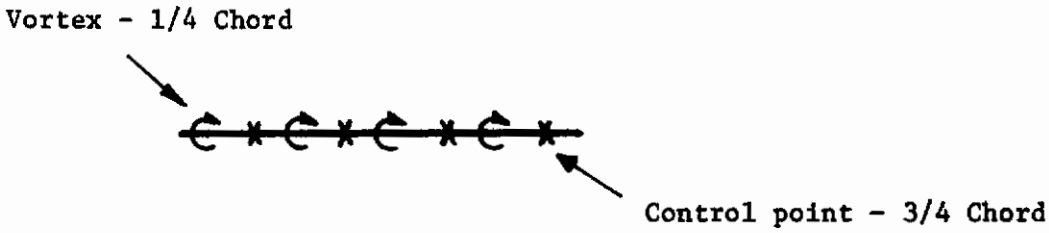

Figure 17. Chordwise Vortex Spacing

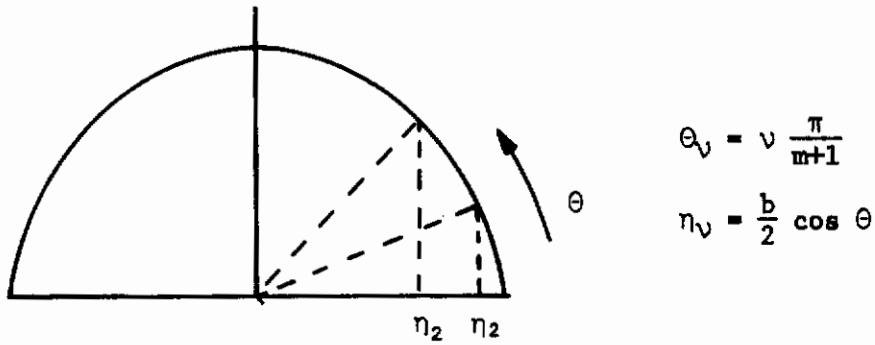

Figure 18. Vortex Spacing Spanwise

$$\theta_v = v \frac{\pi}{m+1}$$

Multhopp's transformation

$$\bar{\eta}_v = \cos \theta_v$$

where

m = number of stations (spanwise)

v = identifying subscript of a particular station

$\bar{\eta}_v$ = nondimensional distance $\bar{\eta} = y/b/2$

For further clarification see Figure 18. The influence coefficient matrices are determined by using the integrated form of the Biot-Savart law for a straight line segment. Applying this equation to each side of the closed horseshoe filament one can determine the induced velocity at any control point due to the vortex box.

The algorithm used to solve for the unknown circulations is listed below.

Step 1. Filaments are placed on the wing as previously described.

Step 2. Influence coefficients [A] are determined.

Step 3. {W} is computed. For example the normalwash and wake induced normal velocity.

Step 4. Unknown circulations are determined

$\{\Gamma\} = [A]^{-1}\{W\}$

Step 5. Shed vortices are moved downstream by the distance $V\Delta t$.

Step 6. Repeat steps 3 through 5.

The above numerical procedure yields the circulation on the wing at discrete points in time. The lift on the wing panels is determined

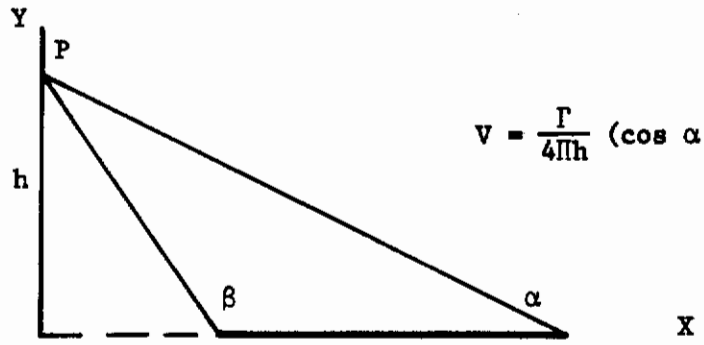

$$V = \frac{\Gamma}{4\pi h} (\cos \alpha + \cos \beta)$$

Figure 19. Biot - Savart Law for a Straight Line Vortex

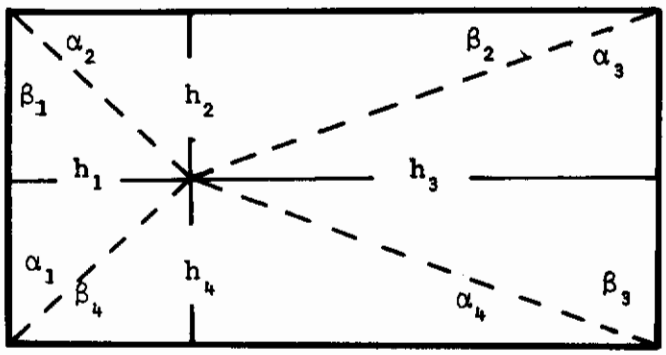

$$A_{ij} = \frac{1}{4\pi} \sum_{k=1}^{4} \frac{1}{h_k} (\cos \alpha_k + \cos \beta_k)$$

Figure 20. Velocity Induced by the Vortex Box

by integrating the pressure difference.

$$\Delta P = \rho V \gamma(x) + \rho \frac{\partial}{\partial t} \int_0^x \gamma(x)\, dx$$

This equation is obtained from the unsteady Bernoulli equation. Expressing Euler's equation in vector form

$$\frac{\partial \bar{q}}{\partial t} + \frac{1}{2} \nabla q^2 = - \frac{1}{\rho} \nabla P$$

and the velocity in terms of the velocity potential

$$\bar{q} = \text{grad } \phi$$

then the following equation can be obtained.

$$\nabla \left[\frac{\partial \phi}{\partial t} + \frac{q^2}{2} + \frac{P}{\rho} \right] = 0$$

Integrating this expression yields

$$\frac{\partial \phi}{\partial t} + \frac{q^2}{2} + \frac{P}{\rho} = \text{const.}$$

The above is known as Kelvin's equation or the unsteady Bernoulli equation. Note that this equation only applies along a streamline. If this equation is applied to the thin airfoil shown in Figure 21, one can determine an expression for the unsteady lift. Consider a small segment of the above airfoil section shown in Figure 22. The circulation around this segment is

$$\gamma dx = 2\Delta V\, dx$$

or

$$\Delta V = \gamma(x)/2$$

The definition of the potential between two points A and B is given by

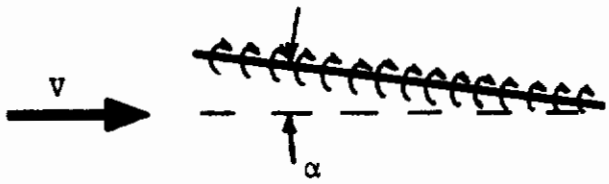

Figure 21. Thin Airfoil

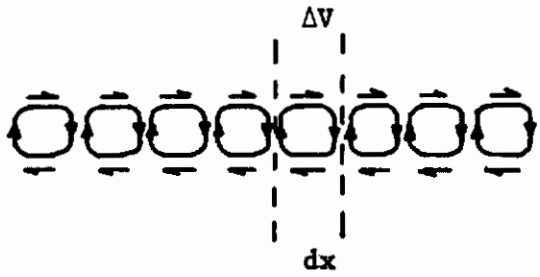

$$\gamma\, dx = 2\Delta V dx$$

or

$$\Delta V = \frac{\gamma(x)}{2}$$

Figure 22. Segment of Vortex Sheet

$$\phi(B) - \phi(A) = \int_A^B V_s \, ds$$

Since the potential at the leading edge of the airfoil can be arbitrarily set equal to zero ($\phi(L.E.) = 0$) the above expression reduces to

$$\phi(x) = \int_o^x V_s \, ds$$

or

$$\phi_u(x) = \int_o^x (V + \frac{\gamma(x)}{2}) \, dx$$

$$\phi_\ell(x) = \int_o^x (V - \frac{\gamma(x)}{2}) \, dx$$

where u and ℓ indicate the upper and lower surfaces respectively. Substituting back into the unsteady Bernoulli equation yields the pressure difference.

$$P_\ell - P_u = - \rho \frac{\partial}{\partial t} (\phi_\ell - \phi_u) - \rho/2 \, (V_\ell^2 - V_u^2)$$

or

$$\Delta P = \rho V \gamma(x) + \rho \frac{\partial}{\partial t} \int_o^x \gamma(x) \, dx$$

The lift on the panel can now be found by integrating the pressure difference from the leading edge to the trailing edge.

$$\ell = \int_o^c \Delta P \, dx = \rho V \int_o^c \gamma(x) \, dx + \rho \frac{\partial}{\partial t} \int_o^c \int_o^x \left[\gamma(x) \, dx'\right] \, dx$$

$$\ell = \rho V \Gamma(t) + \rho \frac{\partial}{\partial t} \int_o^c \Gamma(x) \, dx$$

The equations used for calculating the lift for a particular station are shown for five chordwise vortices.

$$\Delta P_1 = \rho V \frac{\Gamma_1}{\Delta x_1} + \rho \frac{\Gamma_1(t+\Delta t) - \Gamma_1(t)}{\Delta t}$$

$$\Delta P_2 = \rho V \frac{\Gamma_2}{\Delta x_2} + \rho \frac{\Gamma_1(t+\Delta t)+\Gamma_2(t+\Delta t)-\Gamma_1(t)-\Gamma_2(t)}{\Delta t}$$

$$\Delta P_5 = \cdots$$

The lift per unit span is as follows.

$$\ell = \Delta P_1 \Delta x_1 + \frac{(\Delta P_1+\Delta P_2)}{2} \Delta x_2 + \cdots \frac{\Delta P_5}{2} x_6$$

$$\ell = \Delta P_1 (\Delta x_1 + \frac{\Delta x_2}{2}) + \Delta P_2 (\frac{\Delta x_2}{2} + \frac{\Delta x_3}{2})$$

$$+ \Delta P_3 (\frac{\Delta x_3}{2} + \frac{\Delta x_4}{2}) + \Delta P_4 (\frac{\Delta x_4}{2} + \frac{\Delta x_5}{2})$$

$$+ \Delta P_5 (\frac{\Delta x_5}{2} + \frac{\Delta x_6}{2})$$

The moment can also be found in a similar manner. The total lift and moment are calculated by summing the increments of lift in the spanwise direction.

The technique described in this section could be used to determine the induced drag. However, the interpretation of the drag results computed from lifting surface theories still remains a question of some uncertainty in the subsonic speed regime. Another point that should be made is that the technique does not take into

account thickness effects. This could be taken into account by using source distributions.

The unsteady vortex lattice method was programmed and various test cases were run. Comparisons were made with both two- and three-dimensional results. Figures 23 and 24 show the excellent agreement between the classical two-dimensional solution of Theodorsen, Wagner and Kussner with the results calculated from the vortex lattice program. There is a difference between the computed values and the theoretical Kussner and Wagner functions for the first few semichord lengths traveled by the airfoil. However, the Kussner and Wagner functions describe only the circulatory lift due to a gust penetration and a step change in angle of attack respectively, whereas, the computations based on the equations developed for the vortex lattice method include both the noncirculatory and circulatory lift. Since the added mass effects are important at the beginning of an impulsive start then this would account for the difference between the curves. Figures 25 and 26 show the results for a finite wing having an aspect ratio of 6. Again the difference can be explained by the absence of the added mass effects in the classical solution.

An interesting comparison between a simple strip theory and the more exact lifting surface theory is presented in Figure 27. This figure shows a comparison for a step change in gust velocity (Kussner Problem). The difference in the lift coefficient is almost negligible. Figure 28 shows a comparison of the roll moment coefficient computed by both techniques for a gust field which varies linearly from the wing centerline to the wing tip.

Although the vortex lattice method yields extremely accurate

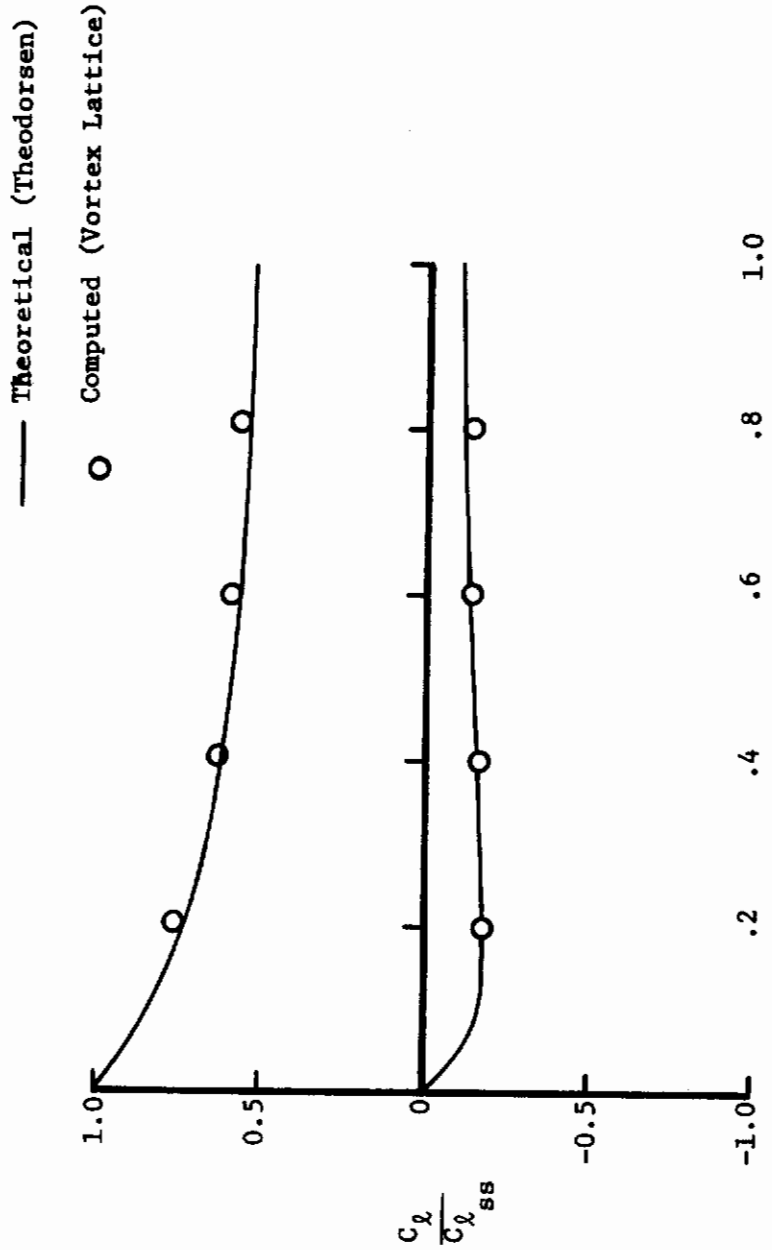

Figure 23. Comparison of Unsteady Vortex Lattice with Theodorsen's Function

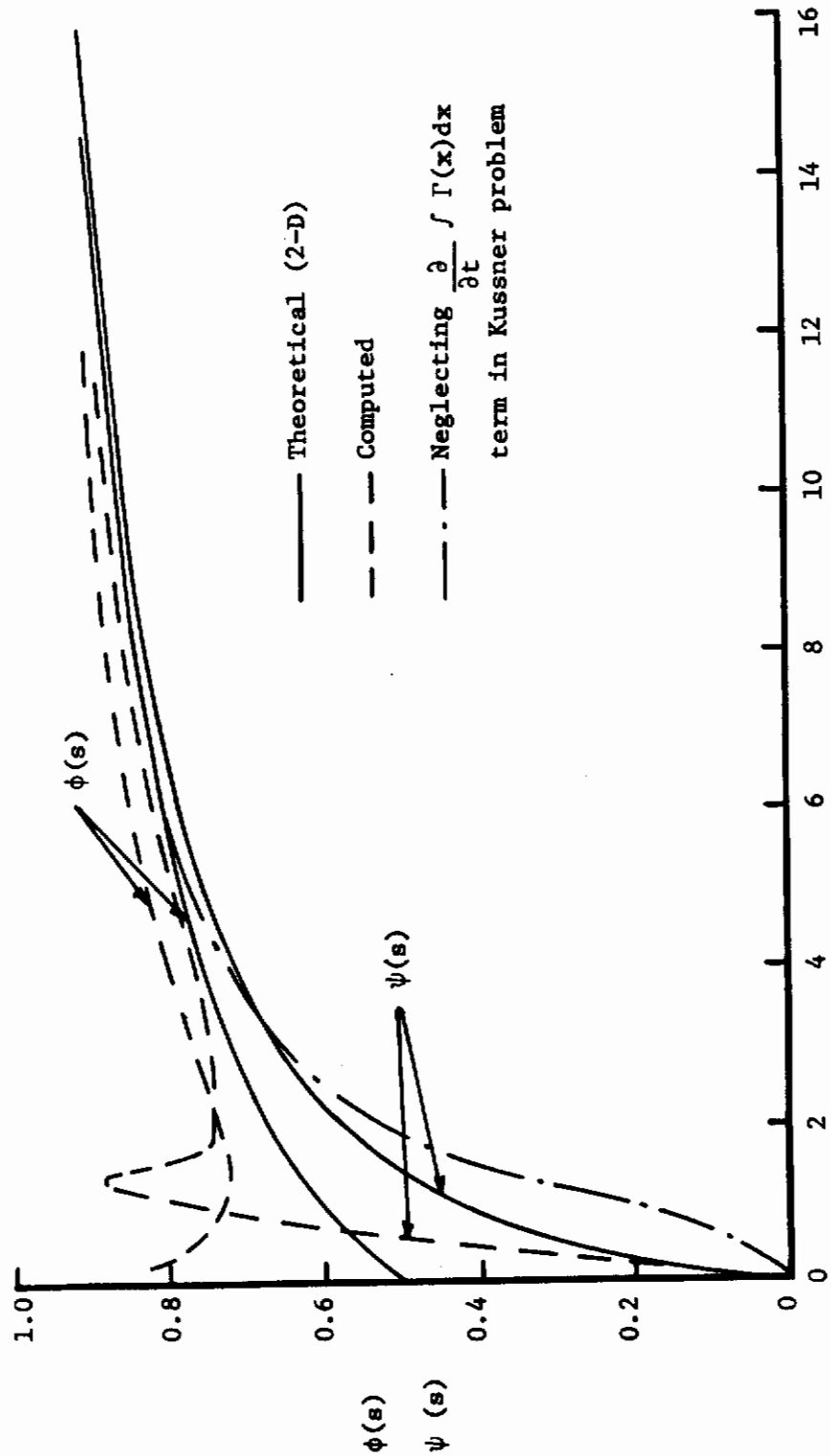

Figure 24. Comparison of Unsteady Vortex Lattice with Kussner and Wagner Functions

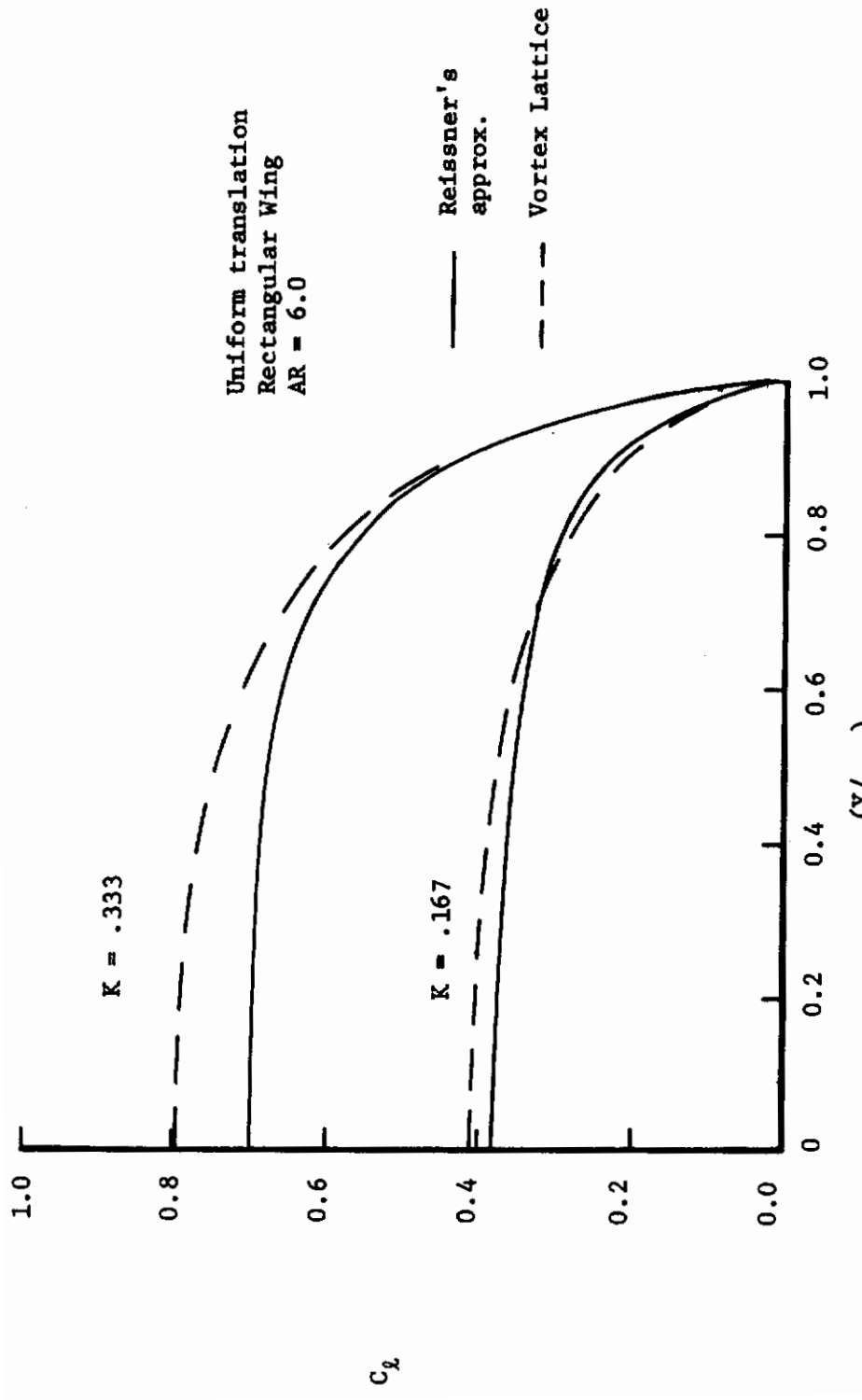

Figure 25. Comparison of Unsteady Vortex Lattice with Reissner's Approximation AR = 6.

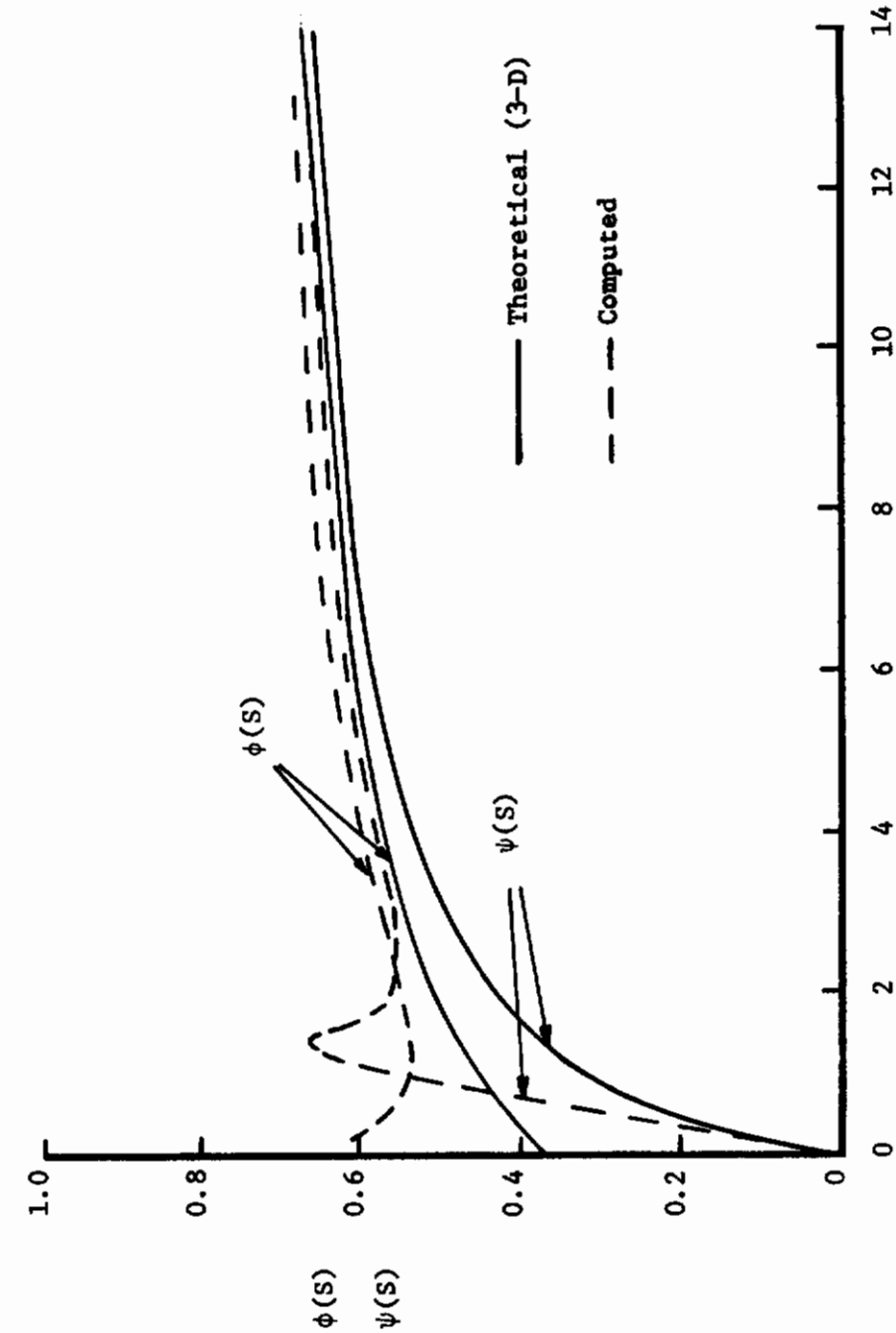

Figure 26. Comparison of Unsteady Vortex Lattice with Kussner and Wagner Functions

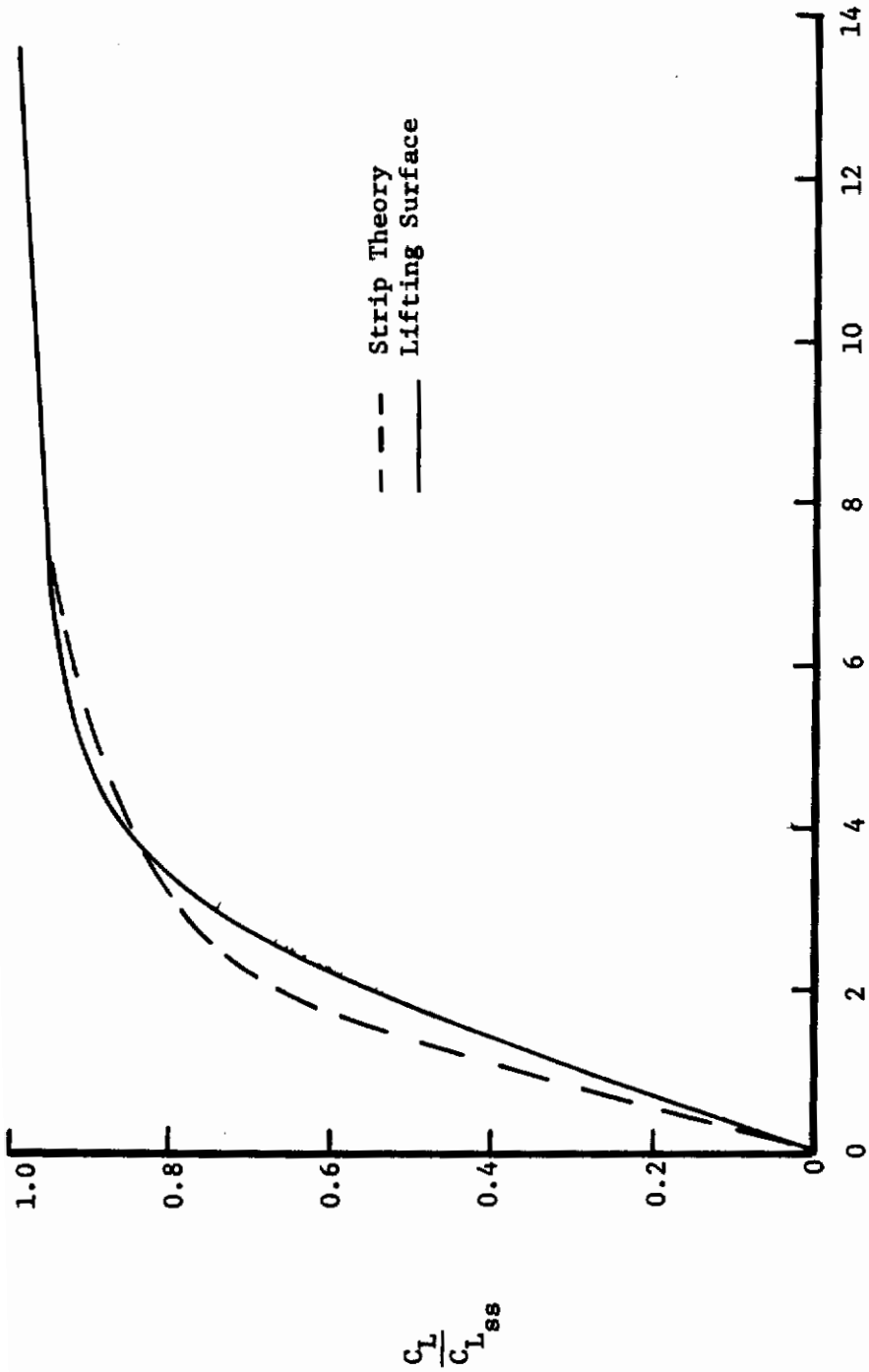

Figure 27. Comparison Between Vortex Lattice Method and a Simple Strip Theory

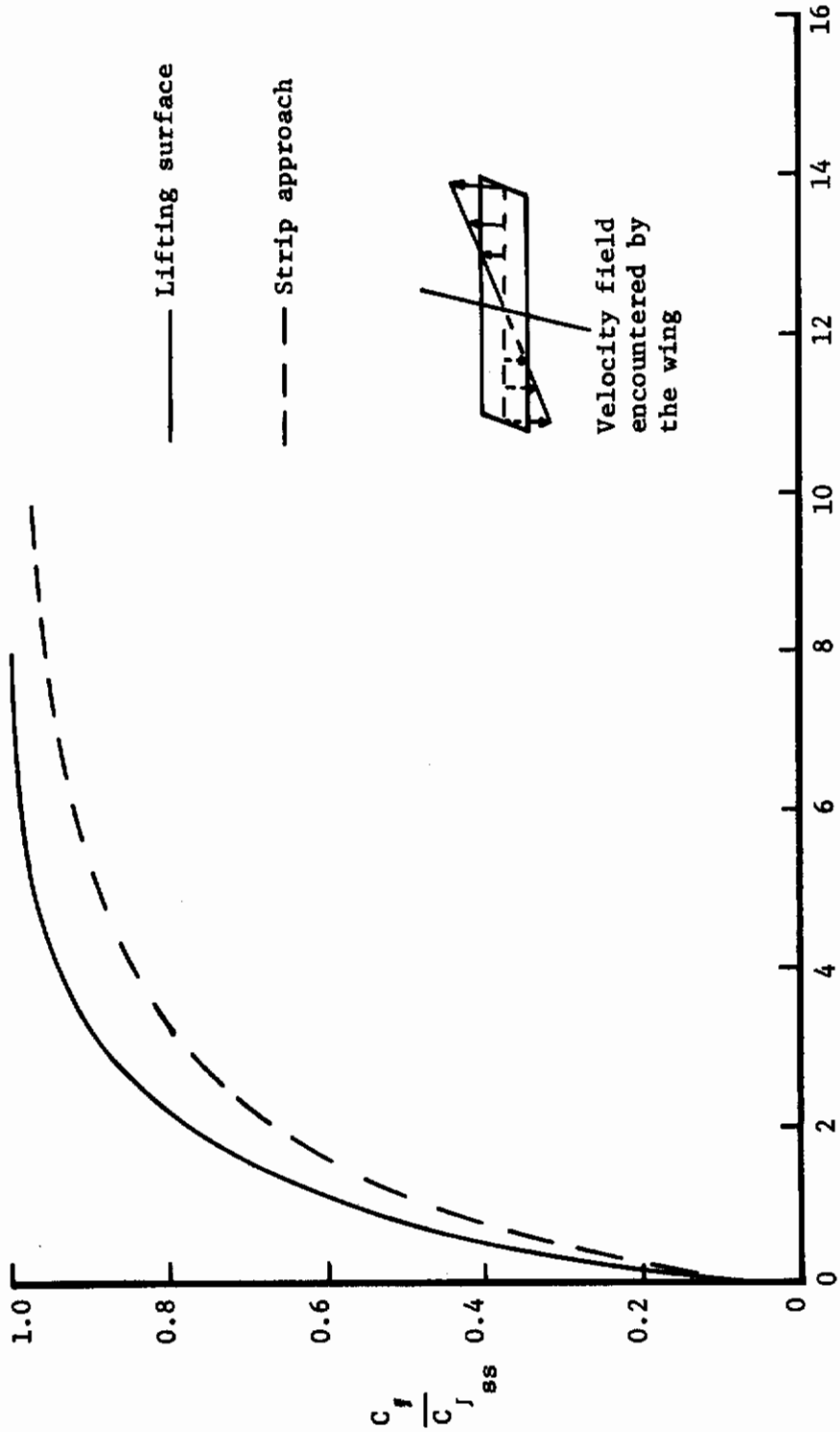

Figure 28. Comparison of Roll Moment Coefficients Calculated by Vortex Lattice and Strip Theory

results, the feasibility of using a complete lifting surface theory to calculate the loads on an aircraft penetrating a trailing vortex system seems to be unwarranted in view of the results shown in this section. Therefore the forces and moments due to the gust penetration and the vehicle's motion are calculated by using a modified strip theory. The strip theory concept is a means of applying two-dimensional aerodynamic theory to wings of finite span. The more rigorous lifting surface theories have largely superseded the strip theory approach. However, approximate methods such as the strip theory still remain useful for practical applications where their simplicity, flexibility, and economy are advantageous.

The strip theory method assumes that the aerodynamic forces on each strip are taken to be those associated with a two-dimensional wing undergoing the same motion as the particular section of a finite wing. This assumption implies that the aerodynamic interaction between strips is ignored. This simplification is not a very good approximation of the three-dimensional loading near the wing tip. However, it is acceptable if the aspect ratio is high.

The loads developed on each strip can be calculated from the following formulas described in References 45-48.

$$\ell_g = m_a \frac{1}{2} \rho U c \ell a \int_o^t \frac{\partial W_g}{\partial \tau} \psi(t-\tau) d\tau$$

$$\ell_m = m_a \frac{1}{2} \rho U c \ell a \left[W_{\frac{3c}{4}} (o) \Phi (t) + \int_o^t \Phi (t-\tau) \frac{dw_{\frac{3c}{4}}(\tau)}{d\tau} d\tau \right]$$

$$\ell_1 = \frac{\pi \rho c^2 \ell}{4} U \dot{\theta}$$

$$\ell_2 = \frac{\pi \rho c^2 \ell}{4} [-\ddot{W} + (c/2 - X_{cg})\ddot{\theta}]$$

where

m_a = aspect ratio correction

ℓ = width of the panel

a = slope of the lift curve

W_g = gust velocity

$W_{\frac{3c}{4}}$ = vehicle velocity

X_{cg} = distance to c.g. location

$\Phi(t)$ = Wagner function

$\psi(t)$ = Kussner function

The aspect ratio correction is obtained from the formula.

$$m_a = \frac{a_o}{1 + (a_o/\pi AR_e)(1+\tau)}$$

AR_e = AR for symmetrical lift distribution

AR_e = AR/2 for antisymmetrical lift distribution

τ = Glauert's correction factor

The above integral equations can be put into a form more suitable for programming by replacing the integrals by summations.

$$\ell_g = m_a \frac{1}{2} \rho U c \ell a \sum_{o}^{n=t/\Delta t} \Delta W(t_i) \psi(t-\tau_i)$$

$$\ell_m = m_a \frac{1}{2} \rho U c \ell a \left[W_{\frac{3c}{4}}(o) \quad \Phi(t) + \sum_{o}^{n=t/\Delta t} \Delta W_{\frac{3c}{4}}(t_i) \quad \Phi(t-\tau_i) \right.$$

By summing the contributions of each panel the total lift can be obtained. In a similar manner the other forces and moments can be calculated.

The general form of the equations used to calculate the forces and moments acting on the aircraft were divided into four parts. For example the Z force is

$$Z(t) = Z_o + Z_g(t) + Z_m(t) + Z_c(t)$$

where the sub o, g, m and c refer to the contribution due to the trimmed condition, gust penetration, vehicle motion and control input respectively. The components are defined as

$$Z_g(t) = - \int_o^t \int_{-b/2}^{b/2} h_{Z_{g_w}}(t,y) \frac{dw_g}{dt_1}(t_1,y) \, dy \, dt_1$$

$$Z_m(t) = \int_o^t \int_{-b/2}^{b/2} h_{Z_{m_w}}(t_1,y) \frac{dw_{\frac{3c}{4}}(t_1, y)}{dt_1} \, dy \, dt_1 + \int_{-b/2}^{b/2} \bar{h} \, W_{\frac{3c}{4}}(o,y) k_m(t_1) \, dy$$

$$Z_c(t) = C_{z_{\delta_e}} \delta_e(t) \, QS$$

where

$$h_{z_{g_w}} = \frac{a\ Q\ c(y)}{U}\ k_g(t_1)$$

$$h_{z_{m_w}} = \frac{a\ Q\ c(y)}{U}\ k_m(t_1)$$

$$\bar{h} = \frac{a\ Q\ c(y)}{U}$$

It was determined by numerical experimentation that the forces and moments acting on the aircraft due to the vehicle's motion could be accurately modeled by using the classical dynamic stability derivatives. Thus the integrals representing $Z_m(t)$, $Y_m(t)$, $L_m(t)$, etc. were replaced by the damping derivatives.

As the aircraft approaches the vortex core the induced velocities at some of the control points could become quite large. The equations developed in this section would then over predict the forces acting on the aircraft. In order to prevent this from occurring a check was incorporated into the aerodynamics subroutine. The check simply limited the maximum sectional lift coefficient to the sectional $C_{\ell_{max}}$. This assumption is not very restrictive when one considers the velocities of the probe aircraft. For this study the probe aircraft had approach velocities in the neighborhood of 200 ft/sec. Therefore very large induced velocities could be tolerated before the angle of attack approached the stall region.

Equations of Motion

The rigid body equations of motion of an aircraft having six degrees of freedom and referred to a rotating axes system can be obtained from the following vector equations as presented by Etkin[49].

$$\bar{F} = m \frac{d\bar{V}_c}{dt} + m\bar{\omega} \times \bar{V}_c$$

$$\bar{M} = \frac{d\bar{H}}{dt} + \bar{\omega} \times \bar{H}$$

The rotating axes system is fixed to the aircraft's center of gravity. The main advantage of using a body axes system is that the moments and products of inertia remain constant with respect to the body axes system. The coordinate systems are shown in Figure 29. Now the scalar equations can be written in the dimensional nonlinearized form as follows:

$$X(t) - m g \sin\theta = m (\dot{U} + QW - RV)$$

$$Y(t) + m g \cos\theta \sin\phi = m (\dot{V} + RU - PW)$$

$$Z(t) + m g \cos\theta \cos\phi = m (\dot{W} + PV - QU)$$

$$L(t) = I_{xx}\dot{P} + QR (I_{zz} - I_{yy})$$

$$M(t) = I_{yy}\dot{Q} + RP (I_{xx} - I_{zz})$$

$$N(t) = I_{zz}\dot{R} + PQ (I_{yy} - I_{xx})$$

The Euler angles (ψ, θ, ϕ) can be obtained by integrating the Euler rates which are expressed in terms of the angular velocities [P, Q, R] by the transformation

$$\begin{bmatrix} \dot{\theta} \\ \dot{\phi} \\ \dot{\psi} \end{bmatrix} = \begin{bmatrix} 0 & \cos\phi & -\sin\phi \\ 1 & \sin\phi \tan\theta & \cos\phi \tan\theta \\ 0 & \sin\phi \sec\theta & \cos\phi \sec\theta \end{bmatrix} \begin{bmatrix} P \\ Q \\ R \end{bmatrix}$$

The coordinates of the aircraft relative to the inertial frame are expressed as a function of the Euler angles and the velocity components [U, V, W].

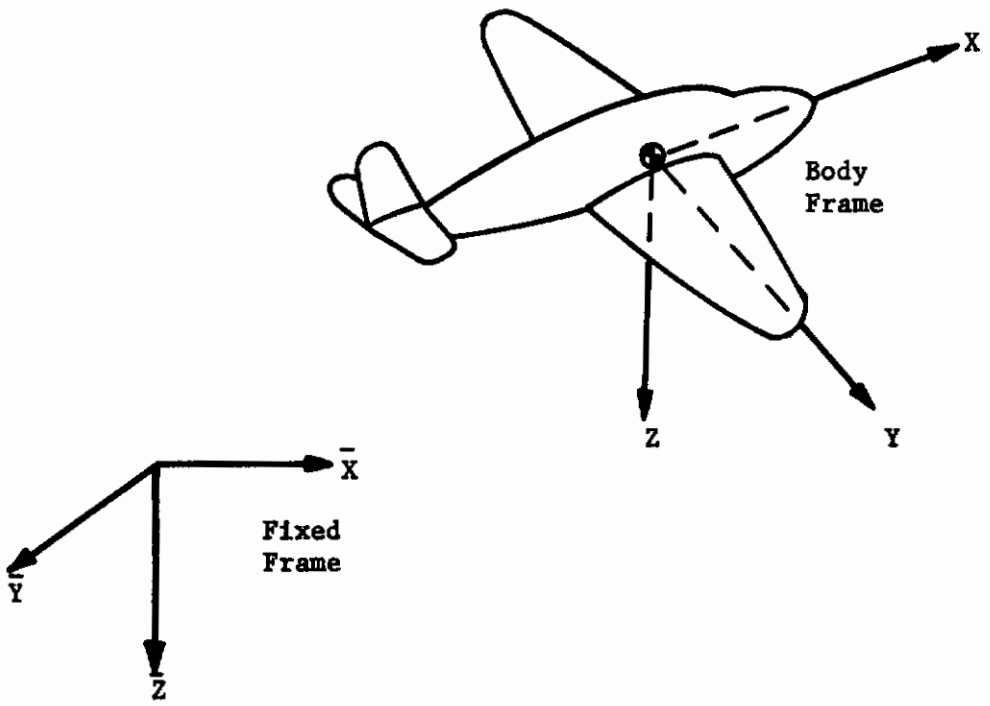

Figure 29. Coordinate System

$$\begin{bmatrix} \frac{dx'}{dt} \\ \frac{dy'}{dt} \\ \frac{dz'}{dt} \end{bmatrix} = \begin{bmatrix} C_\phi C_\psi & S_\phi S_\theta C_\psi - C_\phi S_\psi & C_\phi S_\theta C_\psi + S_\phi S_\psi \\ C_\theta S_\psi & S_\phi S_\theta S_\psi + C_\phi C_\psi & C_\phi S_\theta S_\psi - S_\phi C_\psi \\ -S_\theta & S_\phi C_\theta & C_\phi C_\theta \end{bmatrix} \begin{bmatrix} U \\ V \\ W \end{bmatrix}$$

where C ≡ cos S ≡ sin

The forces and moments acting on the aircraft were divided into four components

$$\begin{bmatrix} X(t) \\ Y(t) \\ Z(t) \\ L(t) \\ M(t) \\ N(t) \end{bmatrix} = \begin{bmatrix} X_o \\ Y_o \\ Z_o \\ L_o \\ M_o \\ N_o \end{bmatrix} + \begin{bmatrix} X_g(t) \\ Y_g(t) \\ Z_g(t) \\ L_g(t) \\ M_g(t) \\ N_g(t) \end{bmatrix} + \begin{bmatrix} X_m(t) \\ Y_m(t) \\ Z_m(t) \\ L_m(t) \\ M_m(t) \\ N_m(t) \end{bmatrix} + \begin{bmatrix} X_c(t) \\ Y_c(t) \\ Z_c(t) \\ L_c(t) \\ M_c(t) \\ N_c(t) \end{bmatrix}$$

initial flight conditions — gust — motion — control

Usually the initial conditions were such that

$Y_o = L_o = M_o = N_o = 0.$

Control - Human Pilot

One of the earliest attempts to model mathematically the behavior of a human being was conducted by Diamantides[50] at the

Goodyear Aircraft Corporation. Diamantides and his associates developed a pilot model with the aid of an analog computer. This was accomplished by postulating various mathematical models to describe the human dynamics and then by comparing the results of the analog with human pilot actions. The test consisted of a movable simulator equipped with a control column and display. The longitudinal equations of motion for a fighter aircraft were used to test the pilot's reaction to pitch disturbances. The human pilot and the analog were run in parallel. This allowed easy evaluation of the postulated human dynamics. The test engineers adjusted the various parameters in the analog model until the pilot was unable to detect that the analog was flying the simulator. Figure 30 shows a block diagram representation of Diamantides' pilot model. This figure indicates that upon perception of the stimulus the human controller performs two linear operations. First he makes a mental computation of the stimulus. That is, position, rate and acceleration are sensed and weighed, then a decision to act occurs. Secondly, there are certain physical limitations on the corrective hand motions which are caused by the neuromuscular or motor feedback loop. Another characteristic of the human operator is that he normally does not react to a stimulus until it is above a certain threshold. Once the magnitude of the stimulus is higher than the threshold value the information is sensed and a mental computation is performed. The brain then commands the appropriate muscle reaction. This all takes place in a fraction of a second. The time lag is called the "reaction time". It has been found that the reaction time is almost constant in normal people.

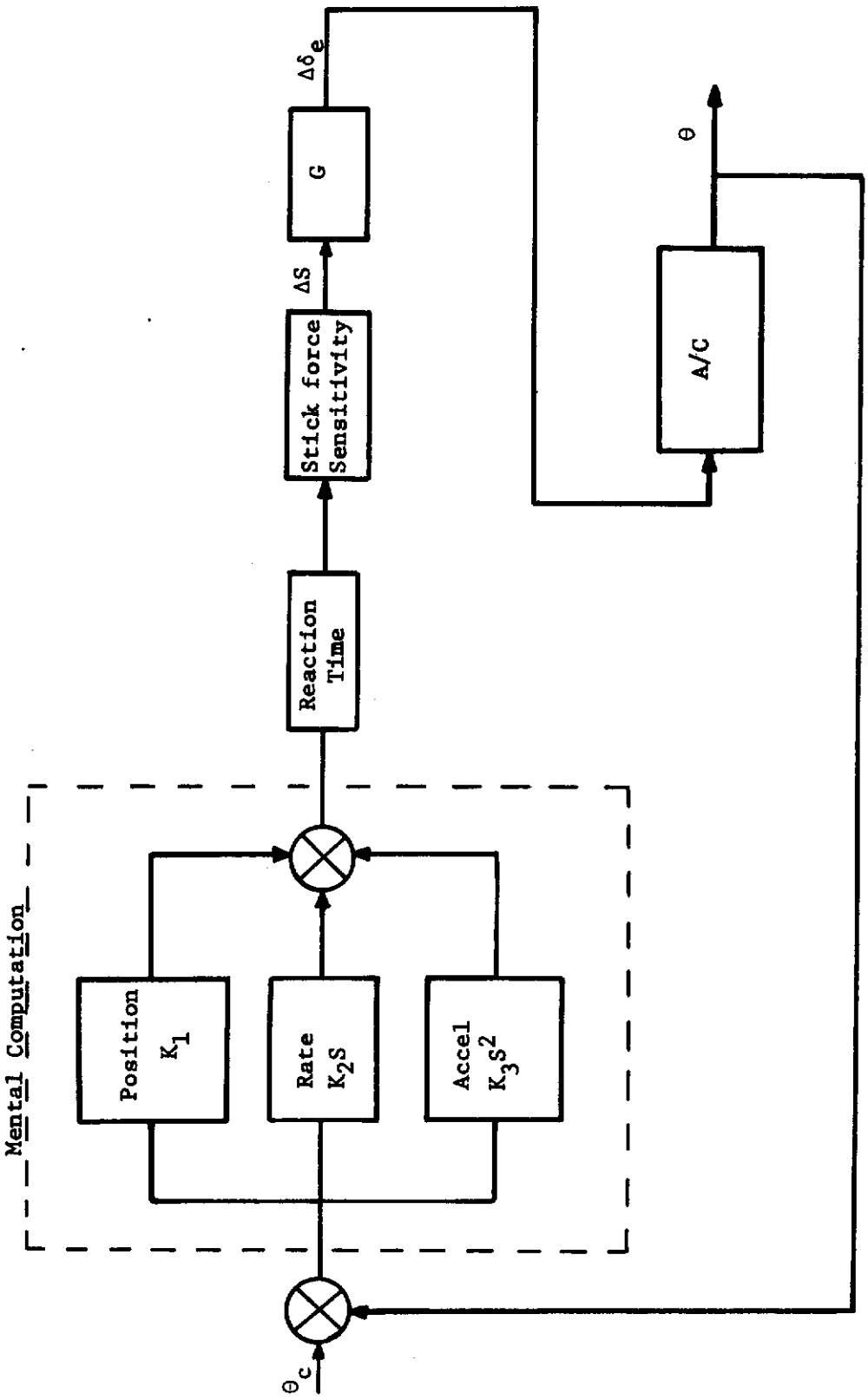

Figure 30. Diamantides Pilot Model

There are two types of control possible. They are pursuit and compensatory. In pursuit tracking past experience provides the tracker with information about what to expect in a future input. In compensatory tracking this is not possible[51]. Figure 31 is a block diagram representation of both pursuit and compensatory tracking. In studying the dynamic behavior of an aircraft penetrating a vortex system it is quite apparent that the compensatory control is the only type which is applicable.

The pilot model for compensatory control case can be expressed in terms of the following transfer function.

$$Y_p(s) = \frac{k_p\, e^{-\tau s}\, (1 + \tau_L s)}{(1 + \tau_N s)(1 + \tau_I s)}$$

k_p = pilot gain

$e^{-\tau s}$ = reaction time delay

τ_L = lead time constant

τ_N = neuromuscular lag time constant

τ_I = lag time constant

The above expression can be put into a more convenient form by assuming that the neuromuscular lag can be accounted for by modifying the reaction time delay.

$$Y_p(s) = k_p \frac{(\tau_L s + 1)}{(\tau_I s + 1)}\, e^{-\tau s}$$

The parameters included in these expressions should not be interpreted as constants. In addition to the transfer function, adjustment rules are required to specify the pilot model parameters. These rules have been determined by numerous investigators.[51, 52]

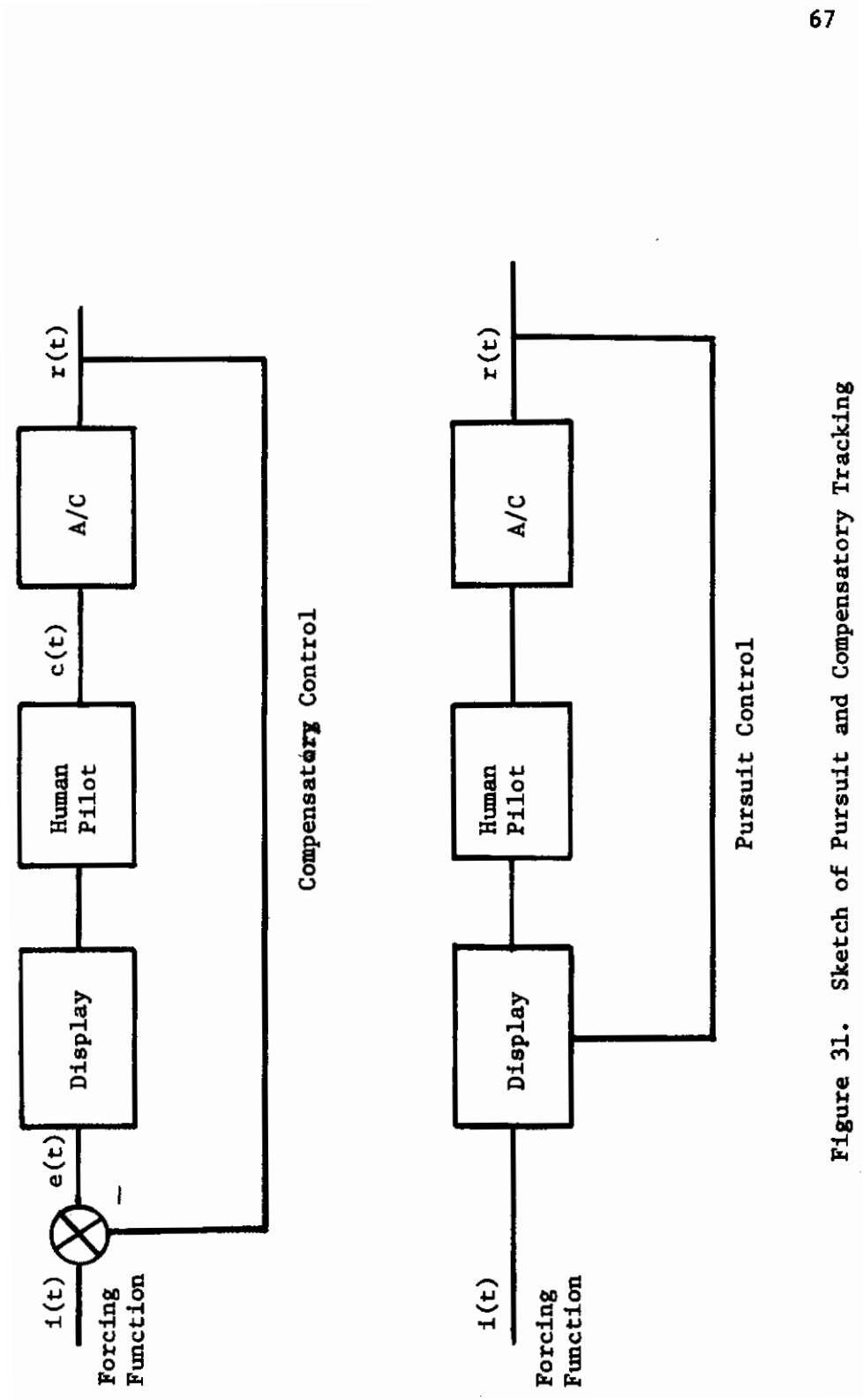

Figure 31. Sketch of Pursuit and Compensatory Tracking

It has been found that the gain k_p is easily and rapidly varied by the pilot to an appropriate value. The equalization term, that is $(\tau_L s+1)/(\tau_I s+1)$, is varied within certain limits so that the system has a good frequency response.

The adjustment rules can be stated as follows:

1. The human adapts so that his gain and equalization characteristics are appropriate for a stable system.

2. The human adapts so that the form of his equalization characteristics is appropriate to good low-frequency closed-loop response to the forcing function.

The adjustment rules were determined by analyzing experimental data obtained from tests on human operators. To put the adjustment rules in a more practical format we can use the following:

1. The open-loop phase margin. The pilot adapts an equalization to obtain 50 to 110 degrees of phase margin. It has been found that an open-loop phase margin in this range yields a closed loop system with a satisfactory time domain performance.

2. Open-loop crossover frequency. For good high frequency characteristics the crossover frequency should be at least 1 rad/sec.

Using these rules the constants τ_L and τ_I can be determined from either a Bode or Polar plot of the open loop transfer function $[Y_p\ Y_a]$, where Y_a is the transfer function of the aircraft. Another technique which can be employed to determine the pilot parameters is the root locus method.

Both single and multi axis control were incorporated into the program. Based on the work in References 47, 48, and 53-59 it was

decided that the pitch and roll axis controllers could be modeled accurately by the simple transfer function

$$Y_{p_\phi} = k_{p_\phi}(\tau_{L_\phi}s+1)e^{-\tau s} \qquad \text{(Roll)}$$

$$Y_{p_\theta} = k_{p_\theta}(\tau_{L_\theta}s+1)e^{-\tau s} \qquad \text{(Pitch)}$$

Figure 32 shows a block diagram representation of the pilot-vehicle system. The transfer function can be written in the time domain as

$$\delta_e(t+\tau) = k_{p_\theta}\,\theta_e(t) + k_{p_\theta}\,\tau_{L_\theta}\,\frac{d\theta_e}{dt}$$

and

$$\delta_a(t+\tau) = k_{p_\phi}\,\phi_e(t) + k_{p_\phi}\,\tau_{L_\phi}\,\frac{d\phi_e}{dt}$$

where

$$\phi_e = \phi_c - \phi = -\phi \qquad \text{for wings level control}$$

$$\theta_e = \theta_c - \theta.$$

Appendix A gives the details on the selection of the pilot parameters. Figure 33 illustrates the block diagram representation of the roll and heading control task. Again the pilot model was assumed to have the same form as those previously described.

The pilot models used in this study should give a qualitative assessment of the pilot's ability to control the upset due to a vortex encounter.

Numerical Analysis

The twelve first order differential equations needed to describe the aircraft's motion were solved numerically by using a fourth order Runge-Kutta technique. The Runge-Kutta method for a system of

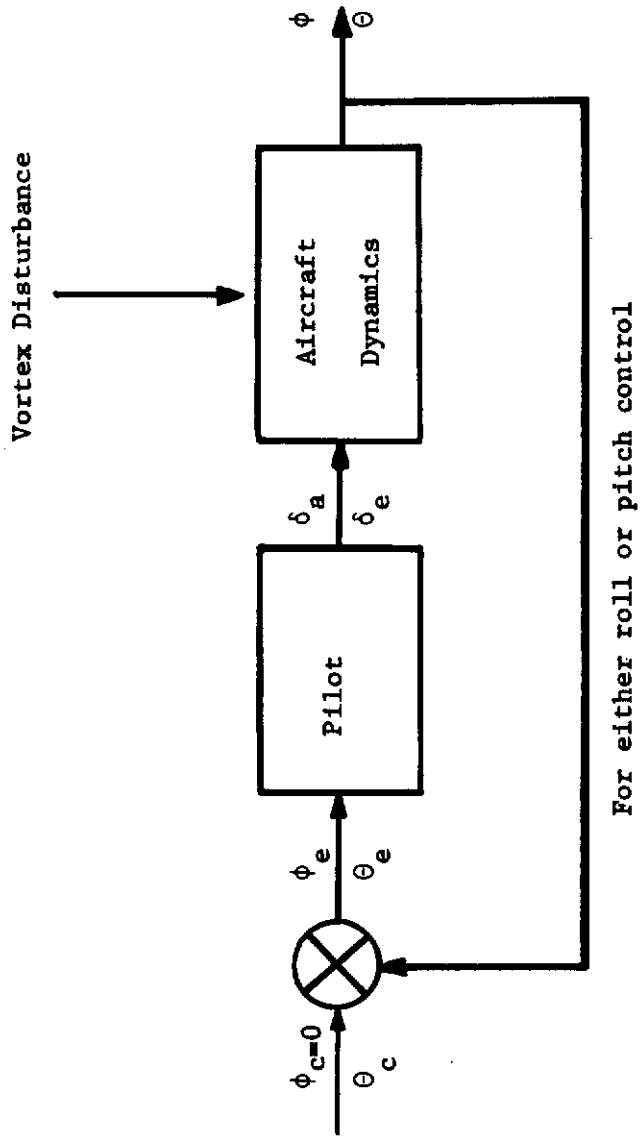

Figure 32. Block Diagram of Single Axis Control of Roll or Pitch

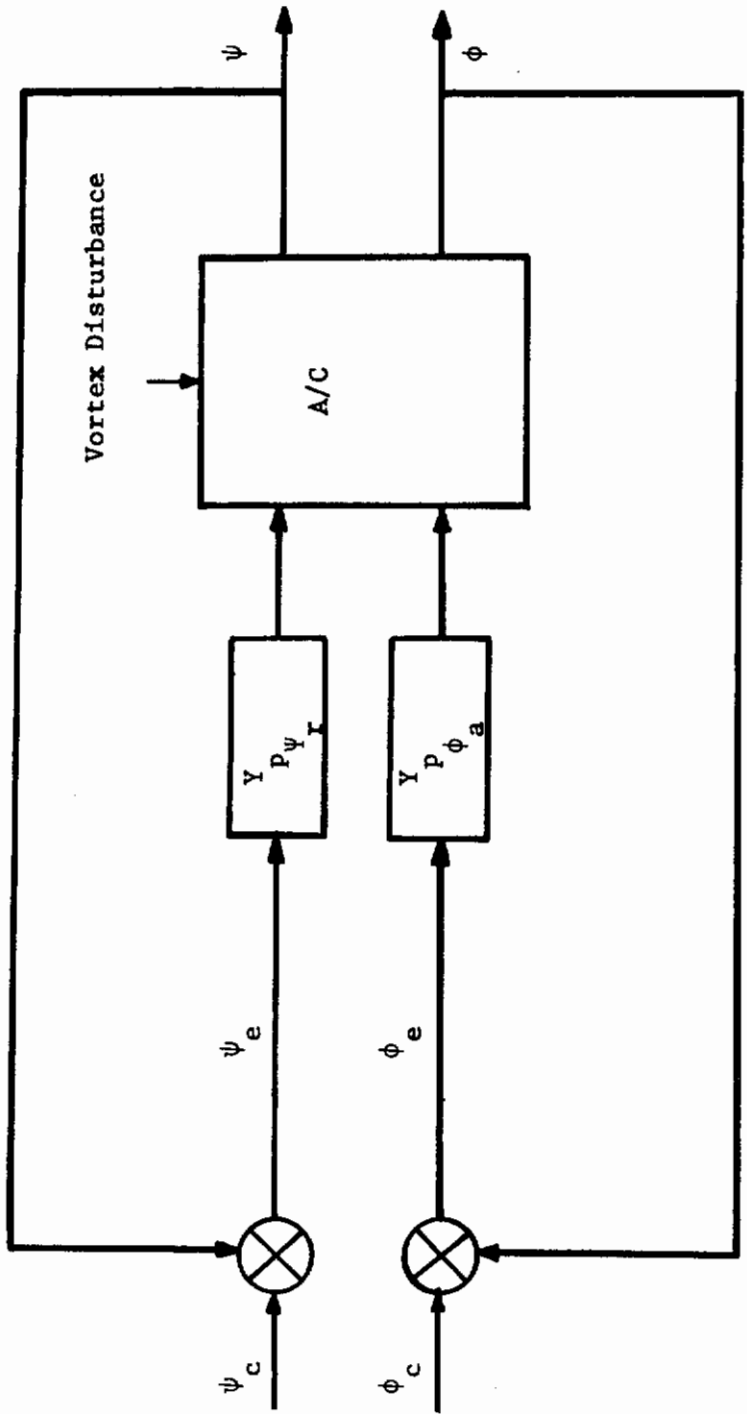

Figure 33. Block Diagram of Roll and Heading Control

differential equations can be found in any text on numerical analysis. For completeness the general form of the Runge-Kutta algorithm is presented below in its functional form.[60]

$$p_k = h\, f_k(x_i, y_{1i}, y_{2,i}, \cdots\cdots y_{n,i})$$

$$q_k = h\, f_k(x_i + {}^{h}/_{2}, y_{1,i} + \frac{p_1}{2}, \cdots\cdots, y_{n,i} + \frac{p_n}{2})$$

$$r_k = h\, f_k(x_i + {}^{h}/_{2}, y_{1,i} + \frac{q_1}{2}, \cdots\cdots, y_{n,i} + \frac{q_n}{2})$$

$$s_k = h\, f_k(x_i + h, y_{1,i} + r_1, \cdots\cdots, y_{n,i} + r_n)$$

$$y_{k,\, i+1} = y_{k,i} + {}^{1}/_{6}\,(p_k + 2q_k + 2r_k + s_k)$$

where $k = 1, 2, 3 \ldots h$

The equations of motion rearranged to a form suitable for integration are as follows:

$$\dot{U} = (X(t) - m\,g \sin\theta)/m - QW + RV$$

$$\dot{V} = (Y(t) + m\,g \cos\theta \sin\phi)/m - RU + PW$$

$$\dot{W} = (Z(t) + m\,g \cos\theta \cos\phi)/m - PV + QU$$

$$\dot{P} = (L(t) - QR\,(I_{zz} - I_{yy}))/I_{xx}$$

$$\dot{Q} = (M(t) - RP\,(I_{xx} - I_{zz}))/I_{yy}$$

$$\dot{R} = (N(t) - PQ\,(I_{yy} - I_{xx}))/I_{zz}$$

$$\dot{\theta} = Q \cos\phi - R \sin\phi$$

$$\dot{\phi} = P + Q \sin\phi \tan\theta + R \cos\phi \tan\theta$$

$$\dot{\psi} = Q \sin\phi \sec\theta + R \cos\phi \sec\theta$$

$$\dot{X} = U\,C_\theta C_\psi + V(S_\phi S_\theta C_\psi - C_\phi S_\psi) + W(C_\phi S_\theta C_\psi + S_\phi S_\psi)$$

Earth axes

$$\dot{Y} = U\,C_\theta S_\psi + V(S_\phi S_\theta S_\psi + C_\phi C_\psi) + W(C_\phi S_\theta S_\psi - S_\phi C_\psi)$$

$$\dot{Z} = -U\,S_\theta + V(S_\phi C_\theta) + W(C_\phi C_\theta)$$

where C = cos S = sin

SECTION IV

RESULTS

Simplified Analysis

Before discussing the results of the computer simulation it would be instructive to examine the results from a simplified analysis. Consider the situation of an aircraft suddenly penetrating along the axis of the vortex core. A measure of the vortex hazard would be a comparison of the vortex induced rolling moment to that available due to maximum aileron deflection. This type of analysis has been discussed previously in Chapter 1. Figure 34 taken from reference 12 indicated the severity of such a vortex encounter. The vortex generated by the leading wing is approximately that of a DC-9 during approach. The separation distance and separation time were 9000 feet and one minute respectively. Examination of this figure reveals that penetrating aircraft would experience induced rolling moments exceeding their roll capability. Figure 35 also taken from reference 12 shows the effect of the lateral displacement on the vortex induced rolling moment. Note that the induced rolling moment reverses sign as the vortex moves toward the wing tip.

Using simple strip theory the induced rolling moment was calculated for aircraft of varying sizes. Table 1 contains the characteristics of the penetrating aircraft while Table 2 contains the information pertaining to the generating aircraft. The results of these calculations are presented in Figures 36 - 38. Figure 36 shows that a light single engine aircraft would experience momentary loss of control for separation distances of up to 9 miles behind a

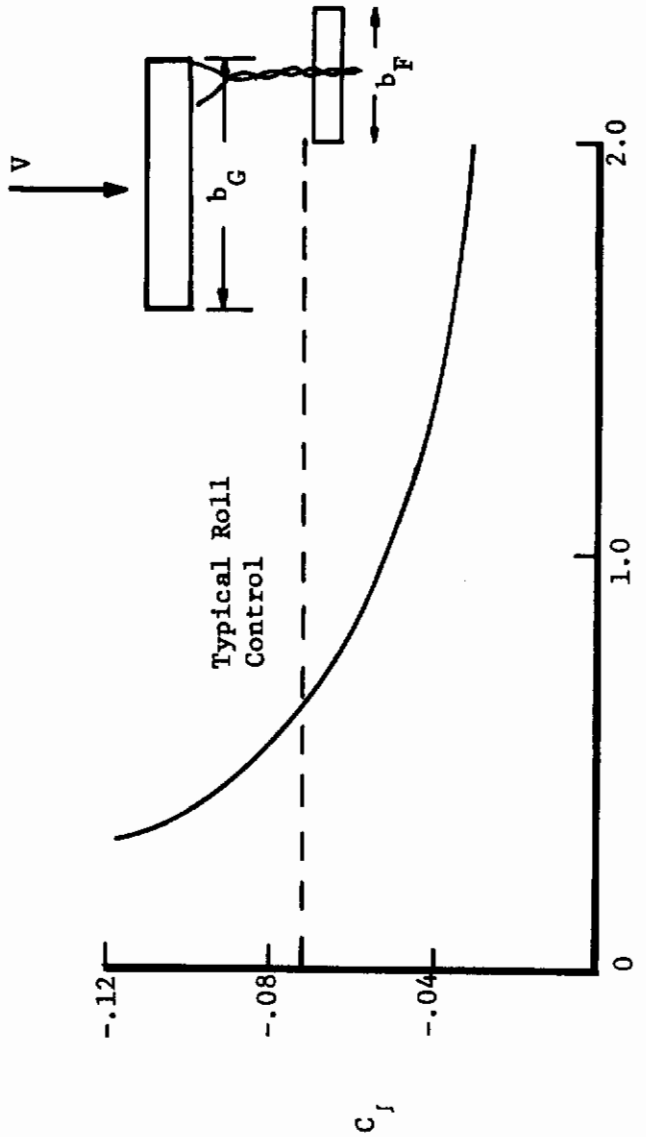

Figure 34. Effect of Relative Span on Vortex-Induced Rolling Moment

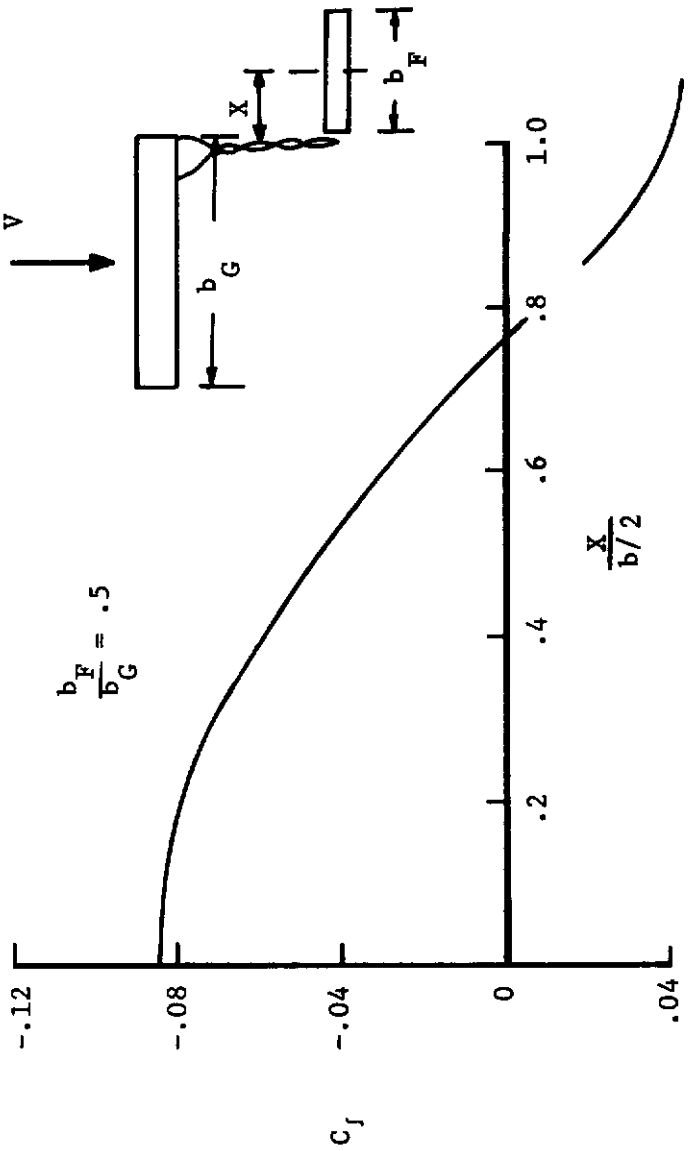

Figure 35. Effect of Lateral Displacement on Vortex Induced Rolling Moment

Table I

Characteristics of Penetrating Aircraft

Aircraft	W(lb)	S(ft^2)	b(ft)	λ	C_o(ft)	Λ	V(fps)
Light Single Engine	2,000	175	29.3	.667	5.33	0	117
Light Twin Engine	3,300	175	36.6	.665	5.33	0	109
Light Business Aircraft	7,700	277	45.9	.50	7.0	0	142
Light Propeller Driven Transport	27,400	750	95	.4	11.33	0	147
Light Jet Transport	70,000	934	89	.215	16.35	24°	236

Table II

Characteristics of Generating Aircraft

Aircraft	W(lb)	S-(ft^2)	b(ft)	V(fps)
C5-A	600,000	6,200	220	320
747	550,000	5,500	195	225
DC-9	70,000	934	90	236
DC-6	90,000	1,457	114	134

DC-6. Also the light twin would be out of control for penetrations under 2.3 miles separation. Figure 37 shows that both the light single and twin engine aircraft are momentarily out of control behind a DC-9. Note that for the light twin to be under control the separation distance must be in excess of 8 miles. Now in Figure 38 we see that even an aircraft the size of a DC-9 would be considered to be out of control for separation distances of up to 13.5 miles behind a 747. Figure 39 taken from a report by Robinson and Larson[61] illustrates that the strip theory approach yields an effective upper bound to the induced rolling moment. The scatter in the flight test data is due largely to the difficulty of penetrating into the vortex core. This will be discussed in more detail later in this section. An interesting result of the flight test program conducted by NASA was that the pilots felt that they had control of the aircraft at separation distances where the ratio of $C_{\ell}/C_{\ell_{\delta_a}}\delta_{a_{max}}$ was greater than one. This is due most likely to two factors. First as the aircraft begins to roll the natural roll damping due to the wing aids the pilot in regaining control of the aircraft. Secondly and probably the most important is that the aircraft is rapidly expelled from the vortex system thus giving the pilots the false impression that they were in complete control of the aircraft.

Along-Track Penetration With Roll Control

Along-track penetration is most likely to occur during final approach or shortly after take-off. In either case the following aircraft can ill-afford to have any large excursions from its normal

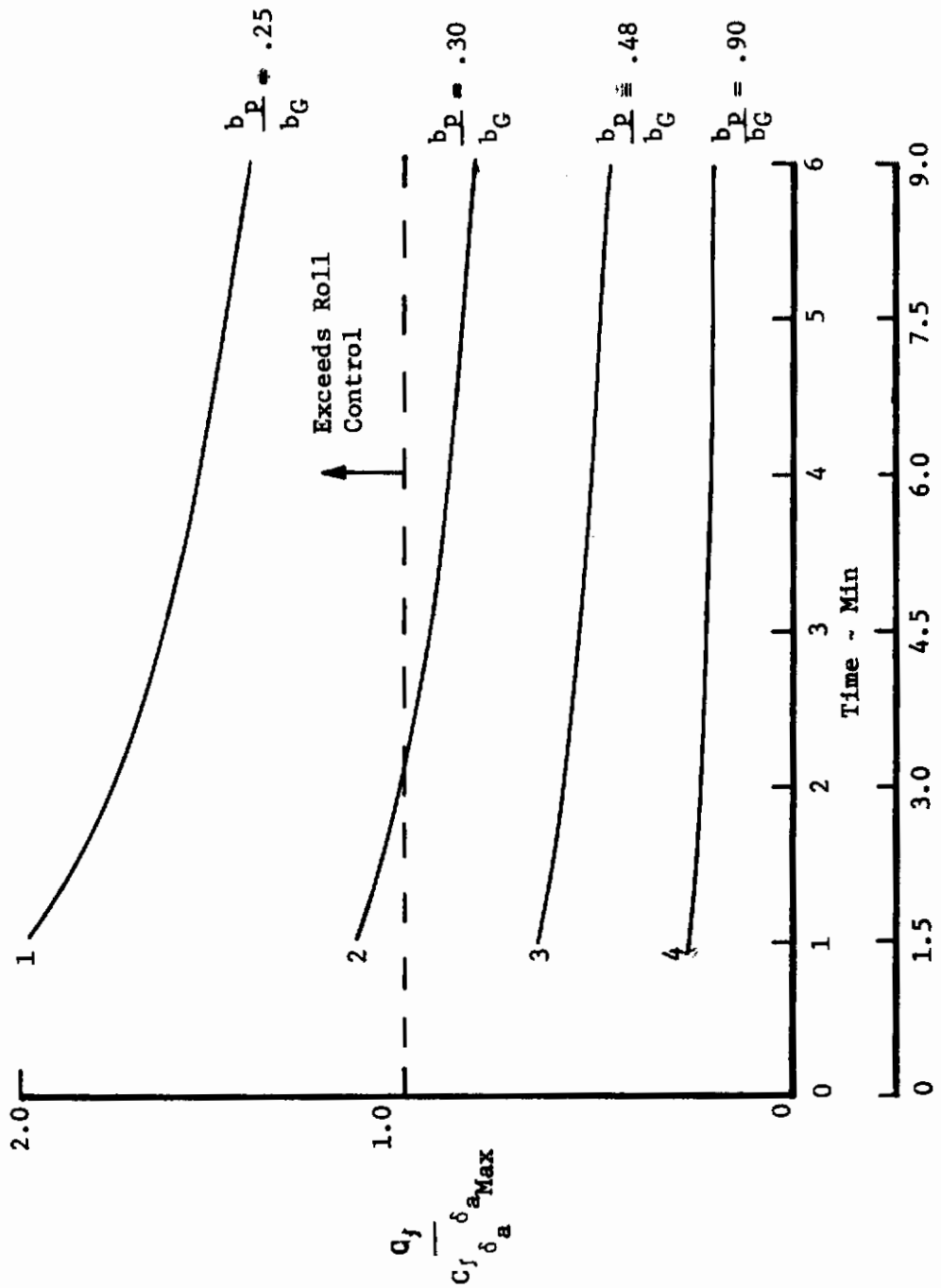

Figure 36. Induced Rolling Moment Due to the Wake of a DC-6

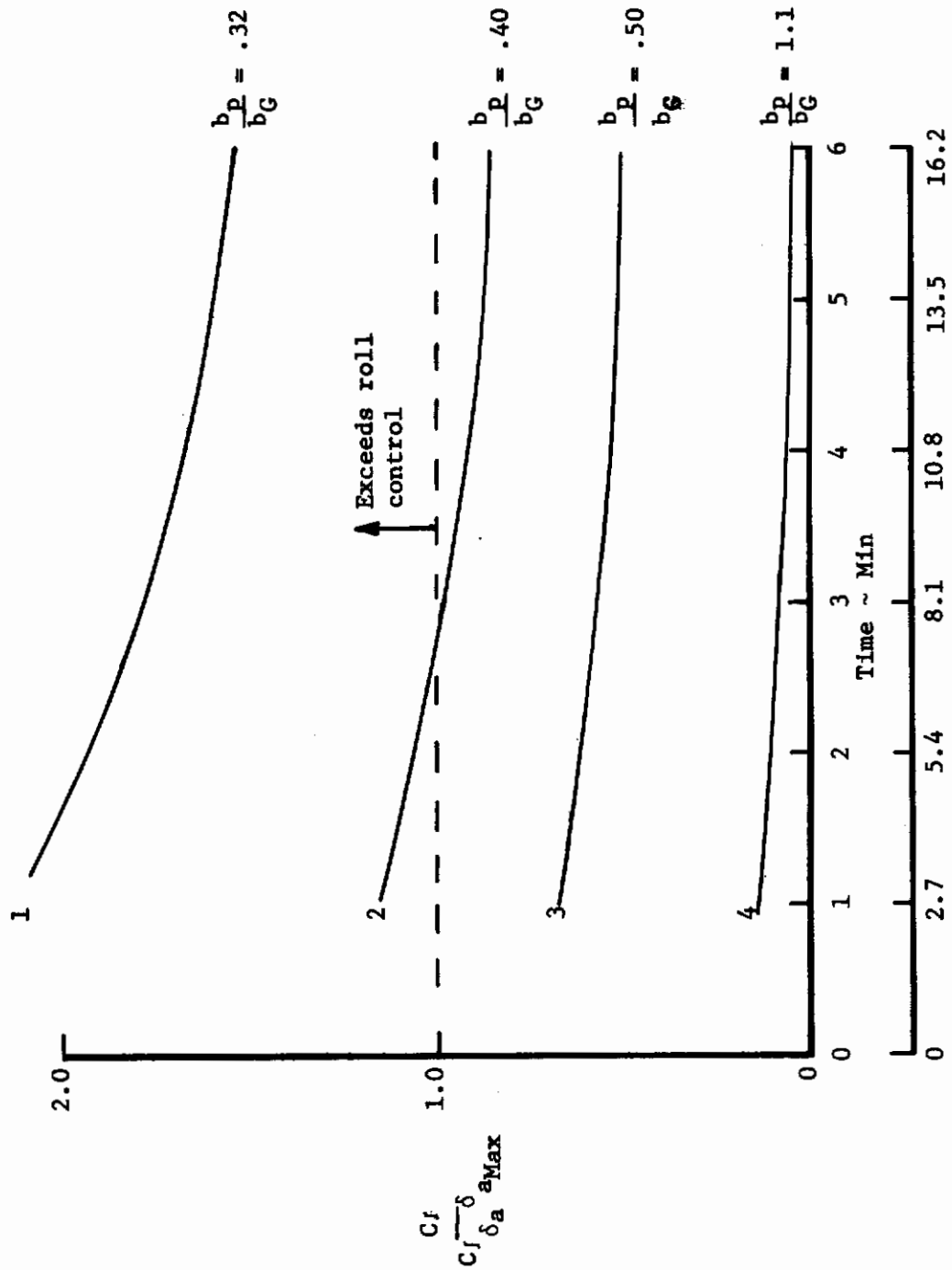

Figure 37. Induced Rolling Moment Due to the Wake of a DC-9

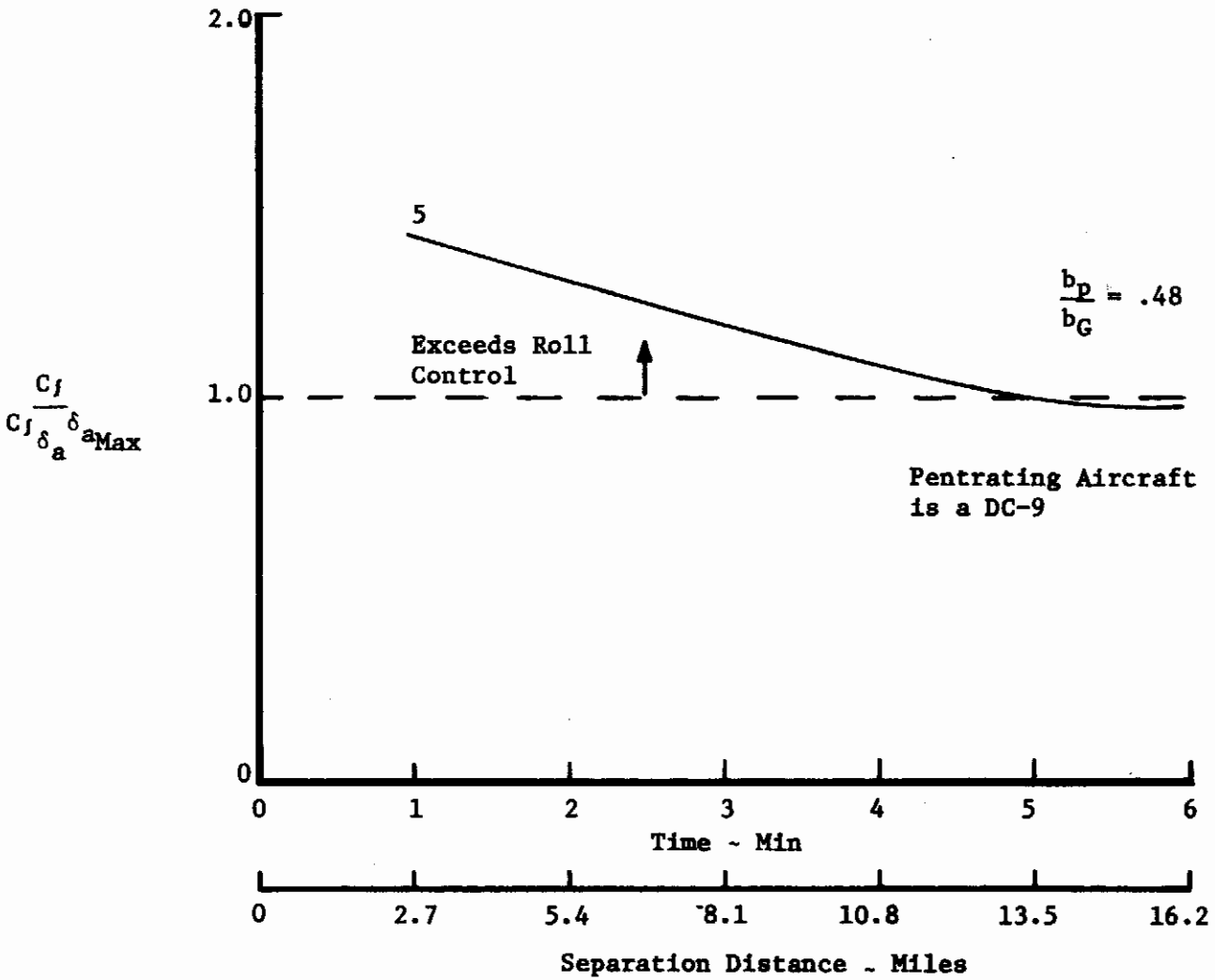

Figure 38. Induced Rolling Moment Due to the Wake of a 747

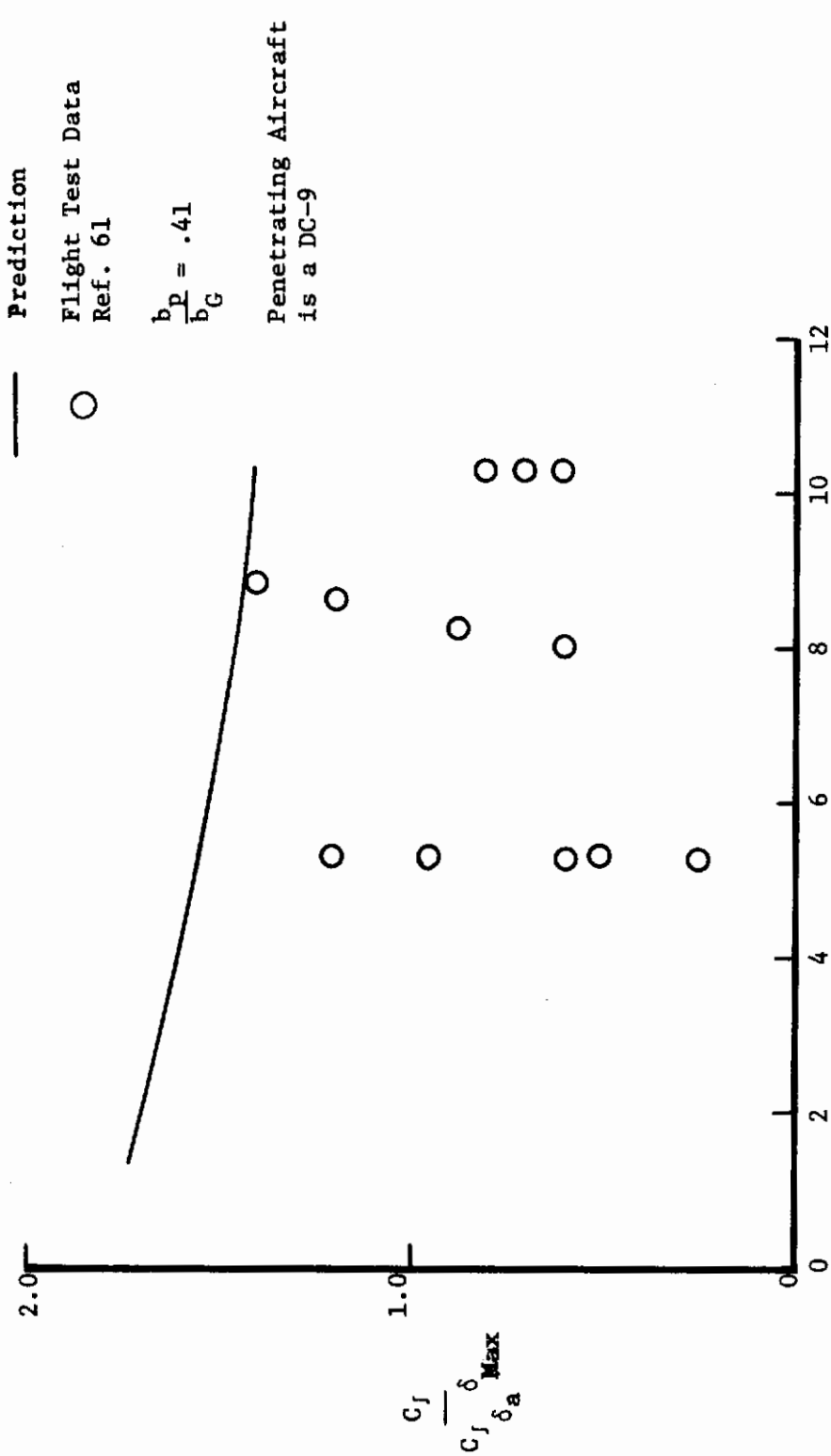

Figure 39. Induced Rolling Moment Due to the Wake of a C5-A

flight path. For the separation times considered in this study the normal downward motion of the vortex system would place the vortices well below the flight path of the following aircraft. However, several investigators have shown that under certain atmospheric conditions the downward motion of the vortex system can be retarded. In fact one investigator has suggested that as the vortex system approaches an inversion layer the vortices behave as though they were approaching the ground. Thus the vortices would cease their downward movement and begin to spread laterally. Another possibility of encountering a vortex wake in the terminal area would be during the execution of a missed approach by the lead aircraft. The wake of the lead aircraft would be laid down at an altitude well above that of the following aircraft and thus could descend into the flight path of the trailing aircraft.

Now consider some typical results from the six degree of freedom computer simulation. First let us examine the response of an aircraft where the pilot controls the roll attitude. That is, the mathematical pilot model attempts to maintain a wings level orientation. The characteristics of the penetrating and generating aircraft are listed in Table III. Figure 40 illustrates the penetrating angles under consideration. θ_p is the angle between the penetrating aircraft's flight path and the plane of the vortices. Whereas ψ_p is defined as the angle between the flight path and the vortex axis when viewed from above. For the cases considered here the separation distance was 27,000 feet or approximately 2 minutes behind the generating aircraft. Also it should be pointed out that the flight path of the penetrating aircraft was selected so that it would

Table III

Aircraft Characteristics

Aircraft Parameters	Penetrating Aircraft ~ P	Generating Aircraft
Wing Area ~ ft^2	350	980
Span ~ ft	55	90
Weight ~ lb	15,000	70,000
Velocity ~ ft/sec	190	232

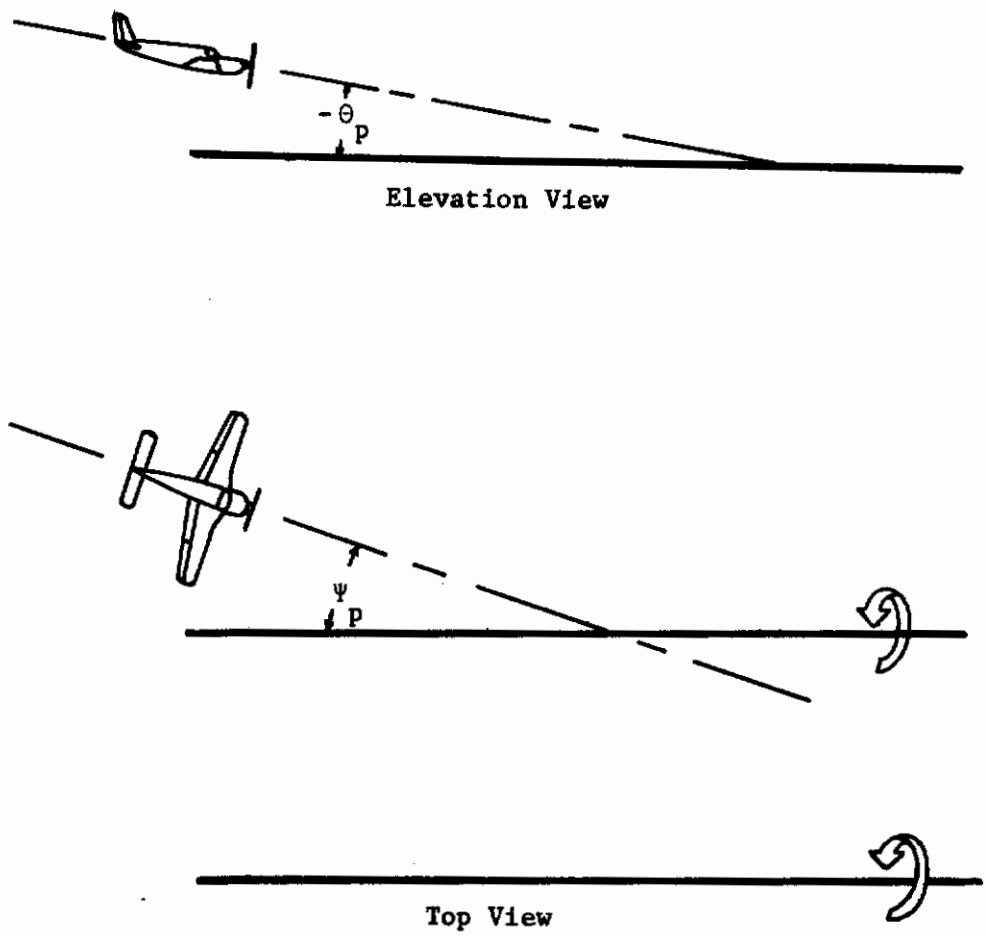

Figure 40. Aircraft Penetrating a Vortex

intersect the vortex core if the aircraft were not influenced by the vortex system.

For an aircraft descending into the vortex system at the angle $\theta_p \simeq 2.5°$, Figures 41 - 43 illustrate the effect of the oblique penetration angle ψ_p on the response of the penetrating aircraft. Notice that the aircraft descending into the vortex with $\psi_p \simeq 3°$ rolls away from the vortex system. The aircraft is seen to roll slightly and climbs away from the vortex. The aircraft climbs since it is flying into the upwash region of the port vortex. Upon increasing the penetration angle to $\psi_p \simeq 6°$ we see a significant difference in the aircraft's response. Figure 42 shows the aircraft rolling sharply to the right and at the same time its rate of descent is increased as the aircraft passes into the strong downwash region between the vortices. Figure 43 illustrates the effect of including the pilot in the simulation. Without pilot control the aircraft rolls to an angle greater than 100 degrees whereas with control input the aircraft rolls approximately 50° before roll recovery takes place. The time history plot of the yaw angle reveals the influence that the vertical tail plays in the aircraft's dynamic behavior. As the aircraft enters the vortex field the aircraft is seen to roll in a counterclockwise direction. This can be explained by referring back to Figure 35 which illustrates the effect of lateral displacement on the induced rolling moment coefficient. Note that the induced rolling moment coefficient reverses sign as the vortex moves toward the wing tip. Thus as the aircraft approaches the port vortex it initially rolls in the opposite direction with respect to the vortex field. The pilot's reaction to the disturbance would be to apply aileron control to roll

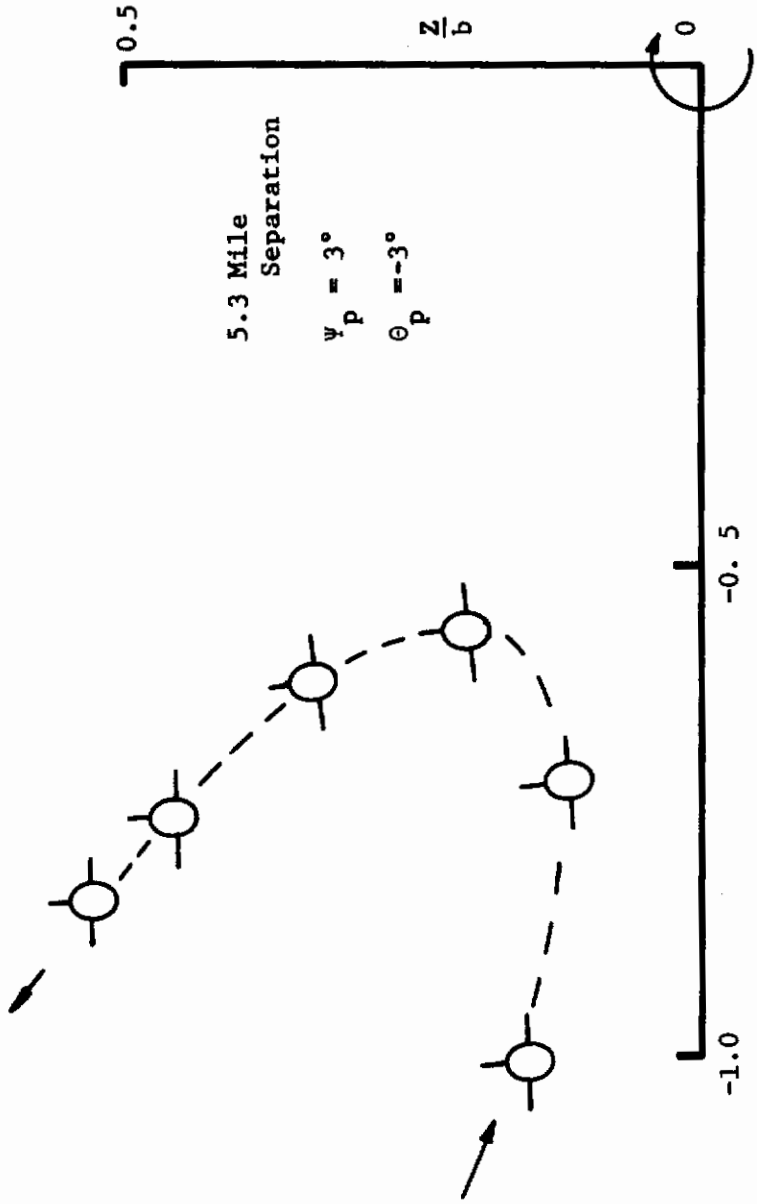

Figure 41. Business Aircraft in the Wake of a Light Jet Transport

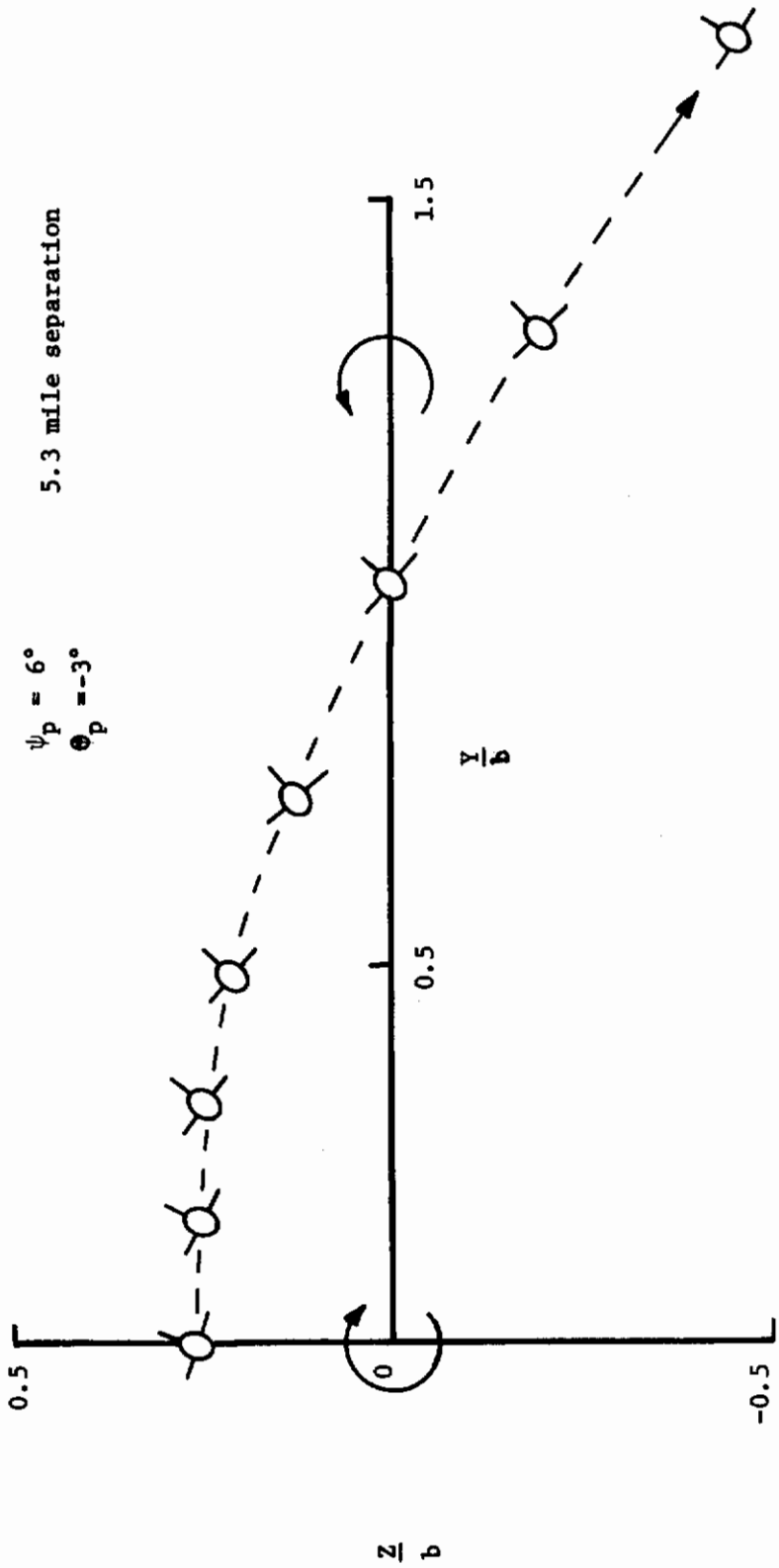

Figure 42. Business Aircraft in the Wake of a Light Jet Transport
ψ_p = 6° Θ_p =-3°

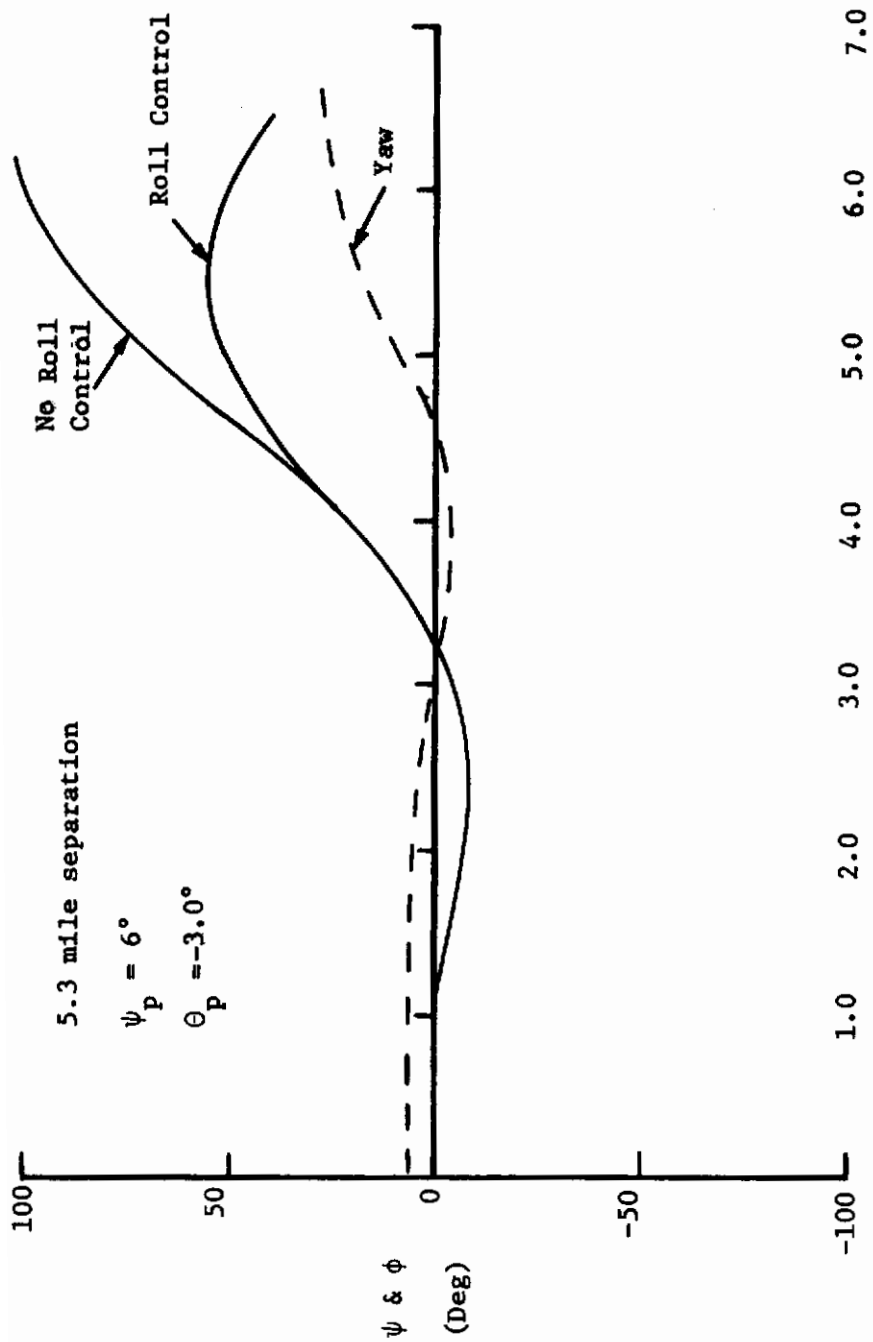

Figure 43. Business Aircraft in the Wake of Light Jet Transport
ψ_p = 6, Θ_p =-3.0°

the aircraft in a clockwise direction. Now as the aircraft nears the vortex the aircraft is rolled sharply in the clockwise direction. Thus we see that the pilot's initial reaction would momentarily be out of phase with the roll disturbance. Also during the vortex encounter the vertical tail experiences an induced velocity from the left which causes the aircraft to yaw to the left by approximately 12°. As the aircraft passes into the field of influence of the starboard vortex the upsetting roll moment tends to aid the pilot in regaining a wings level attitude. The yaw excursion to the right is due primarily to the roll orientation.

Figures 44 - 49 show the effect of varying the angle θ_p. For these calculations ψ_p is held constant. Here the aircraft is climbing into the vortex system. The angle θ_p was varied from 3° to 9°. These figures again indicate the influence of the vertical tail on the aircraft's response. As the aircraft climbs into the velocity field of the port vortex the vertical tail experiences a side velocity from the right. This gives rise to a positive yawing moment which yaws the airplane to the right. As the aircraft passes through the plane of the vortices its rate of climb diminishes and the aircraft rolls in a clockwise direction. The aircraft in Figure 44 is approximately 60 feet below and 80 feet to the left of the port vortex. However, after 8 seconds the aircraft is located 40 feet beneath the vortex plane. If the airplane had not encountered the vortex system the airplane would have been approximately 40 feet above the plane of the vortices. Similar results are shown in Figures 44 - 49. Based on the results presented here several conclusions can be made concerning the dynamic behavior of the following

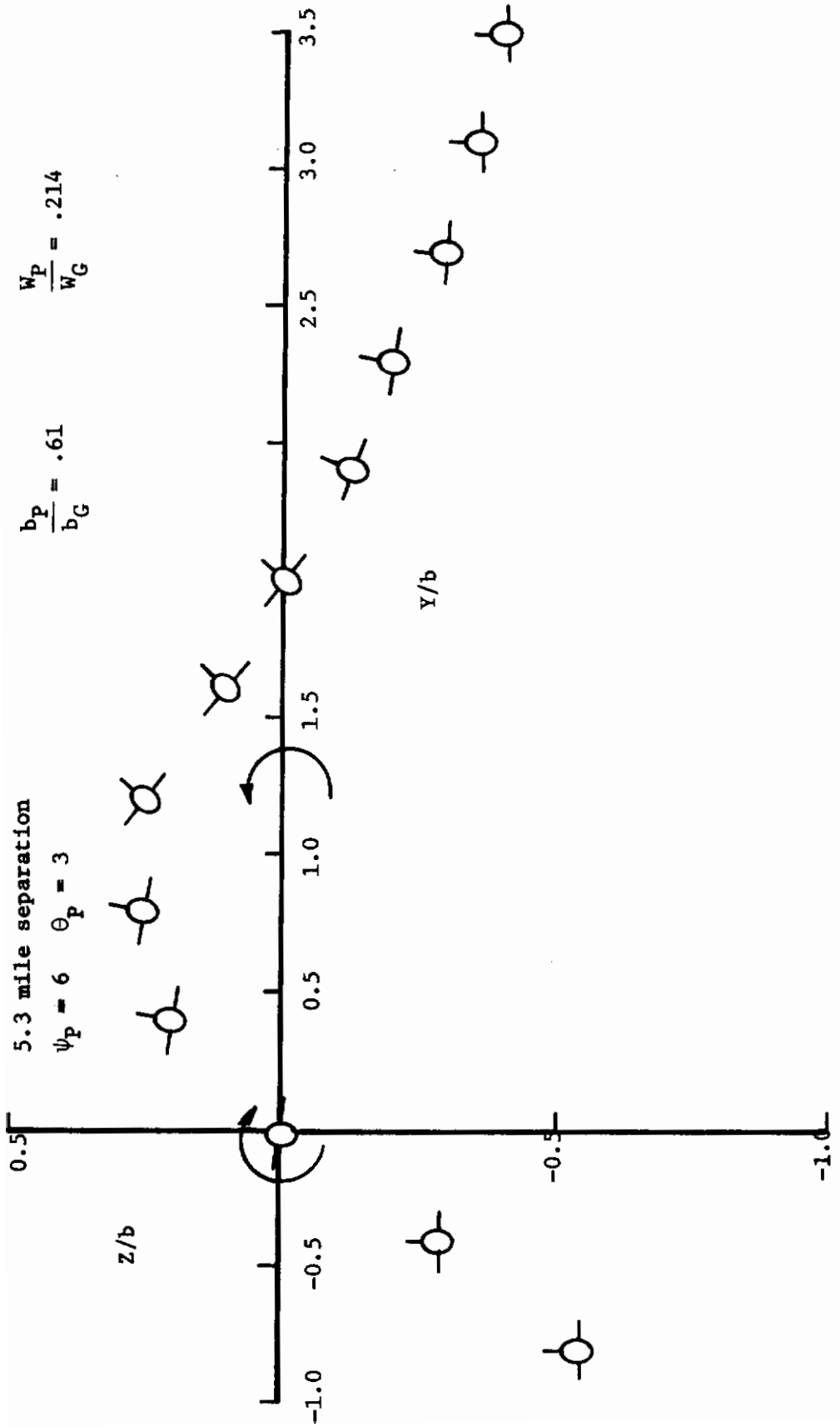

Figure 44. Business Aircraft in the Wake of a Light Transport $\psi_P = 6°$ $\Theta_P = 3°$

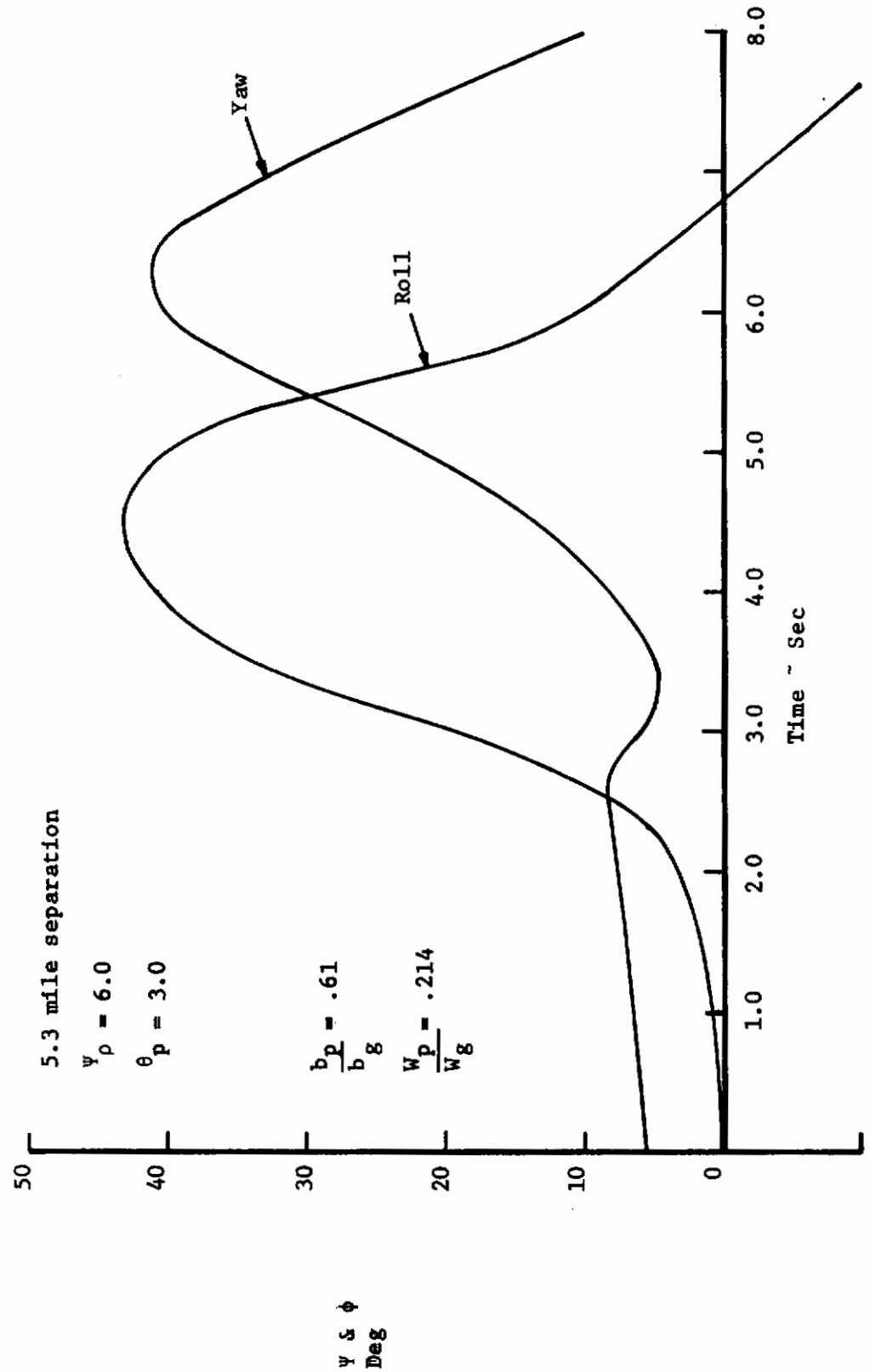

Figure 45. Business Aircraft in the wake of a Light Jet Transport $\Psi_p = 6^o$ $\theta_p = 3^o$

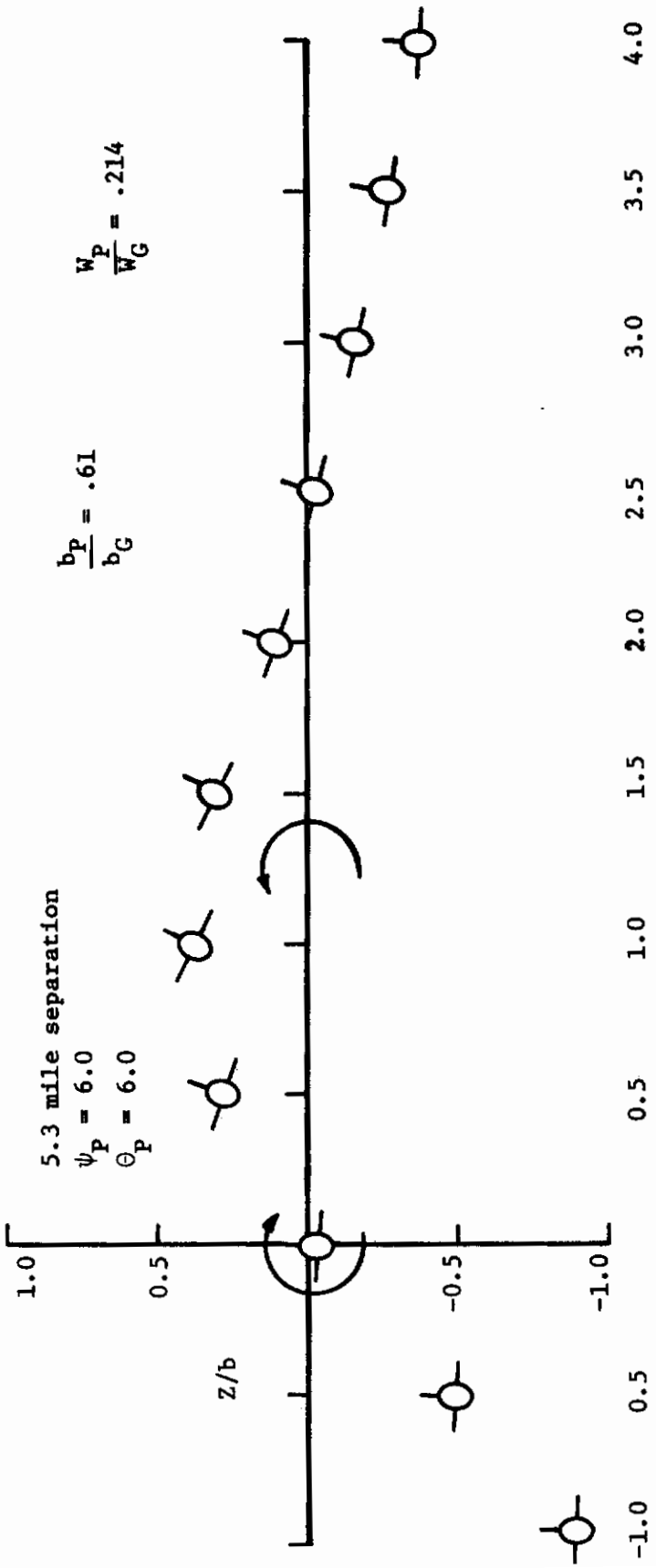

Figure 46. Business Aircraft in the Wake of a Light Jet Transport $\psi_P = 6°$, $\Theta_P = 6°$

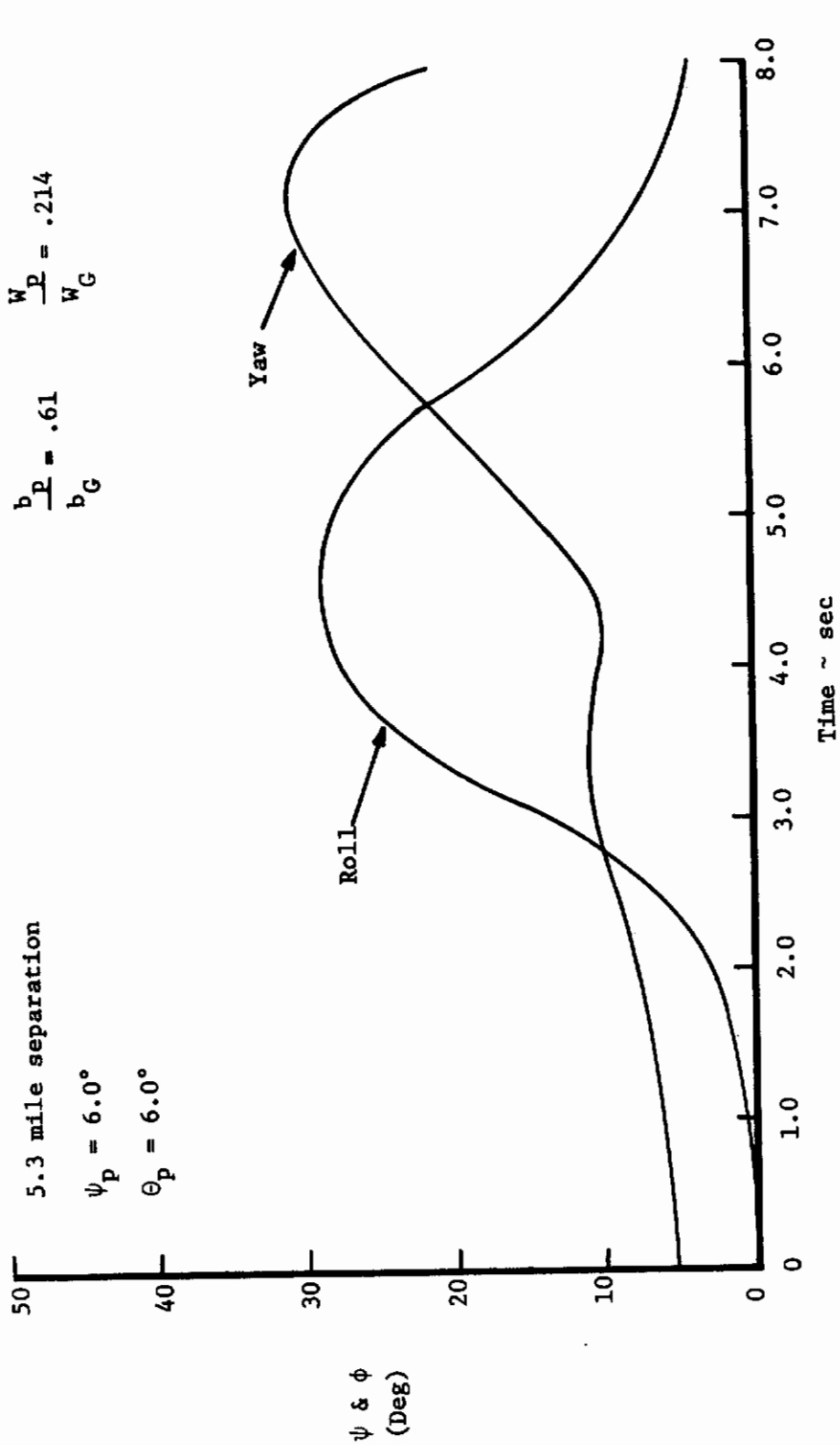

Figure 47. Business Aircraft in the Wake of a Light Jet Transport-Time History Plots

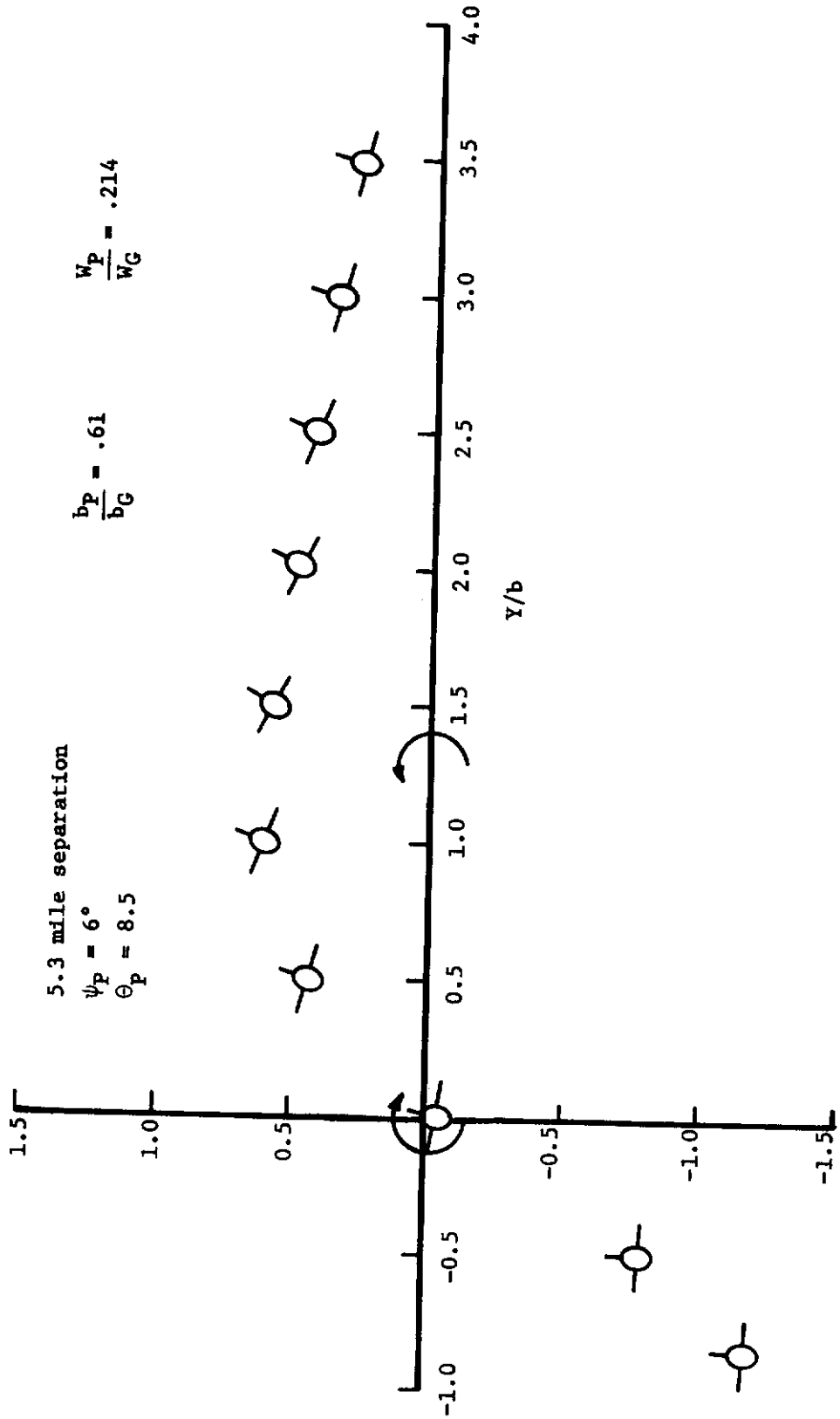

Figure 48. Business Aircraft in the Wake of a Light Jet Transport

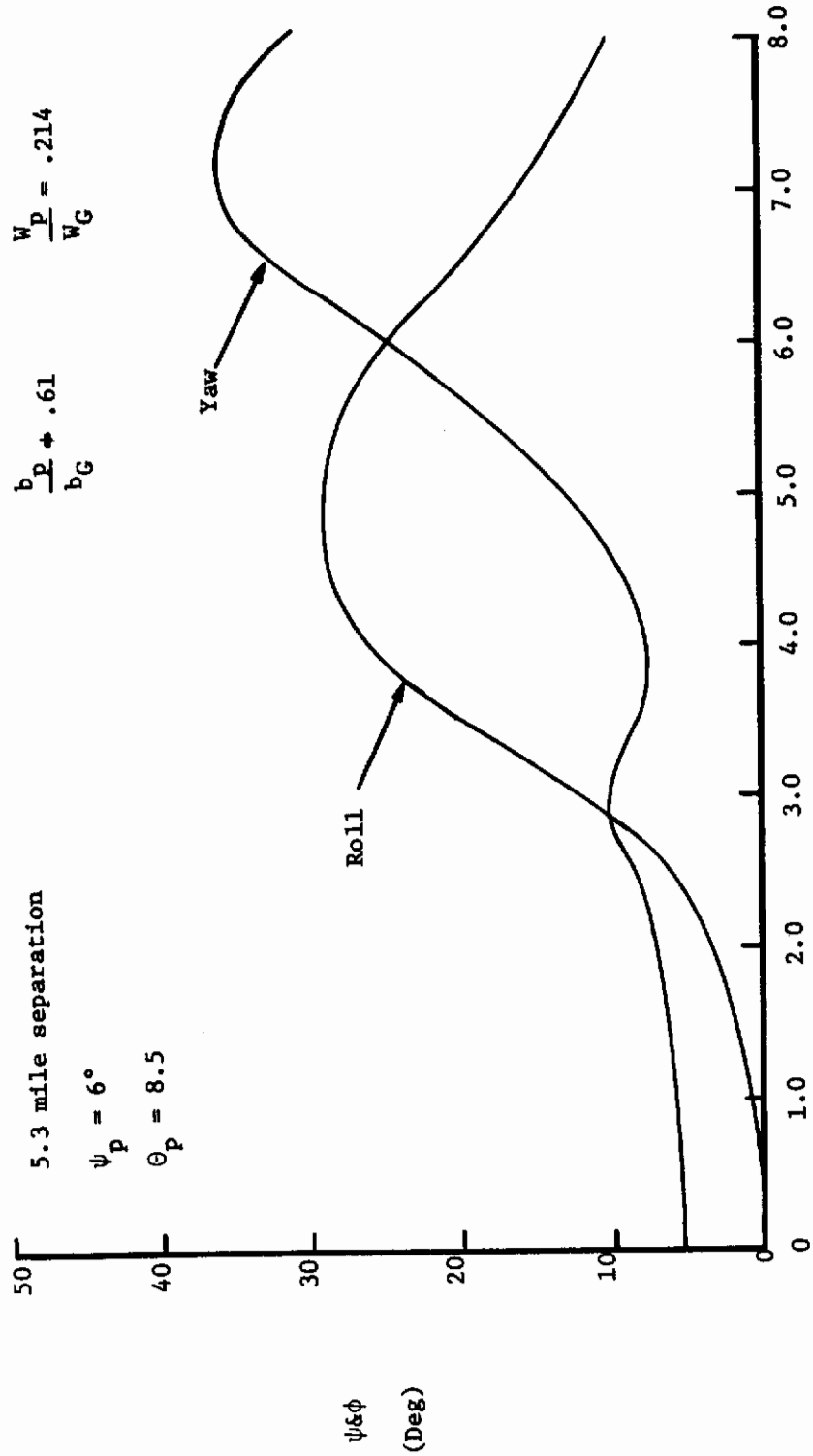

Figure 49. Business Aircraft in the Wake of a Light Jet Transport-Time History Plots

aircraft. The calculations showed that even with pilot control large excursions in roll, yaw, and altitude were experienced by the penetrating aircraft. Also, the results revealed the significant influence that the vertical tail makes to the aircraft's dynamic response. Finally for the cases considered in this section the following aircraft was in close proximity to the ground and thus the excursions shown here are completely unacceptable from a flight safety standpoint.

Additional results of the along track penetration study are shown in Figures 50 - 53. The probe aircraft selected were a Jet Star and DC-9. These aircraft were flown into the wake of either a DC-9, 727 or a DC-10. Figure 50 shows the maximum roll excursion and roll rate of the Jet Star as a function of separation distance. The figure indicates that there is very little difference in the aircraft's response at separation distances from 2 to 8 miles. This can be explained by examining Figure 51 which is a plot of the maximum induced rolling moment coefficient as a function of separation distance. The equation used in computing this curve was taken from reference 12. Note that the rolling moment coefficient decreases slowly with increasing separation distance. This is due to the method used to predict the vortex velocity distribution. Recall that McCormick's equations predict small core radii and large maximum tangential velocities. The lower portion of Figure 51 shows the velocity distributions used in computing the roll coefficient. At distances of several core radii along the span the induced velocities tend to coalesce. This is the region which contributes the major

Table IV

Characteristics of Penetrating Aircraft

Aircraft Parameters	Business Aircraft	Jet Star	DC-9
Wing Area (ft^2)	350	542	980
Span (ft)	55	53	90
Weight (lb)	15,000	38,200	70,000
Velocity (ft/sec)	190	224	232

Table V

Characteristics of Generating Aircraft

Aircraft Parameters	DC-9	727	DC-10	C-990
Wing Area (ft^2)	980	2,600	3,400	2,250.0
Span (ft)	90	142.3	155	118.0
Weight (lb)	70,000	190,000	367,000	153,000
Velocity (ft/sec)	232	243	234	245

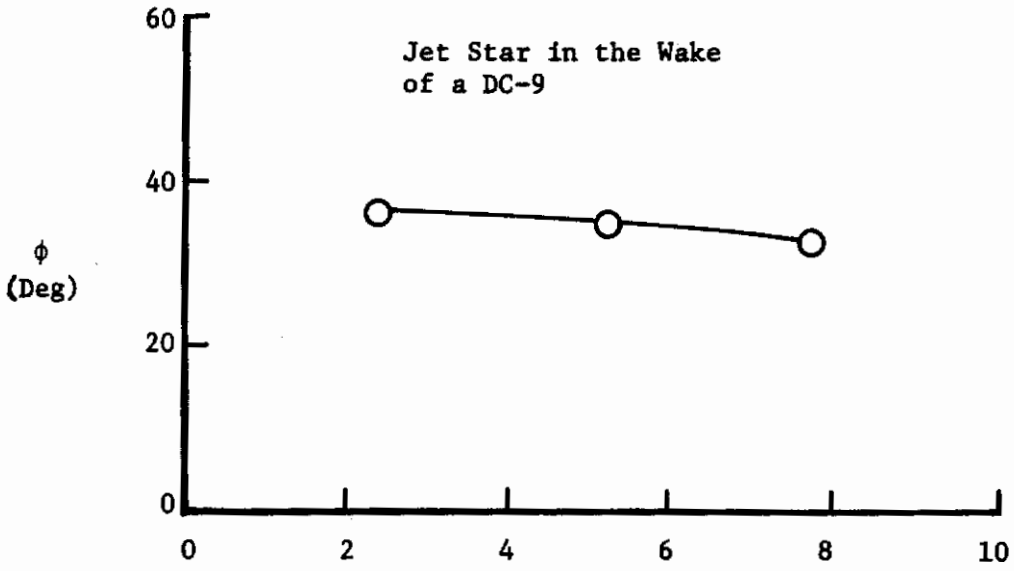

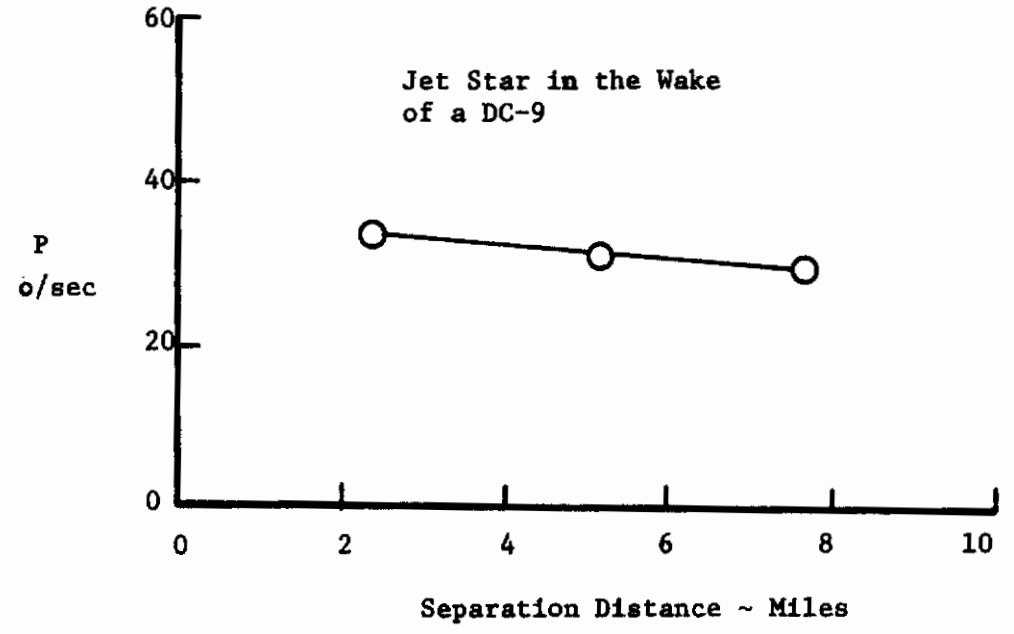

Figure 50. Maximum roll angle and roll rate of a Jet Star in the Wake of a DC-9

portion of the induced rolling moment. Therefore it follows that the roll coefficient will decrease slowly with separation distance.

As mentioned in the introduction various techniques have been proposed to modify the vortex structure. Some of the concepts which have been considered include spoiler deflection and mass injection into the vortex core. Both of these techniques reduce the maximum tangential velocity and increase the core radius. However, at a distance of several core radii from the vortex center the velocity distributions are the same as the unaltered vortex. This can be seen in Figure 11. This figure presents Marchman's data and illustrates the effect that blowing has on the vortex velocity distribution. Based on the results shown in Figure 51 it can be concluded that the vortex abatement devices will not eliminate the vortex hazard unless the device hastens the vortex break-up.

In the literature it has been suggested that the vortex hazard can be assessed by the ratio of the maximum induced acceleration to the maximum acceleration obtained with full aileron deflection. If the ratio $|P|/P_{\delta_{max}}$ is greater than 1 the aircraft is assumed to be out of control. This ratio is of course the same as the ratio $C_\ell/C_{\ell_{\delta_a}}\delta_a$ used previously. Figure 52 shows that the Jet Star flying into the wake of either a DC-9 or 727 would be uncontrollable for the separation distances shown. The roll excursion of the Jet Star in the wake of the DC-10 or 727 exceeded 200 degrees for the same separation distances. Now Figure 53 shows the same type of results for a DC-9 in the wake of either a DC-9, 727 or DC-10. The maximum roll angles exceed 40° for penetration into the wake of the 727 and DC-10.

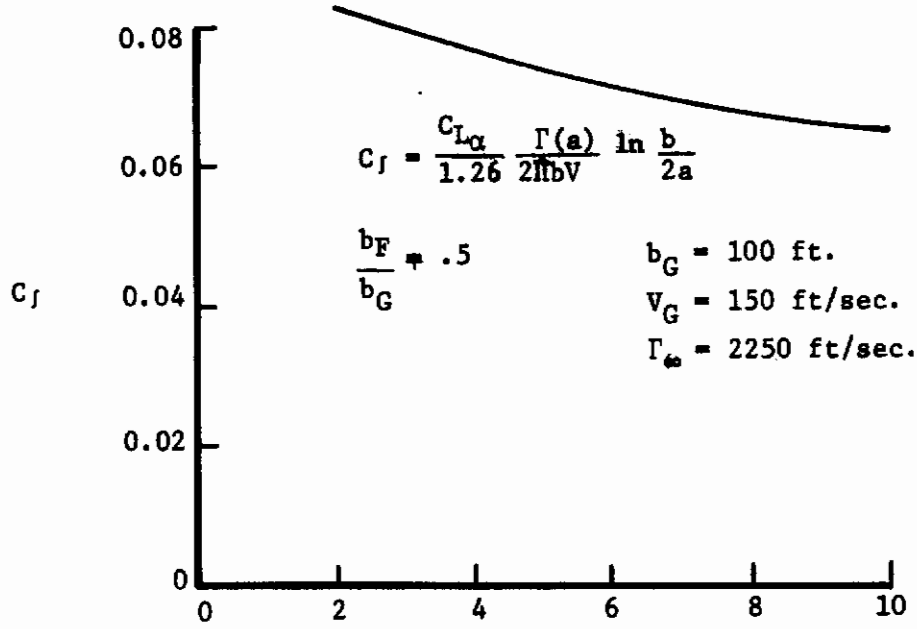

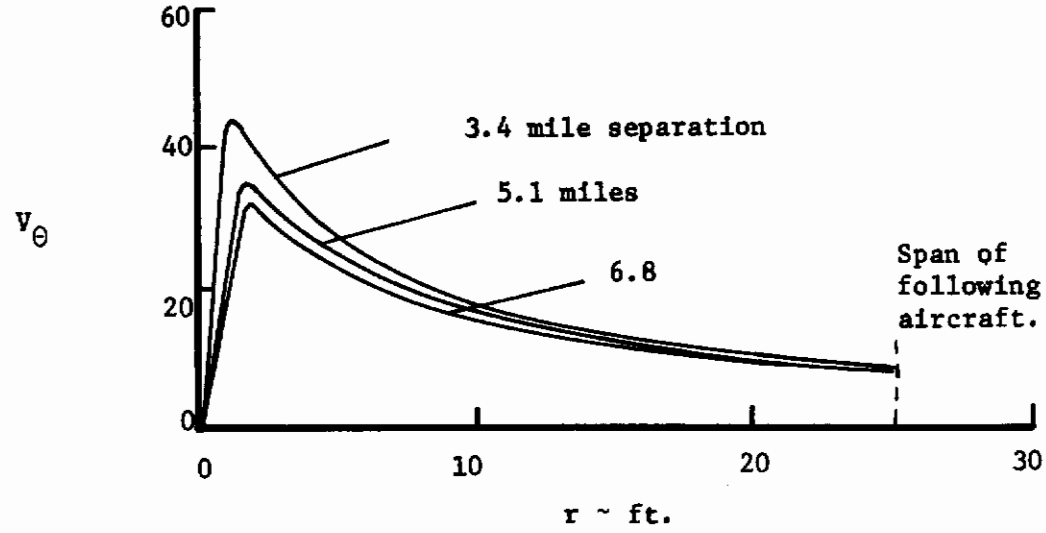

Figure 51. Maximum roll moment coefficient and vortex velocity distributions as a function of separation distance.

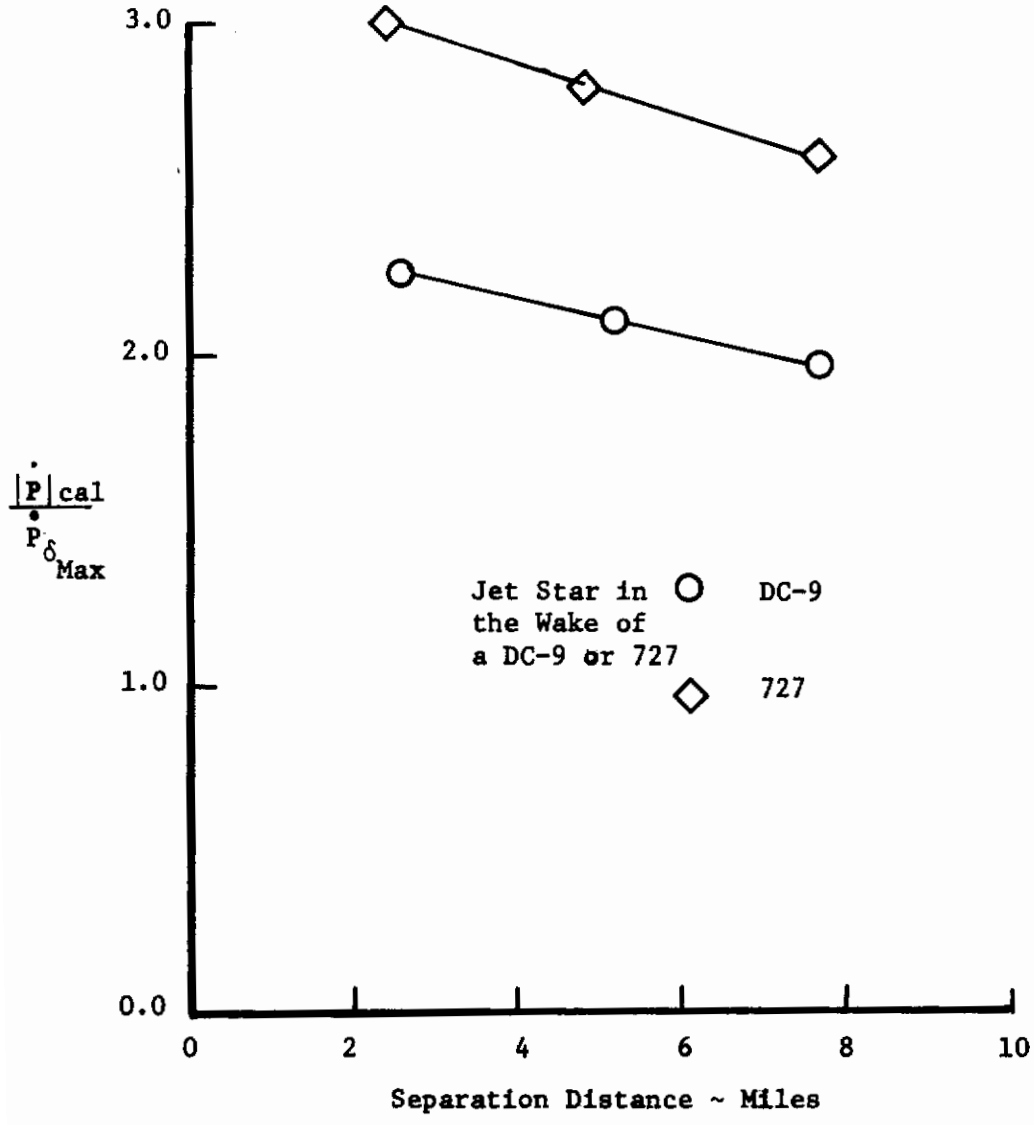

Figure 52. $|\dot{P}|cal/\dot{P}_{\delta_{Max}}$ vs. Separation Distance

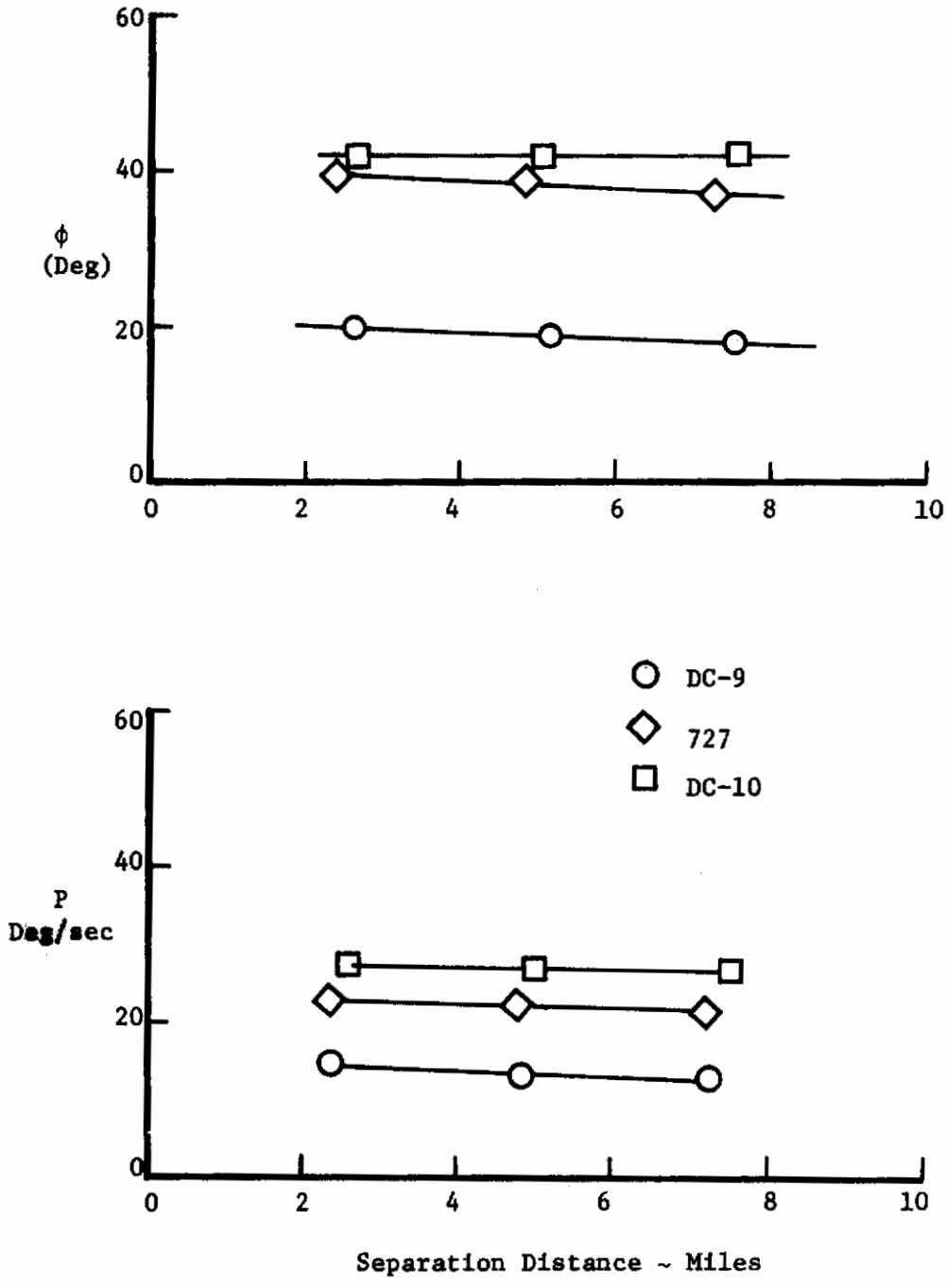

Figure 53. Maximum roll angle and roll rate of a DC-9 in the wake of a DC-9, 727 or DC-10

Whereas the maximum roll angle in the wake of the DC-9 is only 20°. The ratio $|\dot{P}|cal/P_{\delta_{max}}$ shown in Figure 54 indicates that the DC-9 is momentarily out of control when penetrating the wake of a 727, DC-9 and DC-10.

In an effort to assess the validity of the computer simulation the results were compared with flight test data obtained from Reference 62. These data were obtained by the NASA Flight Research Center. The probe aircraft were positioned by radar to a specified distance behind the generating aircraft. The probe aircraft were then flown into the vortex wake for 2 to 3 minutes in order to record sufficient response data. The vortex system of the generating aircraft were marked by entrainment of the smoke generated from the aircraft's engines. However, it was noted that there was a lack of smoke to clearly mark the wake at large separation distances.

The computed results for a DC-9 penetrating the wake of a Convair 990 are presented in Figure 55 along with the flight test data. Two calculated curves are shown in this figure. The solid curve is based on calculations including only roll control and the dashed curve for both roll and heading control. The solid curve is low in comparison to the flight test data for separation distances under 4 miles. In the 5 to 8 mile range the computed results are high. However, the flight test data exhibits considerable scatter. This is due largely to the difficulty of penetrating the vortex system. Recall Figure 35 which illustrates the effect of lateral separation on the vortex induced rolling moment. This figure indicates that if the aircraft missed the vortex core by a relatively small distance the roll excursion would be quite different. Since the pilots had difficulty

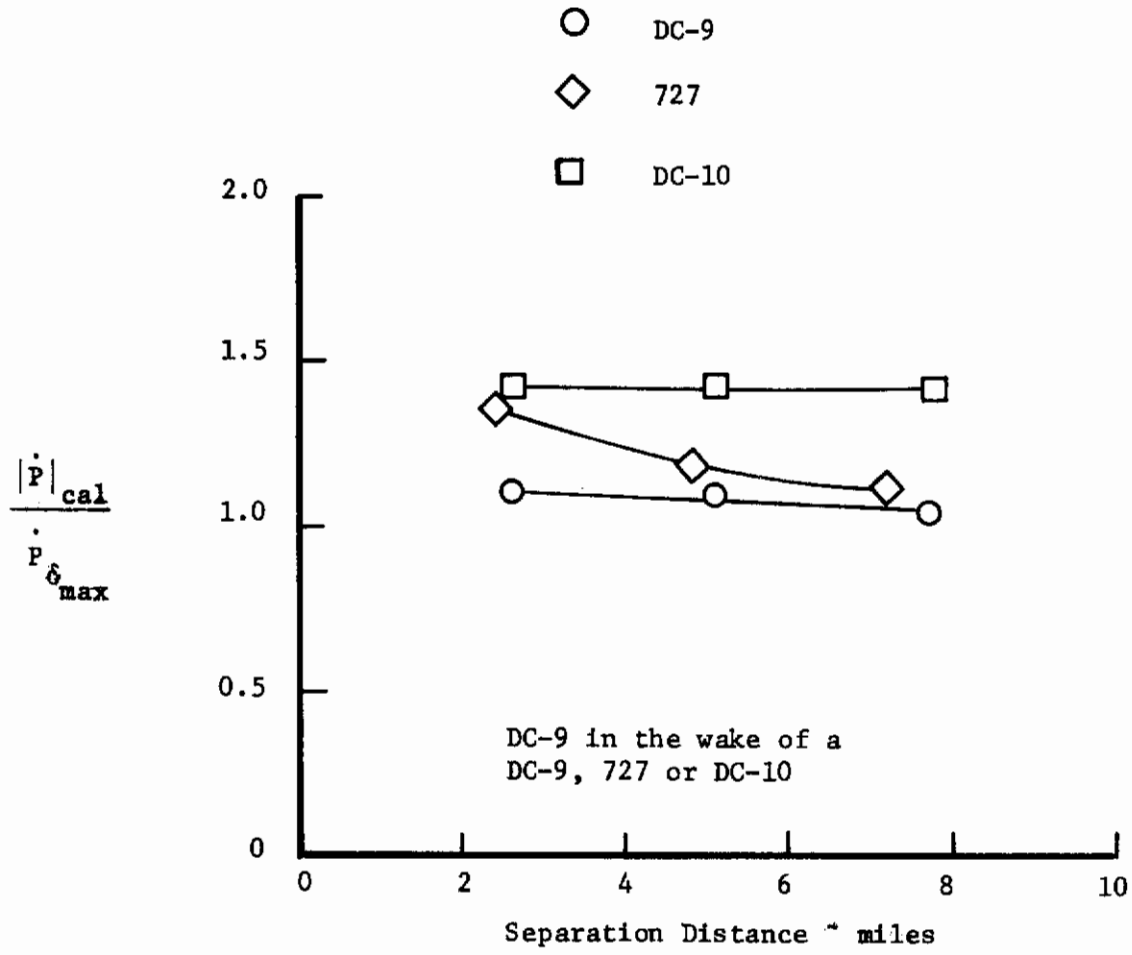

Figure 54. $|\dot{P}|_{cal} / \dot{P}_{\delta_{max}}$ vs. Separation Distance

in seeing the vortex wake at large separation distances one would expect to have scatter in the flight test data. Another factor contributing to the scatter is the break up of the vortex system.

The influence of trying to maintain heading is illustrated by the dashed curve. By maintaining heading the pilot increases the roll upset. As previously shown the aircraft is rapidly expelled from the vortex system and thus by trying to hold his heading the pilot keeps the aircraft in the influence of the vortices for a longer time. This then gives rise to larger roll excursions. Based on this comparison it is felt that the results of the computer simulation are representative of the actual aircraft-vortex encounters.

Figure 56 is a time history plot of the roll and yaw angle. The pilot model is successful in maintaining the aircraft's heading. In this case the roll excursion is essentially the same. The difference between this and the preceding case is the penetration angle ψ_p. In the second example the pilot is attempting to maintain an oblique angle to the vortex axis. However, in the results shown in Figure 55 the pilot is attempting to fly right along the vortex axis.

Numerous cases of cross track penetration were calculated. The results shown in Figures 57 and 58 are representative of the cases studied. The normal load factors without control input compare favorably with the results obtained in previous investigations.[4, 5, 6] However, when pilot control was added the normal load factor was increased slightly which is quite different from the results shown in Figure 3. The results of this study indicate that structural failure is not a serious threat to the penetrating aircraft. Figure 58 shows the angle of attack time history. Notice that the wing is stalled

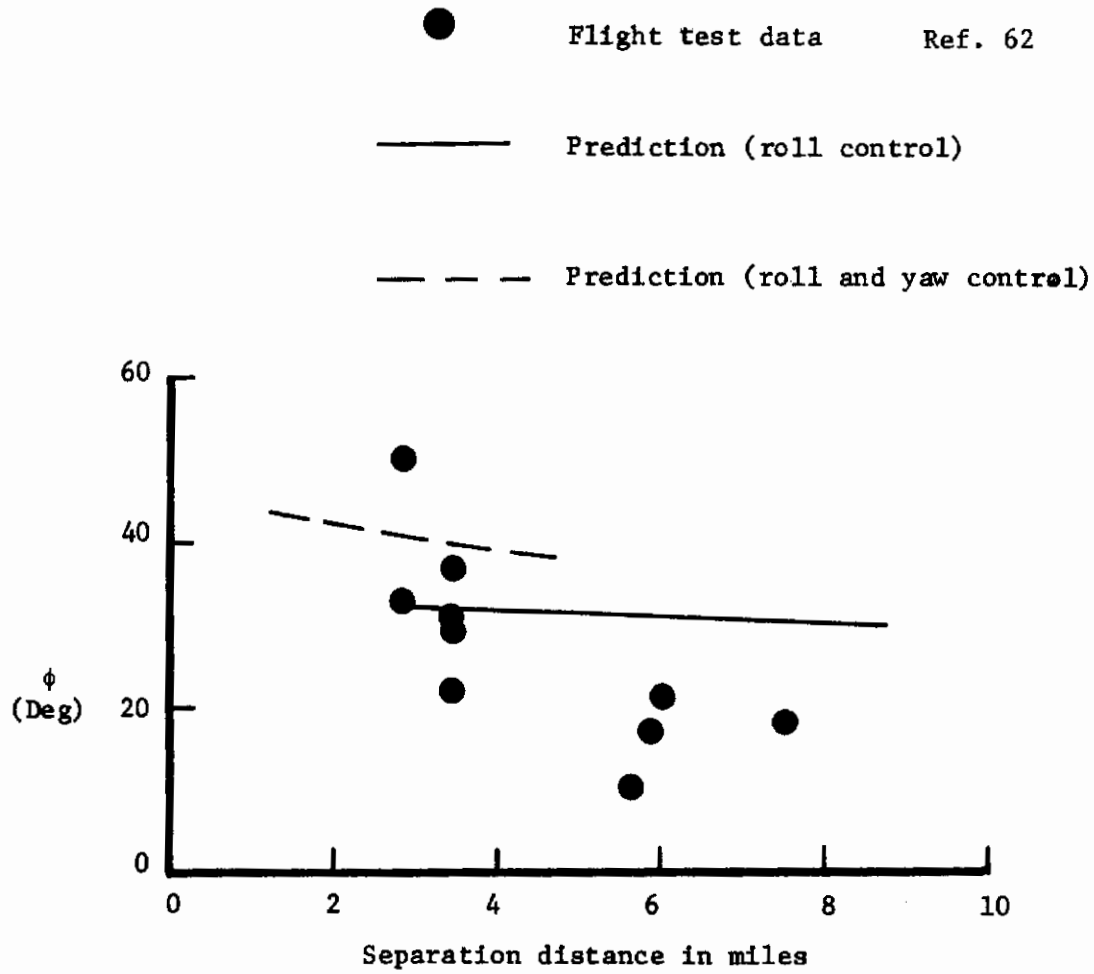

Figure 55. Maximum roll angle of a DC-9 in the Wake of a Convair 990

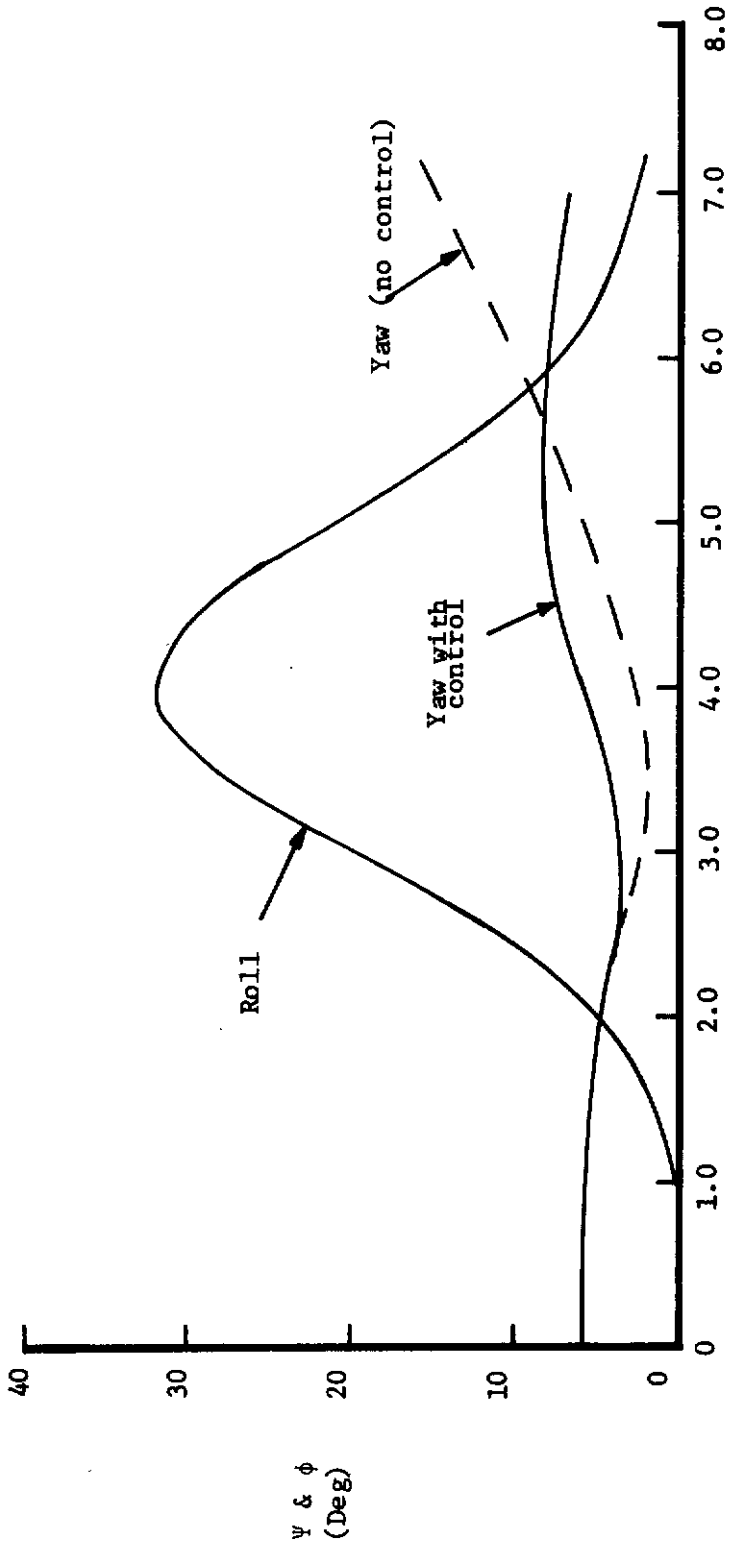

Figure 56. DC-9 in the wake of a Convair 990 - Time History Plot

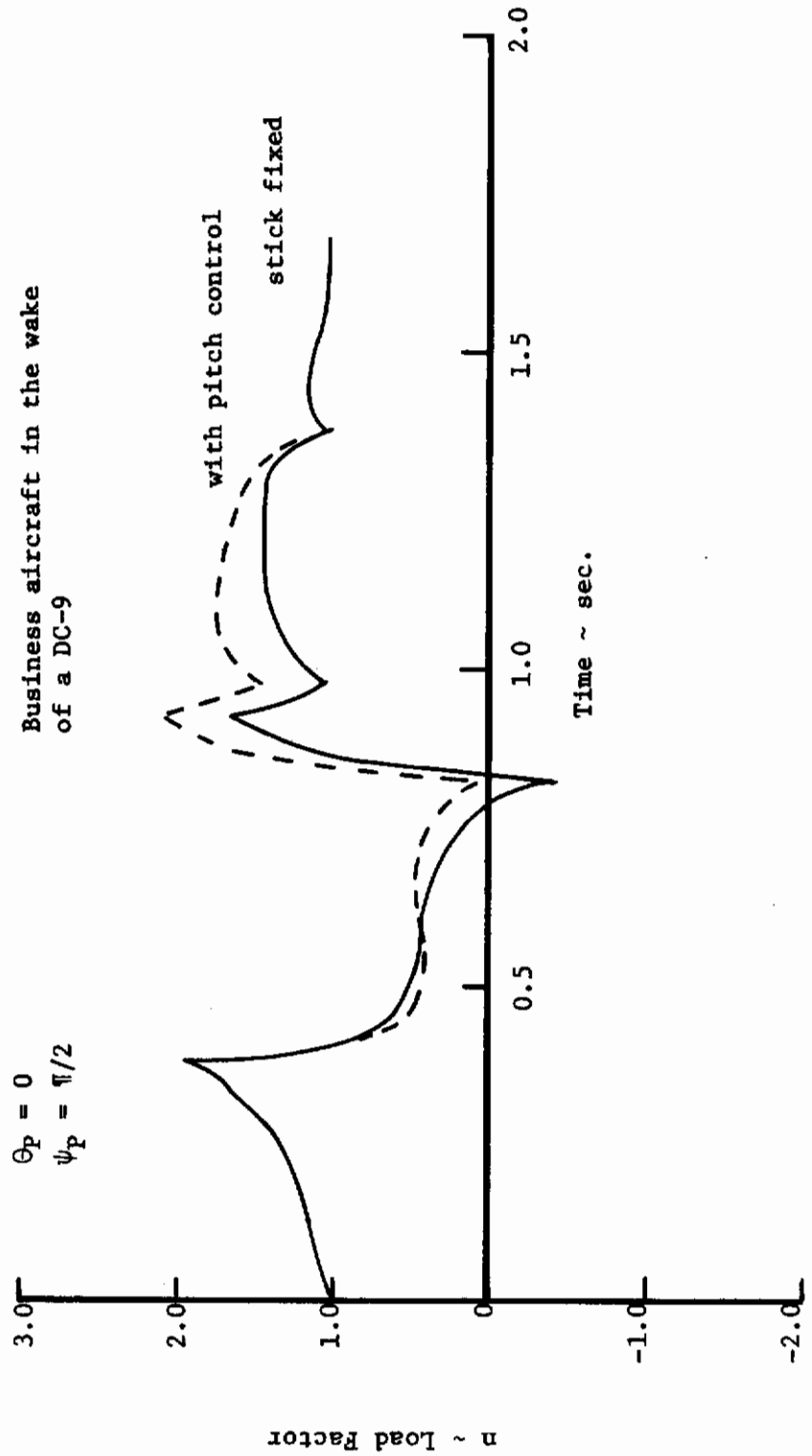

Figure 57. Normal Load Factor vs. Time
(Transverse Penetration)

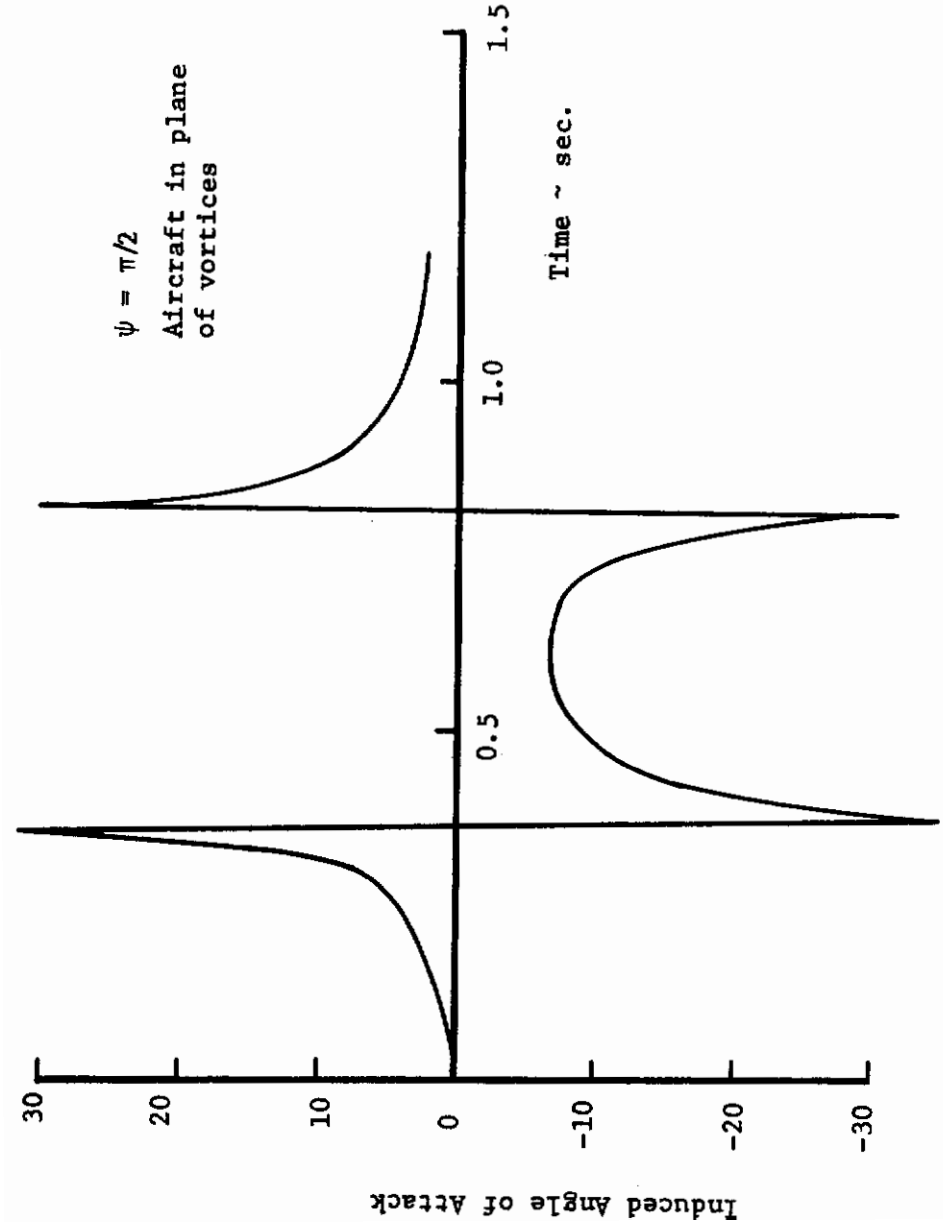

Figure 58. Vortex Induced Angle of Attack (Transverse Penetration)

for a fraction of a second; however, the aircraft does not have time to develop any appreciable vertical velocity.

SECTION V

CONCLUSIONS

Based on the results presented in the previous section the following conclusions have been reached concerning the dynamic behavior of an aircraft penetrating a vortex wake.

1. Encountering a vortex can produce rolling moments on the aircraft in either direction.
2. The pilot's reaction to the roll disturbance can be momentarily out of phase with the upsetting roll moment.
3. An aircraft descending into a vortex can experience completely different types of response depending upon the penetration angle ψ_p. For very shallow angles the aircraft is rolled away from the vortex system. As ψ_p increases the aircraft is rapidly rolled to a very large roll orientation.
4. Aircraft climbing into the vortex system will experience large roll, yaw and altitude excursions.
5. Reduction of the maximum vortex tangential velocity does not significantly reduce the hazard of a vortex encounter.
6. The calculated results agree favorably with flight test data for up to 5 miles. At distances greater than 5 miles the computed results were too high.
7. The pilot can increase the roll upset by trying to maintain his heading. In so doing the aircraft remains in the vortex field for a longer time resulting in a larger roll excursion.
8. In the transverse penetration the pilot's control input did not appreciably increase the load factor as shown in previous

studies. For the aircraft used in this study the results indicate that structural failure is not a serious threat to the penetrating aircraft.

9. The results show that corporate and light jet transports cannot mix safely with the heavier jet transports at distances less than at least 8 miles.

10. Admittedly the probability of encountering a vortex wake is still quite small; however, if the separation distances are reduced the possibility of an encounter will definitely increase. The results of this study indicate that reduced separation distances are unacceptable from a flight safety viewpoint.

References

1. Anon., "The National Aviation System Plan - Ten Year Plan 1973 - 1982", DOT, FAA Appendix 2, March 1972.

2. Corsiglia, V.R., Jacobsen, R.A., and Chigier, N., "An Experimental Investigation of Trailing Vortices Behind a Wing with a Vortex Dissipator", Aircraft Wake Turbulence and its Detection, Edited by J. Olsen, A. Goldberg, and M. Rogers, Plenum Press, New York, 1971.

3. Bleviss, Zegmund O., "Theoretical Analysis of Light Plane Landing and Take-off Accidents Due to Encountering the Wakes of Large Airplanes". Report No. SM-18647, Douglas Aircraft Co., December 1954.

4. McGowan, W.A., "Calculated Normal Load Factors on Light Airplanes Traversing the Trailing Vortices of Heavy Transport Airplanes", NASA TND - 829, March 1961.

5. McGowan, W.A., "Trailing Vortex Hazard", SAE Transactions, Report No. 68-220 Vol 77, 1968.

6. McGowan, W.A., "NASA Aircraft Trailing Vortex Research", Presented at the Federal Aviation Administration's Symposium on Turbulence, March 1971.

7. Wetmore, J.W. and Reader, J.P., "Aircraft Vortex Wakes in Relation to Terminal Operations", NASA TND-1777, April 1973.

8. Hackett, J.E. and Theisen, J.G., "Vortex Wake Development and Aircraft Dynamics" Aircraft Wake Turbulence and its Detection, Edited by J. Olsen, A. Goldberg, and M. Rogers, Plenum Press, New York, 1971.

9. Andrews, A.H., "Flight Evaluation of Wing Vortex Wake Generated by Large Jet Transports", Presented at the Symposium of Aircraft Wake Turbulence held in Seattle, Wash. Sept 1970.

10. Andrews, A.H., "Flight Evaluation of Wing Vortex Wake Generated by Large Jet Transports", Aircraft Wake Turbulence and its Detection, Edited by J. Olsen, A. Goldberg, and M. Rogers, Plenum Press, New York, 1971.

11. Condit, P.M. and Tracy, P.W., "Results of the Boeing Company Wake Turbulence Test Program", Aircraft Wake Turbulence and its Detection, Edited by J. Olsen, A. Goldberg, and M. Rogers, Plenum Press, New York, 1971.

12. Bernstein, S. and Iversen, J.D., "Dynamic Simulation of an Aircraft Under the Effect of Vortex Wake Turbulence", AIAA 2nd Atmospheric Flight Mechanics Conference September 11-13, 1972.

13. Nelson, R.C., and McCormick, B.W., "Aircraft-Vortex Penetration", SAE Paper 730296, April 1973.

14. McCormick, B.W., "Aircraft Wakes; A survey of the Problem", presented at the FAA Symposium on Turbulence, Washington, D.C., March 1971.

15. Lamb, H., "Hydrodynamics" 6th edition, Dover, New York, 1932.

16. Rose, R. and Dee, F.W., "Aircraft Vortex Wakes and their Effects on Aircraft", RAE Technical Note Aero 2934, 1963.

17. Bisgood, P.L., Maltby, R.L., and Dee, F.W., "Some Work at the Royal Aircraft Establishment on the Behavior of Vortex Wakes", Aircraft Wake Turbulence and its Detection, Plenum Press, 1971.

18. Squire, H.B., "The Growth of a Vortex in Turbulent Flow", ARC 1966, 1954.

19. Newman, B.G., "Flow in a Viscous Trailing Vortex", Aero Quarterly Vol 10, Part 2, 1959.

20. Dosanjh, D.S., Gasparek, E.P., Eskinayi, S., "Decoy of a Viscous Vortex", Aeronautical Quarterly, Vol 13, Part 2, May 1962.

21. Kurylowich, G., "Analysis Relating to Aircraft Vortical Wakes", AFFDL/FGC TM-73-32, February 1973.

22. Poppleton, E.D., "Effect of Air Injection into the Core of a Vortex", Engineering note in the Journal of Aircraft, Vol 8, No 3, May 1968.

23. McCormick, B.W., Tangler, J.L., Sherrieb, H.E., "The Structure of Trailing Vortices", Journal of Aircraft, Vol 5, No 3, May 1968.

24. Hoffman, E.R. and Joubert, P.N., "Turbulent Line Vortices", Journal of Fluid Mechanics, Vol 16, Part 3, July 1963.

25. Eisenhuth, J.J., McCormick, B.W., Nelson, R.C. and Garodz, L., "Analysis of Experimental Measurements of Trailing Vortex Systems of Large Jet Transport Aircraft", NAECON 71 Record 1971.

26. Donaldson, C., "A Brief Review of the Aircraft Trailing Vortex Problem", NAECON Conference, Dayton, Ohio, May 1971.

27. Donaldson, C. and Sullivan, H.D., "Calculation of the Wakes of Three Transport Aircraft in Holding Take-off and Landing Configurations and Comparison with Experimental Measurements", ARAP Report No. 190, January 1973.

28. Betz, A., "Behavior of Vortex Systems", NACA-TM-713, June 1973.

29. Garodz, L.J., "NAFEC, Investigation of Relatively Long Time - History Vortex Characteristics of the Convair CV-880 Airplane in Terminal Area - Type Flight Operations", Data Report, Project No. 504-303-03X, November 1970.

30. Garodz, L.J., Hanley, W.J. and Miller, N.J., "Abbreviated Investigation of Lockheed L-1011 Airplane Vortex Wake Characteristics in Terminal Area-Type Operations". FAA Data Report, FS-1-73, June 1972.

31. Garodz, L.J., Hanley, W.J. and Miller, N.J., "Abbreviated Investigation of Douglas DC-10 Airplane Vortex Wake Characteristics In Terminal Area-Type Operations", FAA Data Report FS-2-73, August 1973.

32. Garodz, L.J., "Measurements of Vortex Wake Characteristics of the Boeing 747, Lockheed C5A, and Other Aircraft", FAA Data Report Project No. 177-621-03X, April 1970.

33. Garodz, L.J., "Federal Aviation Administration Full-Scale Aircraft Vortex Wake Turbulence Flight Test Investigations: Past, Present, Future", AIAA Paper 71-97, January 1971.

34. Marchman, J.F. and Mason, W.H., "Farfield Structure of an Aircraft Trailing Vortex, Including Effects of Mass Injection", NASA CR-62078, April 1972.

35. Falkner, V.M., "The Calculation of Aerodynamic Loading on Surfaces of Any Shape", ARC R&M 1910, 1943.

36. Hedman, S.G., "Vortex Lattice Method for Calculation of Quasi Steady State Loading on Thin Elastic Wings", Report 105, Aeronautical Research Institute of Sweden, 1965.

37. Giesing, J.P., Kalman, T.P. and Rodden, W.P., "Subsonic Unsteady Aerodynamics for General Configurations", Parts I and II, AFFDL-TR-71-5, 1971.

38. Rubbert, P.E., "Theoretical Characteristics of Arbitrary Wings by a Nonplanar Vortex Lattice Method", Report D6-9244, Boeing Co., Seattle, Washington, 1964.

39. Woodward, F.A., "Analysis and Design of Wing-Body Combinations at Subsonic and Supersonic Speeds", Journal of Aircraft, Vol 5, No 6, December 1968.

40. Albano, E. and Rodden, W.P., "A Doublet-Lattice Method for Calculating Lift Distributions on Oscillating Surfaces in Subsonic Flows", AJAA Journal, Vol 7, No 2, February 1969.

41. Rudhman, W.E., "A Numerical Solution of the Unsteady Airfoil with Application to the Vortex Interaction Problem" Master Thesis, Aerospace Engineering Department, Pennsylvania State University, December 1970.

42. Reissner, E., "Effect of Finite Span on the Airload Distribution for Oscillating Wings", NACA TN 1194, 1947.

43. James, R.M., "On the Remarkable Accuracy of the Vortex Lattice Discretization in Thin Wing Theory", Douglas Aircraft Company, February 1969.

44. DeYoung, J., "Convergence-Proof of Discrete-Panel Wing Loading Theories", Journal of Aircraft, Vol 8, No 10., October 1971.

45. Houbolt, J. C., and Kordes, E.E., "Structural Response to Discrete and Continuous Gusts of an Airplane Having Wing Bending Flexibility and a Correlation of Calculated and Flight Results", NACA Report 1181, 1954.

46. Jackson, C.E. and Wherry, J.E., "A Comparison of Theoretical and Experimental Loads on the B-47 Resulting From Discrete Vertical Gusts", Journal of Aerospace Sciences, Vol 26, No 1, January 1959.

47. Franklin, J.A., "Turbulence and Lateral Directional Flying Qualities", NASA CR-1718, 1971.

48. Franklin, J.A., "Turbulence and Longitudinal Flying Qualities", NASA CR-1821, 1971.

49. Ekin, B., "Dynamics of Atmospheric Flight", John Wiley and Sons, New York, 1972.

50. Diamantides, N.D., "A Pilot Analog for Airplane Pitch Control", Journal of the Aeronautical Sciences, Vol 25, No 6. June 1958.

51. McRuer, D.T., "Analysis of Multiloop Vehicular Control Systems", ASD-TR 62-1014, March 1964.

52. Magdaleno, R.E. and McRuer, D.T., "Effect of Manipulator Restraints on Human Operator Performance", AFFDL TR-66-72, December 1966.

53. Anderson, R.O., "A New Approach to Specification and Evaluation of Flying Qualities", AFFDL-TR-69-120, December 1969.

54. Dillow, J., "The 'Paper Pilot' - A Computer Program to Predict Pilot Rating for the Hover Task", AFFDL TR-70-40.

55. Naylor, F., "Predicting Roll Task Flying Qualities with 'Paper Pilot'", Masters Thesis, Air Force Institute of Technology, Dayton, Ohio 1972.

56. Adams, J., "Analysis of Aircraft Lateral-Directional Handling Qualities using Pilot Models", AIAA Paper No 72-962, September 1972.

57. Adams, J., "Human Transfer Functions in Multiaxis and Multiloop Control Systems", NASA TN-D-3305, April 1966.

58. Onstott, E.D., and Salmon, E.P., "Airplane Flying Characteristics in Turbulence", AFFDL-TR-70-143, February 1971.

59. Skelton, G.B., "Investigation of the Effects of Gusts on V/STOL craft in Transition and Hover", AFFDL-TR 68-85, October 1968.

60. Beckett, R., and Hurt, J., "Numerical Calculations and Algorithms", McGraw Hill Book Company, New York, 1967.

61. Robinson, G.H., and Larson, R.R., "A Flight Evaluation of Methods for Predicting Vortex Wake Effects on Trailing Aircraft", NASA TN-D 6904, November 1972.

62. Andrews, W.H., Robinson, G.H, and Larson, R.R., "Exploratory Flight Investigation of Aircraft Response to the Wing Vortex Wake by Jet Transport Aircraft", NASA TN 6655, March 1972.

63. Seckel, E., "Stability and Control of Airplanes and Helicopters", Academic Press, New York 1964.

64. Ashkenas, I.L., and McRuer, D.T., "Approximate Airframe Transfer Functions and Applications to Single Sensor Control Systems", WADC 58-82, 1958.

65. McRuer, D.T., Graham, D., and Krendel, E.S., "Manual Control of Single-Loop Systems," Part II, Journal of the Franklin Institute Vol 283, No. 2, February 1967.

Appendix A

Selection of Pilot Parameters

The pilot parameters were selected on the basis of the rules presented in Chapter III. In order to apply these rules the open loop transfer function for the desired control task must be developed. The equations used in selecting the pilot parameters are presented for the following control tasks:

1. Pure Roll
2. Roll and Heading Control
3. Pure Pitch

Roll Control

The equation governing the rolling motion of an airplane can be expressed in terms of the Laplace transform variable as

$$(s^2-L_p s)\phi = L_{\delta_a}\delta a$$

or rewritten to form the roll angle/aileron deflection transfer function

$$\frac{\phi(s)}{\delta_a(s)} = \frac{L\delta_a}{s(s-L_p)}$$

Previously it was stated that the pilot could be modeled by a gain, simple lead term, and a time delay which in mathematical notation yields

$$Y_{p_\phi} = \frac{\delta_a(s)}{\phi_e(s)} = K_{p_\phi}\ (\tau_{L_\phi}s+1)e^{-\tau_e s}$$

where $\tau_e = .25$ seconds. Now the open loop transfer function can be formed by taking the product of the aircraft and pilot transfer functions.

$$Y_{O.L.} = Y_{p_\phi} Y_A = \frac{\delta_a(s)}{\phi_e(s)} \frac{\phi(s)}{\delta_a(s)} = \frac{\phi(s)}{\phi_e(s)}$$

$$Y_{O.L.} = \frac{\phi(s)}{\phi_e(s)} = \frac{K_{p_\phi} \tau_{L_\phi} L_{\delta_a} (s+1/\tau_{L_\phi})}{s(s-L_p)} e^{-\tau_e s}$$

It has been found by experimentation that pilots adopt an equalization term so that they cancel the roll mode. That is the pilots lead term is fixed by the roll root $T_R = 1/L_p$. The pilot's gain K_{p_ϕ} was calculated from an expression taken from Reference 63. For a well damped response K_{p_ϕ} was related to the L_p and L_{δ_a} as follows:

$$K_{p_\phi} = \frac{L_p^2}{2L_{\delta_a}}$$

Heading and Roll Control

Assuming the roll axis to be handled as explained above the heading transfer function can be approximated by the following expression.

$$\frac{\psi}{\delta} = \frac{N_\delta (s+1/\tau_{\psi_1})}{s(s^2+2\zeta_d \omega_d s+\omega_d{}^2)}$$

where

$$1/\tau_{\psi_1} = (Y_v - \frac{Y_\delta}{N_\delta} N_\beta)$$

$$2\zeta_d \omega_d = -(Y_v + N_r)$$

$$\omega_d{}^2 = N_\beta$$

Now the open loop transfer function can be written.

$$\frac{\psi}{\psi_e} = \frac{K_{p_\psi} T_{L_\psi} N_\delta (s+1/\tau_{\psi_1})(s+1/T_{L_\psi}) e^{-\tau s}}{s(s^2+2\zeta_d \omega_d s+\omega_d{}^2)}$$

The rules stated in Chapter III call for a selection of pilot lead and gain so that the phase margin lies between 50 and 100 degrees. The lead term can therefore be adjusted to satisfy the phase margin requirement while the gain can be varied to ensure that the open loop crossover frequency falls in the vicinity of 1.0 radians per second. Figure 59 shows a block diagram sketch of the pilot-vehicle system as well as a Bode plot of the open loop transfer function.

Pitch Control

The pitch angle/elevator deflection transfer function can be obtained by solving the longitudinal set of equations.

$$(s-X_u)u - (X_w s + X_w)w - (X_q s - g)\theta = X_\delta \delta$$
$$-Z_u u + (s-Z_w s - Z_w)w - (U_o + Z_q)s\theta = Z_\delta \delta$$
$$-M_u u - (M_w s + M_w)w + (s^2 - M_q s)\theta = M_\delta \delta$$

solving for $\theta(s)/\delta(s)$ yields

$$\frac{\theta(s)}{\delta(s)} = \frac{A_\theta s^2 + B_\theta s + C_\theta}{\Delta long}$$

where

$$\Delta long = [s^2+2(\delta\omega)_p s+\omega_p{}^2][s^2+2(\zeta\omega)_{sp} s+\omega_{sp}{}^2]$$

The terms A_θ, B_θ, C_θ, $(\zeta\omega)_p$ etc. are related to the aircraft's stability derivatives. Ashkenas and McRuer[64] have shown that the following approximations can be made for the numerator

$$A_\theta s^2 + B_\theta s + C_\theta \simeq A_\theta (s+\frac{1}{\tau_\theta})(s+1/\tau_{\theta_2})$$

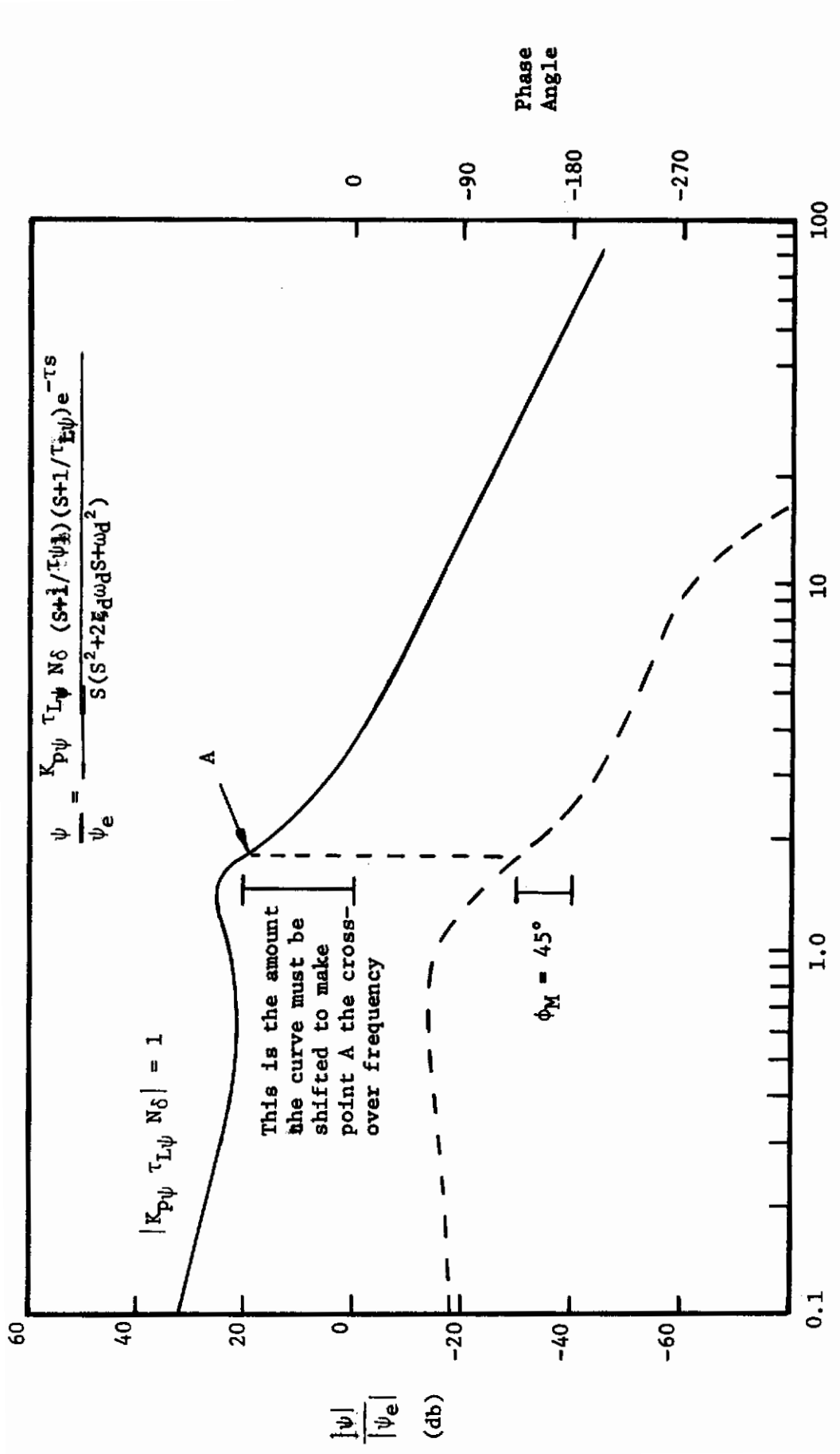

Figure 59. Bode Plot of Heading Transfer Function

where

$$A_\theta = M_\delta$$

$$1/T_{\theta_1} = -X_u + X_w \frac{Z_u}{Z_w}$$

$$1/T_{\theta_2} = -Z_w$$

and for the denominator

$$2\,\delta\,\omega_{sp} = -\,(Z_w + M_q + M_\alpha)$$

$$\omega_{sp} = Z_w\,M_q - M_\alpha$$

$$2\,\delta\,\omega_p = -X_u\,\frac{M_u(X_\alpha - g)}{Z_w\,M_q - M_\alpha}$$

$$\omega_p^2 = \frac{(M_w Z_u - M_u Z_w)}{Z_w\,M_q - M_\alpha}$$

Again the open loop transfer function is obtained by multiplying the aircraft transfer function by the pilot transfer function.

$$Y_{O.L.} = [Y_{p_\theta}]\,\left[\frac{\theta(s)}{\delta(s)}\right]$$

$$\frac{\theta(s)}{\theta_e(s)} = \frac{M_\delta\,k_{p\theta}\,T_{L_\theta}(s+1/T_{L_\theta})(s+1/T_{\theta_1})(s+1/T_{\theta_2})e^{-\tau s}}{(s^2+2(\delta\omega)_p s + \omega_p{}^2)(s^2+2(\delta\omega)_{sp}\,s + \omega_{sp}{}^2)}$$

Figure 60 shows a block diagram sketch and Bode plot of the open loop transfer function. Note that the crossover frequency is approximately 4.5 radians/second. This value was selected based on the information contained in a paper by McRuer, Graham and Krendel[65]. They found that for good pitch attitude control a crossover frequency of 4.5 radians/second is required for an effective time delay of .25 seconds.

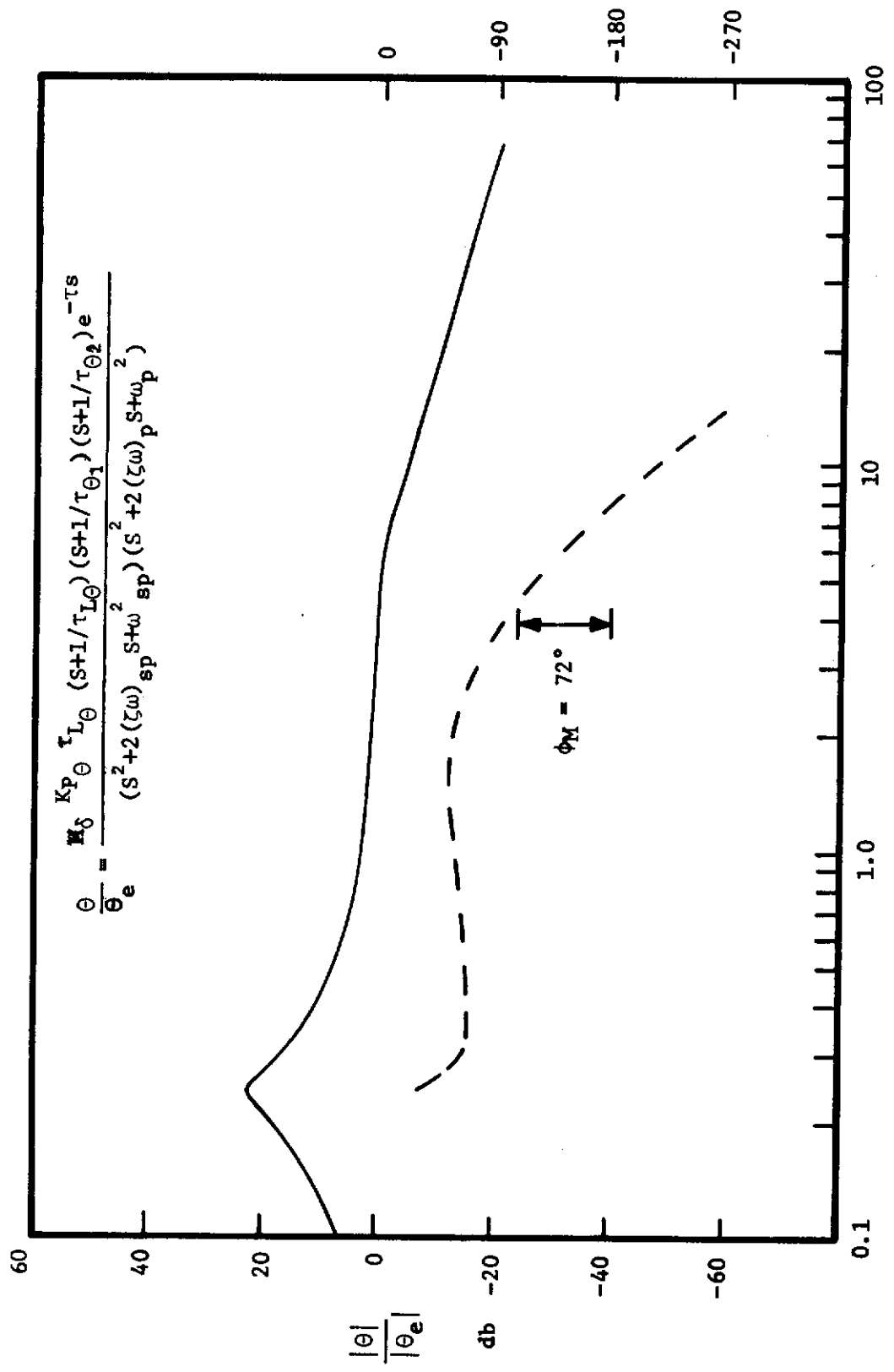

Figure 60. Bode Plot of Pitch Transfer Function

☆U.S.Government Printing Office: 1974 — 657-013/67